



JOHANNES GUTENBERG
UNIVERSITÄT MAINZ

Adjuvant-loaded protein-based nanocapsules induce effective anti-cancer immunity

Dissertation

zur Erlangung des Grades
„Doktor rerum naturalium“
(Dr. rer. nat.)
im Promotionsfach Biologie

am Fachbereich Biologie
der Johannes Gutenberg-Universität Mainz

vorgelegt von

Jenny Schunke

geb. am 06.03.1996

in Querfurt

Dekan: Univ.-Prof. Dr. Eckhard Thines

1. Berichterstatter:

2. Berichterstatter:

Datum der mündlichen Prüfung: 05.10.2023

Declaration of Authorship

The research studies presented in this dissertation were performed from November 2019 until April 2023 at the University Medical Center in Mainz in the department of dermatology as well as at the Max Planck Institute for Polymer Research in Mainz in the department of Prof. Dr. Katharina Landfester under the supervision of Prof. Dr. Volker Mailänder.

I, Jenny Schunke, hereby declare that this dissertation entitled “Adjuvant-loaded protein-based nanocapsules induce effective anti-cancer immunity” was written by myself without unauthorized external assistance and that only sources (materials, apparatus, literature) acknowledged in this work were used. I have not submitted the work presented for any scientific examination and I have not submitted the work or any part of it to any other faculty or department as a dissertation.

Jenny Schunke

Mainz, July 2023

Content

Abstract.....	VII
Zusammenfassung.....	IX
Publication List.....	XI
Introduction.....	1
Chapter A.....	17
Multicomponent Encapsulation into Fully Degradable Protein Nanocarriers via Interfacial Azide-Alkyne Click Reaction in Miniemulsion Allows the Co-Delivery of Immunotherapeutics.....	18
Abstract.....	18
Introduction.....	19
Results and Discussion.....	21
Conclusion.....	28
Acknowledgments.....	28
Supporting Information.....	29
Chapter B.....	50
Adjuvant-loaded ovalbumin-based nanocarriers for the induction of DC-mediated anti-melanoma immune responses.....	50
Material and Methods.....	50
Results and Discussion.....	51
Acknowledgement.....	59
Chapter C.....	60
Co-delivery of STING and TLR7/8 agonists in antigen-based nanocapsules to dendritic cells enhances CD8⁺ T cell-mediated melanoma remission.....	60
Abstract.....	61
Introduction.....	61
Materials and Methods.....	63
Results and Discussion.....	71
Conclusion.....	84
Acknowledgement.....	85

Supplementary Information	86
Conclusion and Outlook	99
References.....	101
Curriculum Vitae.....	Fehler! Textmarke nicht definiert.
Acknowledgements	115

Abstract

Nanocarrier-based vaccines enable the simultaneous transport of antigens and adjuvants for specific activation of the immune system for cancer therapy. In this context, the targeting of dendritic cells (DCs), whose maturation can be induced and directed by specific adjuvants and which can prime naïve T cells in an antigen-specific manner, is particularly relevant.

Within the scope of this PhD project, protein-based nanocapsules with a shell/core morphology were evaluated. Human serum albumin (HSA) and ovalbumin (OVA) with high biocompatibility, degradability, and low cytotoxicity were used as shell materials. Combinatorial encapsulation of multiple adjuvants, which stimulate different signaling pathways, into the aqueous capsule core was successfully established. The uptake of HSA capsules loaded with the adjuvants muramyl dipeptide (MDP), resiquimod (R848) and polyinosinic:polycytidylic acid (Poly(I:C)) by dendritic cells and the subsequent DC maturation were demonstrated. Additionally, it could be shown that the combination of adjuvants in particular is necessary to sufficiently stimulate DCs. Flow cytometric analyses were performed to evaluate the expression of costimulatory molecules and the secretion of pro-inflammatory cytokines and chemokines.

OVA-NCs allowed the simultaneous transport of the model antigen with the adjuvants MDP, R848, and Poly(I:C) to dendritic cells. Effective OVA peptide presentation to naïve T cells via loading on MHC class I and MHC class II molecules inducing T cell proliferation could be demonstrated *in vitro*. Subsequently, the potential of adjuvant-loaded OVA nanocapsules to induce anti-tumor immune responses was evaluated in a murine melanoma model. For this purpose, C57BL/6J mice were injected with OVA-expressing B16/F10 melanoma cells and subsequently treated with different OVA-NC formulations. Significant reduction of tumor growth, in particular by combined encapsulating of R848 and MDP, was obtained.

Furthermore, it could be shown that only the transport of antigen and adjuvants in nanocapsules to DCs induced an efficient anti-tumor immune response, whereas the administration of soluble adjuvants and antigens did not achieve comparable results. Through a comparative study including different NC amounts and injection routes, the optimal therapeutic regimen was established.

To induce complete tumor remission, R848, a Toll-like receptor 7/8 agonist, was encapsulated in combination with the potent STING agonist diamidobenzimidazole (diABZI, compound 3), in OVA nanocapsules. This adjuvant combination induced synergistic effects *in vitro* with respect to the expression of DC maturation markers as well as the production of a broad spectrum of pro-inflammatory cytokines and chemokines. In particular, the induction of type I interferons, which are required for an efficient anti-tumor immune response, by diABZI offered an

advantage over the previously established adjuvant combination. In subsequent tumor studies, animals with OVA-expressing B16/F10 melanomas were cured by triple injection of diABZI- and R848/diABZI-loaded nanocapsules. The nanovaccine was evolved by supplemental encapsulation of the melanoma-specific antigen tyrosinase-related protein 2 (TRP2). This melanoma-specific nanovaccine elicited a significant reduction of wild-type B16/F10 melanomas.

Another focus was set on the characterization of the NC-induced immune response. The infiltration of different immune cells into tumor-draining lymph nodes and the tumor tissue *in vivo* was demonstrated. In particular, the anti-tumor immune response was shown to be mediated by antigen-specific activation of CD8⁺ cytotoxic T cells. In addition, the effect of NC treatment on the expression of immune checkpoint receptors by CD8⁺ T cells was investigated.

The nanoparticle-based tumor vaccine presented in this PhD thesis can be flexibly adapted for personalized cancer therapies by encapsulation of patient-specific peptides and further modified with immune cell-addressing molecules.

Zusammenfassung

Die Vakzinierung mit Nanocarriern ermöglicht den simultanen Transport von Antigenen und Adjuvantien zur spezifischen Aktivierung des Immunsystems im Kontext der Krebstherapie. Hierbei ist insbesondere die Adressierung von dendritischen Zellen (DCs), deren Reifung durch Adjuvantien induziert und gelenkt werden kann und welche naive T Zellen antigen-spezifisch primen können, relevant.

Im Rahmen dieser Doktorarbeit wurden proteinbasierte Nanokapseln angewendet, welche eine Hülle/Kern-Morphologie aufweisen. Hierbei wurden Humanes Serum Albumin (HSA) und Ovalbumin (OVA) mit hoher Biokompatibilität, Abbaubarkeit und geringer Zytotoxizität als Hüllenmaterialien verwendet. Eine kombinatorische Verkapselung mehrerer Adjuvantien, welche unterschiedliche Signalwege anregen, in den flüssigen Kapselkern konnte erfolgreich etabliert werden. Die Aufnahme der HSA-Kapseln, welche mit den Adjuvantien Muramyl-Dipeptid (MDP), Resiquimod (R848) und Polyinosinsäure:Polycytidylsäure (Poly(I:C)) beladen wurden, in primäre dendritische Zellen sowie die hierdurch ausgelöste DC-Maturierung wurden nachgewiesen. Zudem konnte demonstriert werden, dass insbesondere die Kombination von Adjuvantien notwendig ist, um DCs hinreichend zu stimulieren. Die Analyse der Expression von kostimulatorischen Molekülen sowie der Sezernierung von Zytokinen und Chemokinen erfolgte mittels Durchflusszytometrie.

OVA-Nanokapseln ermöglichen den zeitgleichen Transport des Modell-Antigens mit den Adjuvantien MDP, R848 und Poly(I:C) zu dendritischen Zellen. Eine effektive OVA-Peptid-Präsentation über die Beladung von MHC-I- und MHC-II-Molekülen an naive T Zellen und die hierdurch induzierte Proliferation konnten *in vitro* gezeigt werden. Nachfolgend wurde die Wirksamkeit der adjuvansbeladenen OVA-Nanokapseln in einem murinen Melanommodell überprüft. Hierfür wurden C57BL/6J Mäusen OVA-exprimierende B16/F10 Melanomzellen injiziert und nach Anwachsen der Tumore wurden verschiedene OVA-NC-Formulierungen appliziert. Es konnte eine signifikante Reduktion des Tumorwachstums, insbesondere durch die Verkapselung von R848 und MDP in Kombination, erzielt werden. Zudem wurde gezeigt, dass nur durch den Transport von Antigen und Adjuvantien mittels Nanokapseln eine effiziente anti-tumorale Immunantwort ausgelöst wurde und die Verabreichung löslicher Adjuvantien und Antigene keine vergleichbaren Resultate erzielte. Durch eine Vergleichsstudie, welche verschiedene NC-Mengen und Injektionsrouten umfasste, konnte das optimale Therapieschema etabliert werden.

Um eine komplette Tumorremission zu induzieren, wurde in darauffolgenden Experimenten Resiquimod, ein *Toll-like* Rezeptor 7/8-Agonist, mit dem STING-Agonisten diABZI (compound

3), in OVA-Nanokapseln eingekapselt. Hierdurch konnten *in vitro* synergistische Effekte in Bezug auf die Expression von DC-Maturierungsmarkern als auch die Produktion eines breiten Spektrums an proinflammatorischen Zytokinen/Chemokinen erzeugt werden. Insbesondere die Induktion von Typ-I Interferonen, welche für eine anti-tumorale Immunantwort erforderlich sind, durch diABZI bot einen Vorteil im Vergleich zu der zuvor etablierten Adjuvantienkombination. In darauffolgenden Tumormodellen konnten Tiere mit OVA-exprimierenden B16/F10 Melanomen durch Injektion von diABZI- und R848/diABZI-beladenen Nanokapseln dauerhaft geheilt werden. Weiterentwickelt wurde die Nanovakzine durch die ergänzende Verkapselung des melanomspezifischen Antigens TRP2. Diese wurde in weiteren Tumorstudien getestet und induzierte eine signifikante Reduktion des Wachstums muriner B16/F10 Tumore.

Ein weiterer Schwerpunkt dieser Arbeit liegt auf der Charakterisierung der NC-induzierten Immunantwort. Im Mausmodell konnte die Infiltration verschiedener Immunzellen in drainierende Lymphknoten und das Tumorgewebe nachgewiesen werden. Insbesondere konnte gezeigt werden, dass die anti-tumorale Immunantwort auf CD8⁺ zytotoxischen T Zellen basiert und antigenspezifisch ist. Zusätzlich wurde die Expression von Immuncheckpoints untersucht.

Die im Rahmen dieser Doktorarbeit entwickelte und etablierte nanopartikelbasierte Tumorstudie kann für personalisierte Krebstherapien flexibel angepasst werden und weiterhin mit immunzelladressierenden Molekülen modifiziert werden.

Publication List

J. Schunke, N. Hüppe, N. Mangazeev, K.R. Speth, T. Klaus, V. Bolduan, M. Kuske, P. Schneider, S. Grabbe, K. Landfester, V. Mailänder, M. Fichter. Co-delivery of STING and TLR7/8 agonists in antigen-based nanocapsules to dendritic cells enhances CD8⁺ T cell-mediated melanoma remission. Submitted to *Advanced Materials*, **2023**.

J. Schunke, V. Mailänder, K. Landfester, M. Fichter. Delivery of Immunostimulatory Cargos in Nanocarriers Enhances Anti-tumoral Nanovaccine Efficacy. Submitted to *International Journal of Molecular Sciences*, **2023**.

L. Dietz, J. Oberländer, A.M. Maroto, **J. Schunke**, M. Fichter, E.-M. Krämer-Albers, K. Landfester, V. Mailänder. Submitted to *Journal of Extracellular Vesicles*, **2023**.

N. Hüppe, **J. Schunke**, M. Fichter, V. Mailänder, F.R. Wurm, K. Landfester. Multicomponent encapsulation into fully degradable protein nanocarriers *via* interfacial azide-alkyne click reaction in miniemulsion allows the co-delivery of immunotherapeutics. *Nanoscale Horizons*, **2022**, 25;7(8).

J. Simon, M. Fichter, G. Kuhn, M. Brückner, C. Kappel, **J. Schunke**, T. Klaus, S. Grabbe, K. Landfester, V. Mailänder. Achieving dendritic cell subset-specific targeting *in vivo* by site-directed conjugation of targeting antibodies to nanocarriers. *Nano Today*, **2022**, 43.

T. Klaus, A. S. Wilson, E. Vicari, E. Hadaschik, M. Klein, S.S.C. Helbich, N. Kamenjarin, K. Hodapp, **J. Schunke**, M. Haist, F. Butsch, H.C. Probst, A.H. Enk, K. Mahnke, A. Waisman, M. Bednarczyk, M. Bros, T. Bopp, S. Grabbe. Impaired Treg-DC interactions contribute to autoimmunity in leukocyte adhesion deficiency type 1. *JCI Insight*, **2022**, 22;7(24).

M. Bednarczyk, V. Bolduan, M. Haist, H. Stege, C. Hieber, L. Johann, C. Schelmbauer, M. Blanfeld, K. Karram, **J. Schunke**, T. Klaus, I. Tubbe, E. Montermann, N. Röhrig, M. Hartmann, J. Schlosser, T. Bopp, B.E. Clausen, A. Waisman, M. Bros, S. Grabbe. β 2 Integrins on Dendritic Cells Modulate Cytokine Signaling and Inflammation-Associated Gene Expression, and Are Required for Induction of Autoimmune Encephalomyelitis. *Cells*, **2022**, 13;11(14).

C. Kappel, C. Seidl, C. Medina-Montano, M. Schinnerer, I. Alberg, C. Leps, J. Sohl, A.K. Hartmann, M. Fichter, M. Kuske, **J. Schunke**, G. Kuhn, I. Tubbe, D. Paßlick, D. Hobernik, R. Bent, K. Haas, E. Montermann, K. Walzer, M. Diken, M. Schmidt, R. Zentel, L. Nuhn, H. Schild, S. Tenzer, V. Mailänder, M. Barz, M. Bros, S. Grabbe. Density of Conjugated Antibody Determines the Extent of Fc Receptor Dependent Capture of Nanoparticles by Liver Sinusoidal Endothelial Cells. *ACS Nano*, **2021**, 28;15(9).

Introduction

The introduction is mainly based on the submitted paper in the peer-reviewed journal *International Journal of Molecular Sciences* and was only slightly modified by addition of short text parts. Figures were created with BioRender.com. This work was supported by the Deutsche Forschungsgemeinschaft (DFG) through the CRC1066 in subproject Q2 and Q6.

Delivery of Immunostimulatory Cargos in Nanocarriers Enhances Anti-tumoral Nanovaccine Efficacy

Jenny Schunke^{a,b}, Volker Mailänder^{a,b}, Katharina Landfester^b, Michael Fichter^{a,b,*}

^a Department of Dermatology, University Medical Center Mainz, Langenbeckstraße 1, 55131 Mainz, Germany

^b Max Planck Institute for Polymer Research, Ackermannweg 10, 55128 Mainz, Germany

* corresponding author

Abstract

Long-term cure of tumor patients still represents a major challenge. Immunotherapies offer promising therapy options since they are designed to specifically prime the immune system against the tumor and modulate the immunosuppressive tumor microenvironment. Using nucleic acid-based vaccines or cellular vaccines often does not achieve sufficient activation of the immune system in clinical trials. Additionally, the rapid degradation of drugs and their non-specific uptake into tissues and cells as well as severe side effects pose a challenge. The encapsulation of immunomodulatory molecules into nanocarriers provides the opportunity of protected cargo transport and targeted uptake by antigen-presenting cells. In addition, different immunomodulatory cargos can be co-delivered, which enables a versatile stimulation of the immune system, enhances anti-tumor immune responses and improves the toxicity profile of conventional chemotherapeutic agents and adjuvants.

1. Different factors establish the immunosuppressive tumor microenvironment

The effective treatment of cancer still holds many challenges due to the heterogeneity of tumors in patients. Moreover, different mechanisms of the immune system are influenced by tumor cell alterations. For example, the downregulation or loss of HLA class I/MHC class I

expression or defects of the antigen-processing machinery in antigen-presenting cells (APCs)^[1-2] is affected, which in turn leads to an impaired T cell activation against tumors. The expression of immune checkpoint ligands, such as programmed death-ligand 1 (PD-L1), by tumor cells and the secretion of inhibitory cytokines, e.g. TGF- β , can also inhibit the function of APCs.^[3-4] Binding of PD-L1 to programmed cell death protein 1 (PD-1) not only inhibits dendritic cells (DCs) but also T cells directly and thereby suppresses their activation. Additionally, the signaling through other expressed immune checkpoints, such as cytotoxic T lymphocyte-associated protein 4 (CTLA-4), lymphocyte-activation gene 3 (LAG3) or T cell immunoglobulin and mucin domain 3 (TIM-3) suppresses the function of immune cells in the tumor microenvironment (TME).^[5-6] To circumvent this immunosuppression, immune checkpoint-blocking antibodies are successfully used in clinic. In particular, patients with advanced melanoma benefit from a therapy with monoclonal anti-PD-1 antibodies (nivolumab) or a combination of PD-1 and CTLA-4 (ipilimumab) blockade.^[7]

Nevertheless, the TME is often composed of immunosuppressive cells such as regulatory T cells (T_{regs}), myeloid-derived suppressor cells (MDSCs) or inhibitory (M2-type) macrophages.^[8-10] FoxP3⁺ T_{regs} not only inhibit the differentiation of naïve T cells to effector cells but also inhibit the function of CD4⁺ and CD8⁺ T cells as well as of NK cells, B cells and DCs.^{[11], [12]} MDSCs are able to suppress T cell activity by the production of ROS^[10] and the expression of arginase and iNOS.^[13-14] It was further shown that MDSCs promote the differentiation of FoxP3⁺ T_{regs} *in vivo*.^[15-16] Immunosuppression by M2-type macrophages is based on the release of anti-inflammatory molecules subsequently promoting tumor growth.^[17]

To overcome immune evasion and to induce tumor-specific T cell responses, immunotherapeutic vaccines are designed based on tumor antigens.^[18] The choice of the tumor antigen and its tumor specificity are critical to the effectiveness of tumor vaccination.^[19] Those tumor-associated antigens (TAA) and tumor-specific antigens (TSA) offer different advantages in their use as vaccine components in terms of prevalence, T cell specificity and generation of immune tolerance or autoimmunity.^[20-22] TAA comprise tissue differentiation antigens as well as overexpressed antigens which are found on both tumor cells and healthy cells.^[19] They often have a low tumor specificity and their use can induce severe side effects. TAA include, among others, the antigens Melan A/MART-1, gp100, p53, and HER2. On the other hand, TSA can also be used for vaccination approaches, comprising for example MAGE, KRAS and HPV E6/E7. They include cancer germline antigens, tumor specific mutated antigens and oncogenic viral antigens.^[19]

Antigen-based vaccination formulations can overcome existing challenges of immunotherapies. They offer advantages such as the protected transport of cargos and the

resulting extended circulation time as well as the possibility of all-in-one delivery of antigens, adjuvants and drugs. In addition, defined quantities of transported cargos can be controlled and non-specific diffusion of small molecules can be prevented. Furthermore, toxicity profiles of chemotherapeutic drugs by their encapsulation into nanocarriers is improved.

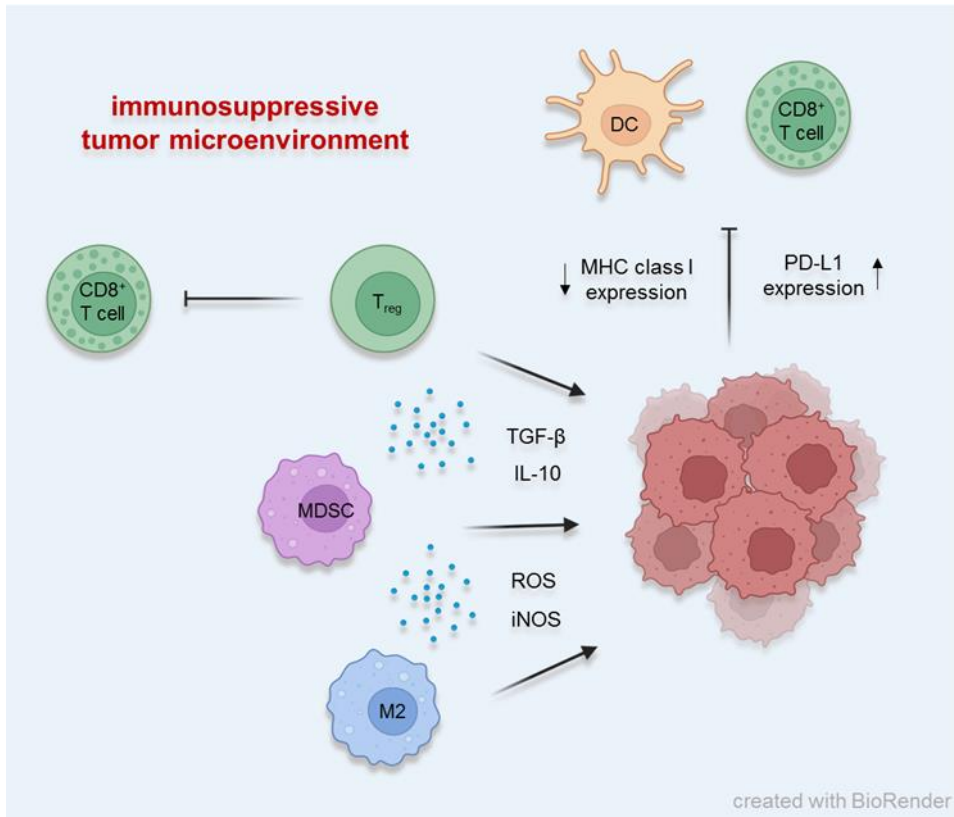


Figure 1. Cellular mechanisms maintaining the immunosuppressive tumor microenvironment.

2. Nucleic acid-based vaccines: DNA and RNA encoding for tumor antigens

Nucleic acid-based vaccines consist of DNA or RNA encoding for TAA as well as for TSA.^[23-24] Research efforts have focused on DNA vaccines due to their ease of production and stability during storage. They can be designed by incorporation of desired sequences into a plasmid backbone.^[25] Furthermore, DNA vaccines offer a way to mimic viral infections^[26] by DNA binding to Toll-like receptors and thereby induce pro-inflammatory immune responses and can be flexibly adapted by genetic modifications.^[25] However, they have shown unsatisfactory results in clinical trials due to low uptake in antigen-presenting cells and the resulting inefficient expression of antigens.^[27] Nevertheless, tumor-specific T cell and IgG responses could be generated with DNA fusion vaccines in pre-clinical studies^[28] using electroporation (EP).^[29-30] For instance, an improved response to an HIV-1 DNA vaccine was induced using EP as application method.^[31]

Since mRNA is translated in the cytoplasm of a target cell, mRNA vaccines do not need to enter the nucleus in contrast to DNA vaccines.^[23] On the other hand, RNA has a lower stability and is rapidly degraded in biological fluids.^[32] Therefore, mRNA vaccine design focuses on the increase of RNA half-life by optimizing the 5'- and 3'-UTR elements via genetic modifications or the encapsulation in delivery vehicles.^[33-34] Non-formulated mRNA is mainly taken up by immature DCs, thus, so-called "naked" mRNA is administered intradermally or intranodally.^[35-36] Even though naked RNA induced antigen-specific T cell responses in pre-clinical studies^[37], mRNA stability is challenging. One way to circumvent mRNA instability is to load DCs *ex vivo*, which in turn is time-consuming and expensive.^[38] Electroporation of DCs with mRNA encoding for CD70, CD40-L, and constitutively active Toll-like receptor 4 (caTLR4) induced effective DC maturation and subsequent T cell stimulation^[39]. This so called TriMix-RNA was combined with additional mRNAs, each encoding for one of four melanoma-associated antigens (MAGE-A3, MAGE-C2, tyrosinase, or gp100), and further introduced into DCs by electroporation. In clinical trials for treatment of stage III/IV melanoma patients this vaccine has shown to be safe and immunogenic and can further be improved in regard to long-term immunity by combining with immune checkpoint blockade.^[40-41] Treatment with TriMix/mRNA-vaccine in combination with ipilimumab resulted in an overall survival of 28% and a progression-free survival of 18% after more than 5 years.

3. Tumor cell-based vaccines

Early vaccination approaches focused on the application of whole cells or cell lysates for antigen delivery.^[42] Designing vaccines based on autologous and allogeneic tumor cells offers the advantage that tumor antigens do not have to be identified in advance by DNA/RNA sequencing techniques. In addition, these vaccines contain a wide range of tumor antigens, which can thus generate a broad immune response. To improve the immunogenicity of whole cell vaccines, tumor cells can be genetically modified to express cytokines and chemokines. GVAX cancer vaccine, first developed in 1993 by Glenn Drandoff, consisting of two replication-deficient prostate-carcinoma cell lines, which were genetically modified to secrete GM-CSF, were tested in clinical trials.^[43-44] This therapy for advanced prostate cancer was well tolerated and prolonged the overall survival dose-dependently. Improved effects were achieved treating patients with advanced melanoma using a polyvalent melanoma vaccine consisting of three irradiated human melanoma cell lines.^[45-46] Intradermal injection of this melanoma vaccine significantly increased the overall survival of stage IIIA and IV melanoma patients by three- or fourfold, respectively. Other approaches, such as the cancer vaccine Melacine, combine allogeneic melanoma cell lysates with adjuvants.^[47-48] This vaccination strategy induced modest anti-tumoral effects in clinical studies and induced strongest anti-tumor activity in

patients expressing the HLA class I antigens A2 or C3 by most efficient induction of CD8⁺ T cell responses.

4. Dendritic cell-based vaccines

Since DCs can prime naïve T cells in an antigen-specific manner, various DC-based vaccines have been explored.^[49-50] Following antigen uptake, DCs mature, migrate into the lymph nodes and present antigenic peptides bound to MHC class I and II molecules to T cells^[51-52] T cell priming and proliferation is based on three DC-mediated signals: (i) T cell receptor (TCR) binding to antigen/MHC-complex, (ii) binding of the costimulatory receptors CD80 and CD86 expressed by DCs, and (iii) cytokine signaling.^[53-54] Cytokines are soluble proteins secreted by different immune cells stimulating either pro-inflammatory or anti-inflammatory immune responses. Pro-inflammatory cytokines include IL-1 β , IL-6, IL-8, IL-12, TNF- α , and interferons.^[55] Not only the secretion of cytokines influences the activity of lymphocytes, but also the production of chemokines regulating the recruitment of immune cells to the tumor site. DCs are attracted by CCL20, CCL5, and CXCL12, whereas CXCL9 and CXCL10 are associated with the recruitment of Natural Killer (NK) cells, CD4⁺ Th1 cells, and CD8⁺ cytotoxic T lymphocytes (CTL).^[56]

DCs can be divided into two subtypes: plasmacytoid DCs (pDCs) and conventional DCs (cDCs).^[57] cDCs can further be subdivided into cDC1 and cDC2 based on their surface marker expression profile^[58]. Crosspresenting cDC1 are characterized by the presence of the markers XCR1, CLEC9A, BTLA, or CD26. Murine cDC1 also express CD8 α and CD103, whereas human cDC1 can be identified by the expression of CD141. The absence of cDC1 markers and the high expression level of CD11b in combination with the presence of CD1c and SIRP α characterize cDC2. Their function in the murine system differs from that in humans. Murine cDC2 mainly present endogenous antigens to CD4⁺ T cells, while human cDC2 also crosspresent endogenous antigens to CD8⁺ T cells. pDCs can also prime naïve T cells and are known for their important role in anti-viral immune responses which is characterized by the vigorous production of type I interferons, IL-6, and TNF- α .^[59] These properties also make them an interesting target in the context of tumor vaccination.

In various studies evaluating the efficacy of DC-mediated vaccines, monocyte-derived DCs cultured with GM-CSF and IL-4 were used. Prior to immunization, they were loaded with tumor antigens *ex vivo*, such as MHC class I-restricted peptides, synthetic long peptides, or full-length proteins.^[60-62] Early clinical trials for the treatment of melanoma patients describe the pulsing of *in vitro*-generated DCs with either a cocktail of melanoma-associated peptides (tyrosinase, Melan-A/MART-1, gp100) or peptides derived from MAGE-1 and MAGE-3.^[63] Those peptide-loaded DCs were repeatedly injected intralymphatically depending on the patients' response

to the vaccination. Another group of patients was injected with tumor lysate-pulsed DCs. In this study, the induction of DC vaccine-mediated antigen-specific T cell activity against melanoma and metastases in different organs could be observed. The suitability of antigen-pulsed DCs was further confirmed in a B cell lymphoma vaccination trial^[64] as well as for the treatment of acute myeloid leukemia^[65] and myeloma.^[66] Furthermore, autologous peptide-loaded DCs were tested for their potential to induce anti-melanoma immune responses.^[42, 67] DCs were loaded with MHC class I- and II-restricted peptides and injected subcutaneously. However, there was no increased response rate or overall survival compared to standard chemotherapy with the cytostatic agent dacarbazine.

5. Adjuvants play a key role in enhancing immune responses to vaccines

Adjuvants are immunomodulatory molecules enhancing antigen-specific immune responses. In this way, they improve the antigen-directed response to vaccines, strengthen the durability of the immune response to vaccine stimuli or trigger a more extensive immune response.^[68-69] In particular, when administering immunotherapeutic vaccines to deliver tumor antigens, the additional application of adjuvants is necessary to circumvent tolerance induction by triggering pro-inflammatory immune responses.^[70] Agonists of pattern recognition receptors (PRRs) play an important role in the development of adjuvants. PRRs are expressed by dendritic cells and macrophages, as well as by epithelial cells, endothelial cells, and fibroblasts. They are involved in the recognition of pathogen-associated molecular patterns (PAMPs) as well as damage-associated molecular patterns (DAMPs).^[71] Four different PRR groups can be distinguished: Toll-like receptors (TLRs), c-type lectin receptors (CLRs), Retinoic acid-inducible gene (RIG)-I-like receptors (RLRs) and NOD-like receptors (NLRs). Binding of PAMPs and DAMPs to those receptor types triggers the upregulation of gene transcription and subsequent release of cytokines, chemokines, and antimicrobial proteins. PAMPs that have been studied in the development of cancer vaccines include, among others, flagellin, LPS as well as the less toxic MPLA, and CpG ODN. Particularly effective DAMPs for anti-tumor vaccination are HMGB1, an endogenous adjuvant, and heat shock protein (HSP).^[72] Additional to pathogen-derived molecules, cytokines such as IL-2, IL-12, interferons or granulocyte-macrophages colony stimulating factor (GM-CSF) can also act as adjuvants.^[19] They can directly circumvent tolerance by the induction of CTLs or trigger a Th1-directed immune response as well as antibody production.^[73]

In the 1920, aluminum salts were first approved for the application as vaccine adjuvant in humans.^[74] Aluminum hydroxide and aluminum phosphate are still important adjuvants present in various licensed vaccines. Their effect is based on the stimulation of DCs, the activation of the complement system and the induction of chemokine production.^[75-77] However, they cannot

elicit antigen-specific CD8⁺ T cell and T_h1 responses and generally enhance T_h2-mediated antibody-based immune responses which are not sufficient for robust tumor killing.^[78] Since then, the development of novel adjuvants is steadily progressing. Nowadays, a broad range of clinically tested and used adjuvants for vaccination approaches is available.^[79] Besides aluminum salts, these include adjuvant-containing emulsions, virosomes, dsRNA analogs, lipid A analogs, or imidazoquinolines.^[79]

TLRs represent important adjuvant targets detecting pathogen-associated molecular patterns and are mainly expressed by antigen-presenting cells. TLR4 is localized in the plasma membrane, while TLR7/8 and 9 are located in endosomal membranes.^[80] The immunomodulatory potential of TLR agonists has been widely used in testing and development of adjuvants for vaccination.

It has been shown that the TLR3 and MDA5 agonist Poly(I:C) induces the production of type I interferons and other pro-inflammatory cytokines subsequently enhancing T cell activity and proliferation^[81]. Furthermore, CpG oligodeoxynucleotides, which interact with TLR9, primarily stimulate B cells, T cells as well as natural killer (NK) cells and macrophages.^[82] In addition to those polymer-like adjuvants, small molecules such as imidazoquinolines bind to TLR7 and TLR8, which play an important role in the induction of anti-viral immune responses by naturally recognizing single-stranded RNA.^[3, 83-84] The imidazoquinoline R848 was shown to activate the MyD88 signaling pathway through binding to TLR7 or TLR8 and subsequently inducing the secretion of pro-inflammatory cytokines by NF- κ B-mediated transcription.^[85] Due to this property R848 became a promising adjuvant not only for vaccination against pathogens but also for use in cancer vaccines. Clinical studies have shown an improvement of pancreatic tumor control by combining radiotherapy and R848 application.^[86] Furthermore, this combination treatment elicited an anti-tumor immune response in pre-clinical studies against melanoma.^[87] In addition, the combination of the TLR3 agonist Poly(I:C) and the TLR7/8 agonist R848 enhanced the polarization of macrophages to inflammatory (M1-like) effectors *in vitro* and induced T cell infiltration followed by tumor regression in murine lung cancer and fibrosarcoma models.^[86] Additionally, single-stranded RNA with uridine- and guanosine-rich sequences can also act as TLR7/8 agonist and thereby promote Th1 responses and the secretion of IFN- α and IL-12 as adjuvant.

Multiple studies demonstrated a correlation of induced high levels of type I interferons upon anti-cancer immunotherapy with a better outcome.^[88-89] Therefore, agents triggering the activation of stimulator of interferons genes (STING) got into the focus.^[88-89] STING, a transmembrane protein located in the endoplasmic reticulum, plays an important role in the sensing of cytosolic DNA which triggers the cGAS/STING pathway.^[54] This leads to the

downstream production of type I interferons affecting T cells, NK cells^[90-91], APCs^[92-93] and tumor cells themselves. It is known that those interferons inhibit the proliferation of tumor cells and induce the expression of MHC class I, while the expression of VEGF is reduced.^[94-96] First generation STING agonists, such as DMXAA, significantly reduced tumor growth but failed to overcome immunosuppressive TME and did not induce long-term immunity in mouse models.^[97-98] Even though DMXAA was successfully applied in pre-clinical studies and was well tolerated in clinical trials, it failed to prolong the overall survival of non-small cell lung cancer patients compared to placebo treatments.^[99-100] Those contrary results in mouse models and clinical trials can be explained by polymorphisms in human STING, which prevent effective binding of DMXAA in many patients rendering therapy with this STING agonist ineffective.^[101] This finding led to the development of synthetic cyclic dinucleotides such as ADU-100. Intratumoral injection of ADU-100 was shown to induce antigen-specific activation of CD8⁺ T cells and to improve cancer therapy with antibodies specific for the immune checkpoints PD-1 and CTLA-4.^[102-105] Next-generation non-cyclic dinucleotides, such as ALG-031048, with higher stability were further developed. Intratumoral application of ALG-031048 increased the regression rate of CT26 colon tumors from 44% following treatment with ADU-100 to 90%. It additionally promoted an effective long-term immune memory in mice.^[106] Nevertheless, the use of these STING agonists was limited by their low stability and their systemic administration was not feasible. Therefore, a new class of STING agonists, amidobenzimidazoles (ABZI), with higher stability and increased potency were developed. In pre-clinical trials ABZI-based compound 3 (diABZI) induced a 400-fold stronger IFN- β production compared to the natural STING agonist cGAMP. Furthermore, the systemic treatment of murine CT26 tumors led to an effective anti-tumoral immune response based on CD8⁺ T cells.^[107-108]

6. Nanomedicine enables the combined delivery of immunostimulatory cargos and reduces side effects elicited by chemotherapeutic drugs

Using nanoparticles (NPs) as delivery vehicles for antigens, adjuvants or drugs ensures their protected transport, prolonged bioavailability, and controlled release.^[109] In addition, different nanocarrier groups can be selected for specific applications, as they differ not only in composition, but also in loading capacity, size, shape, and surface charge.^[110-113] When used as vaccine formulations in cancer immunotherapy, the uptake of NPs by DCs is particularly important to ensure tumor antigen-specific activation of the immune system. In addition, the encapsulation of cargos such as adjuvants has the potential to transport them directly to the target site and prevents diffusion of small molecules. DC uptake cannot exclusively be influenced by NP properties but can also be increased by specific modification of the particle

surfaces. These modifications include the conjugation of antibodies^[114] or other targeting moieties.^[115]

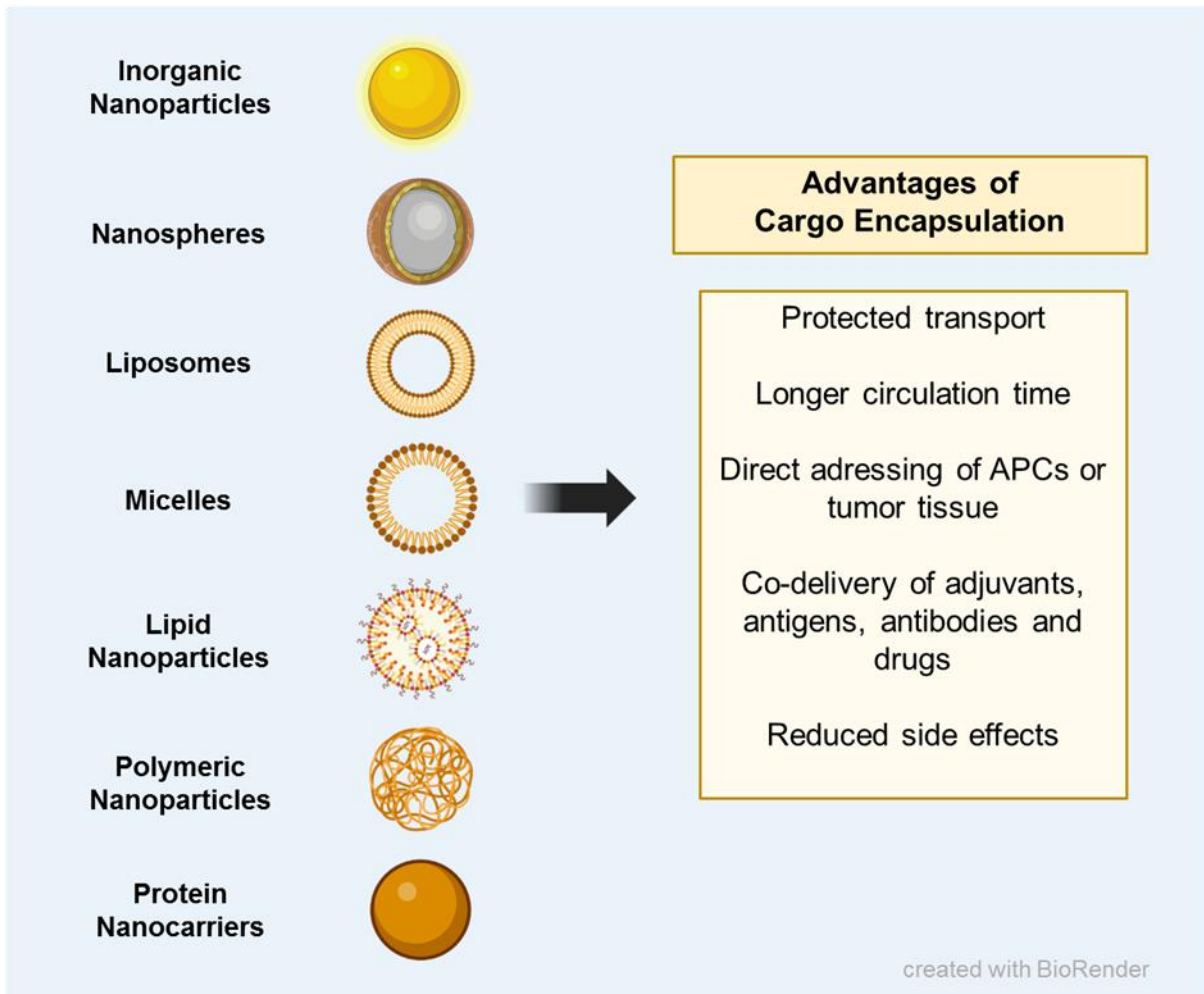


Figure 2. Encapsulation of biomedical cargos into nanocarriers increases anti-tumoral nanovaccine efficacy.

NPs composed of inorganic materials are of interest for the application as tumor vaccines due to their stability in biological fluids and their controllable synthesis.^[116] In addition, depending on the material from which they are synthesized, they inherit various advantages and disadvantages. Gold nanoparticles, for example, were shown to stimulate the immune system by inducing different cytokine pathways. This immune system-activating potential is dependent on size and shape.^[117]

Silica-based NPs are promising inorganic formulations due to their non-toxic profile and biodegradability.^[118-119] *In vitro* studies demonstrated the successful encapsulation of dexamethasone into core-shell silica nanocapsules for the treatment of liver diseases.^[120] Encapsulation of drugs can also enhance their solubility, stability and reduce side effects. This was shown for the encapsulation of four different chemotherapeutic drugs (cisplatin, carboplatin, oxaliplatin, and oxalipalladium) into silica nanocapsules.^[121] Fan *et al.* additionally

demonstrated the efficient covalent conjugation of the anti-cancer drug doxorubicin and folic acids to the NP surface.^[122] Surface modifications enhanced the NP uptake by folate receptor-expressing cancer cells and reduced cytotoxicity due to lower drug release in folate receptor negative cells. However, silanol groups of silica NP surfaces can interact with phospholipids of red blood cells and thereby inducing hemolysis.^[123] Those disadvantages can reduce their applicability *in vivo*. Thus, other inorganic nanoparticles, such as carbon nanospheres, solid carbon nanoparticles or carbon nanotubes consisting of graphite layers came into focus.^[124-125]

Their core-shell morphology provides a large loading space and can be used for the encapsulation of drugs or immune checkpoint inhibitors (ICIs).^[124] Additionally, the biocompatibility of carbon NPs enables oral vaccine administration.^[125] In addition, encapsulation protects cargos against enzymatic degradation in the gastrointestinal tract, which even allows oral administration of unstable molecules.^[126]

Liposomes made of biodegradable phospholipids are uni-, bi- or oligolamellar vesicles which offer another option for effective encapsulation of immunomodulatory compounds.^[127] They were first introduced in 1965^[128] and used for vaccine development in 1974.^[129] Since various parameters such as size, charge, surface modification and loading are variably adjustable, they represent versatile delivery vehicles for adjuvants and antigens.^[130] In particular, the surface charge can modulate uptake in tissues and cells such as APCs. Cationic liposomes, for example, interact with DC surfaces due to their positive zeta potential, which enhances their uptake, and further induce DC maturation.^[131-132] These properties also allow application by various routes, such as oral, topical or mucosal administration. Cargos can be encapsulated into the hydrophilic core of liposomes, embedded into the lipid bilayer or attached to the surface via modification of acyl chains or complexation.^[130] An example of DC-stimulatory liposomes are RNA-lipoplexes (RNA-LPX) synthesized by complexing antigen-encoding RNA with liposomes.^[133] Since single-stranded RNA naturally binds to TLR7 and TLR8, RNA-LPX induce DC maturation and thereby lead to the production of pro-inflammatory cytokines and T cell activation. This has also been proven in pre-clinical studies in which the vaccination of CT26 colon tumor-bearing mice with RNA-LPX induced strong anti-tumoral cellular and humoral immune responses. Intravenously injected RNA-LPX were further described as well-tolerated treatment of melanoma patients and offer the opportunity of personalized cancer treatment.^[134] A vaccine-mediated and dose-dependent production of IFN- α and antigen-specific T cell responses were observed. Protected delivery of mRNA in lipid nanoparticles (LNP) was additionally demonstrated by preventive immunization with COVID-19 mRNA vaccines.^[135] This approach also allows the complexation of mRNA encoding tumor antigens or therapeutic

antibodies.^[136] LNP consist of ionizable cationic lipids, phospholipids, lipids attached to polyethylene glycol (PEG) and cholesterol. Ionizable lipids are needed for mRNA complexation, whereas cholesterol and other helper lipids improve LNP stability.^[136-137] Surface PEGylation further enhances the LNP circulation time.^[137] Cationic 1,2-dioleoyl-3-trimethylammonium-propane (DOTAP)-based LNP were shown to interact with serum proteins and thus aggregate resulting in a short half-life. Furthermore, their hemolytic activity induced severe side effects. Therefore, ionizable LNP with an improved toxicity profile have been developed for pH-sensitive mRNA delivery. Different mRNA-loaded LNP are being evaluated for their efficacy in clinical trials on the treatment of tumors such as lymphoma or melanoma. The packaged mRNA encodes target proteins such as human IL-12, OX40L, or for different neoantigens. Moreover, additive treatment effects are tested by combining the mRNA LNP with monoclonal antibodies blocking immune checkpoints.^[136]

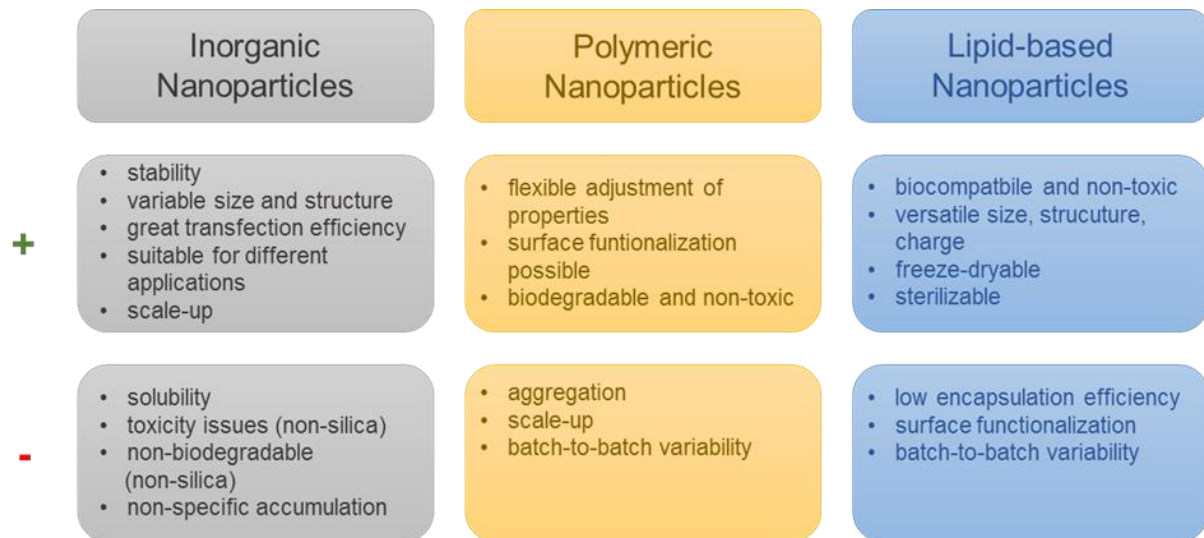


Figure 3. Advantages and challenges of different nanoparticle classes.

Further promising carrier systems for the use as anti-cancer vaccines are micelles. They enable the efficient co-encapsulation of antigens and adjuvants and, thus, enhance DC-mediated antigen-specific T cell activation.^[138] This was demonstrated via the encapsulation of ovalbumin (OVA) and the TLR7 agonist CL264 into micelles based on amphiphilic diblock co-polymers.^[139] Vaccination with these micelles enhanced antigen cross-presentation of DCs to CD8⁺ T cells, resulting in E.G7-OVA tumor growth prevention *in vivo*. Similar results were obtained by Zeng *et al.* with the melanoma antigen TRP2 and TLR9 agonist CpG ODN-loaded self-assembled micelles based on two amphiphilic diblock co-polymers.^[140] Their application *in vivo* led to strong anti-tumoral immune responses mediated by cytotoxic T lymphocytes in a lung metastatic melanoma model.

The synthesis of polymeric NPs for vaccination purposes has been extensively researched.^[141] Different vaccines composed of poly(D,L-lactic-co-glycolic acid) (PLGA)-based NPs were developed and their potential to transport encapsulated bioactive cargos specifically to DCs was verified.^[142] Uptake of PLGA NPs was detected by both, murine and human cells^[143-145], with the uptake rate being highest for cationic NPs.^[146] *In vivo* studies demonstrated that NP sizes below 500 nm is beneficial for the uptake and subsequent activation of cytotoxic T lymphocytes. Small NPs are preferentially taken up by DCs and larger ones by macrophages, explaining these observations.^[142, 147] PLGA-based NPs can be loaded with antigens as well as adjuvants. This allows the co-delivery of multiple adjuvants, such as TLR agonists^[148], as well as the reduction of the adjuvant amount needed for robust DC-mediated T cell priming^[149]. Diwan *et al.* immunized BALB/c mice with CpG-loaded PLGA-NPs and showed that the amount of CpG required for T cell activation could be reduced by 10- to 100-fold by encapsulation into NPs. Further *in vivo* studies additionally demonstrated the induction of antigen-specific T cell responses by encapsulation of antigens and the simultaneous enhancement of immune responses by encapsulated adjuvants.^[150-151] The combined encapsulation of OVA and the TLR4 ligand monophosphoryl lipid A induced antigen-specific T cell activation as well as a strong production of the pro-inflammatory cytokine IFN- γ . IFN- γ plays an important role in anti-cancer immunity by triggering the expression of MHC class I and II molecules on DCs^[152] resulting in enhanced antigen presentation. Furthermore, B16/F10 melanoma-bearing mice could be efficiently treated with TRP2/7-acyl lipid A-loaded PLGA NPs. Vaccination with those PLGA-NPs triggered the production of different pro-inflammatory cytokines, such as IL-6, IL-12, TNF- α , and IFN- γ , as well as strong T cell-mediated reduction of tumor volume.^[153] As an alternative to PLGA, other copolymers can be utilized for the synthesis of polymeric nanoparticles. Amphiphilic hybrid and fully synthetic copolymers such as poly(ethylene glycol), polyoxazolines, synthetic glycopolymers, or hydrophilic poly(amino acids) are used as hydrophilic blocks.^[154] As hydrophobic blocks polycarbonate, polystyrene or aliphatic polyesters (e.g. polycaprolactone and poly(lactic acid)) are used.^[154]

Combined encapsulation of the TAA gp100 with CpG ODN as adjuvant induced strong CD8⁺ T cell proliferation *in vivo* as well as enhanced IFN- γ production. The efficiency of antigen and adjuvant co-delivery in E2 NPs was demonstrated by treating B16/F10 melanoma-bearing mice, with regard to prolonged overall survival.^[155] Moreover, the importance of cargo co-delivery for efficient DC-mediated cancer therapy was further shown by Hüppe *et al.*^[156] This study demonstrated the feasibility of the encapsulation of three adjuvants with different solubility in nanocapsules (NCs) composed of human serum albumin (HSA). Dendritic cells showed the strongest activity in terms of the expression of CD80 and CD86 after uptake of NCs containing all three adjuvants, Poly(I:C), R848 and MDP. This observation additionally

demonstrated the importance of simultaneous cargo encapsulation and delivery, which causes an extensive DC activation and consequently induces anti-tumoral immune response. Moreover, proteins derived from milk or corn can also serve as nanoparticle shell material. Zein, a storage protein present in corn, can be used as biocompatible source for the synthesis of nanocarriers.

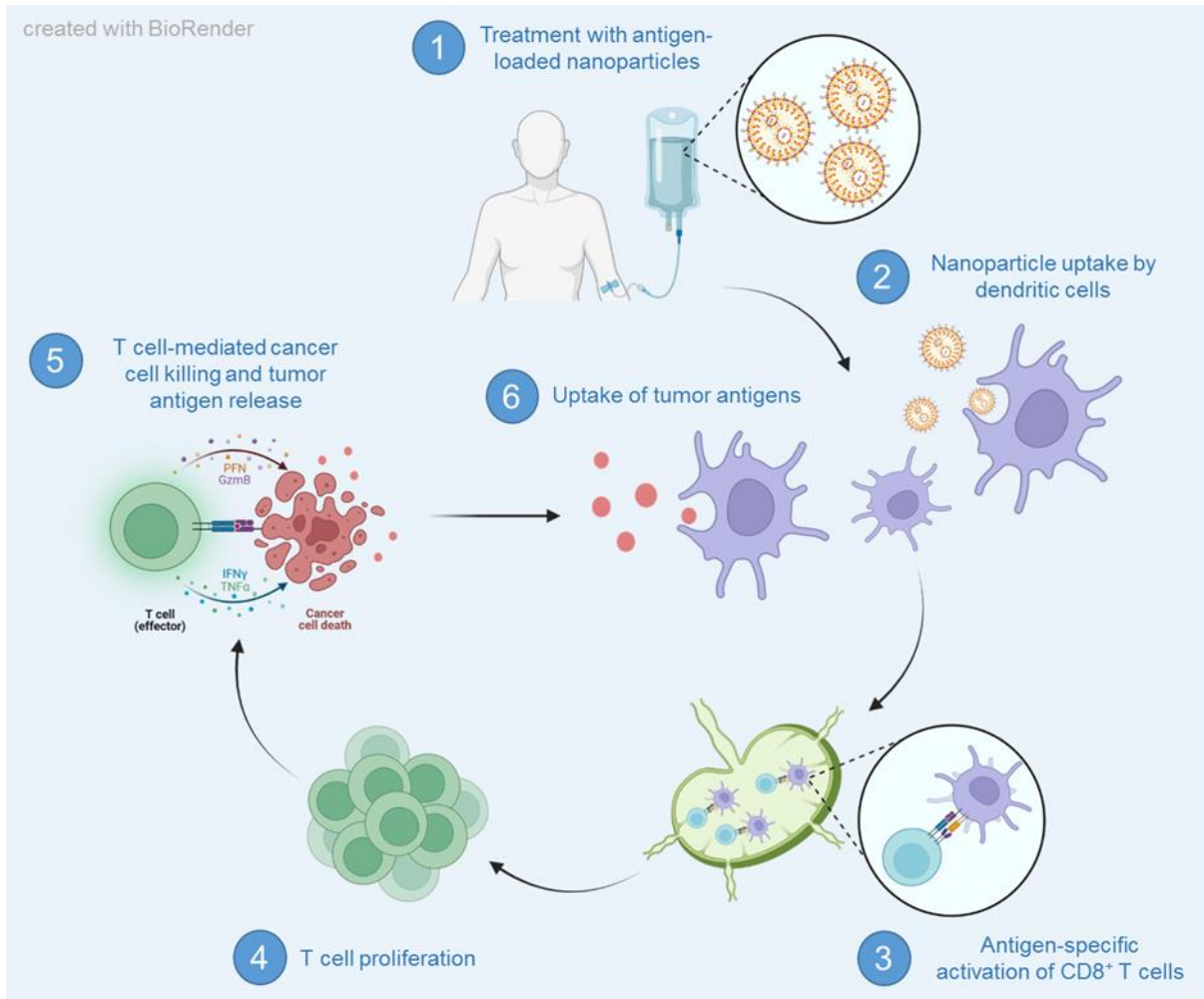


Figure 4. Antigen-loaded nanoparticle vaccines induce specific cancer cell killing. Depicted is the principle of nanoparticulate nanovaccines, which specifically transport antigens in the form of peptides, DNA or RNA to dendritic cells and thereby induce T cell activation.

7. Nanocapsule crosslinking affects immunogenicity of cargos

Biodegradable materials, such as proteins (e.g. ovalbumin) and hydroxyethyl starch, can be crosslinked with 1,4-toluene diisocyanate (TDI) to form nanocarriers using the inverse miniemulsion method.^[157-158] Therefore, the shell material has to provide primary amine or alcohol groups to enable the crosslinking reaction. A disadvantage of this method is the unintentional crosslinking of cargos bearing nucleophilic end groups which can influence their bioactivity and lead to reduced efficacy. Furthermore, the irreversible crosslinking of antigens

may reduce their immunogenicity due to the destruction of epitopes preventing antigen recognition by T cells. Azide-modified proteins can further be crosslinked by metal-free azide-alkyne click reaction. Different studies demonstrated the efficient synthesis of nanocarriers using this method with activated hexanediol dipropiolate (HDDP) acting as crosslinker.^[156, 159] Shell density as well as capsule degradation and cargo release can be varied by using different amounts of crosslinker. Moreover, antigen immunogenicity can be maintained using this synthesis method since epitopes are not affected enabling antigen-specific activation of T cells and subsequent tumor cell killing. Further *in vivo* studies demonstrated an enhanced vaccination potency by combined encapsulation of TRP2-coding mRNA and PD-L1 siRNA into lipid-coated calcium phosphate NPs for the treatment of murine B16/F10 melanoma.^[160] The NP-induced knockdown of PD-L1 enhanced the antigen-specific antitumor immune response. Very recently, treatment of patients with advanced squamous cell carcinoma could also be improved by combining a neoantigen-based vaccine with anti-PD-1 antibodies in a clinical trial.^[161]

8. Combining nanovaccines with immune checkpoint therapy enhances anti-tumoral immune responses

After efficient antigen-specific priming, CD8⁺ T cells proliferate, migrate and infiltrate the TME.^[162] This effector phase is directed by cytokines and chemokines and results in the recognition of tumor antigens and cancer cell killing. Subsequent release of further tumor antigens by destroyed cells leads to an increased breadth and depth of the anti-tumoral immune response due to APC-mediated activation of different immune cells.^[163] Nevertheless, T cell activity can be inhibited by binding of immune checkpoints such as PD-1, CTLA-4, TIM-3 or LAG3 to their agonists which in turn are expressed by APCs and tumor cells.^[162] This tumor cell-induced inhibition of T cells often reduces the effectiveness of immunotherapies. For this reason, immune checkpoint-blocking antibodies were developed. Treatment of patients with anti-PD-1 antibodies alone or in combination with anti-CTLA-4 antibodies led to a significantly reduced tumor growth and a prolonged overall survival.^[164]

To enhance the efficacy of nanovaccines, different combination studies with immune checkpoint inhibitors (ICI) were performed. Liu *et al.* combined aerosolized nanoparticles (NPs) containing cyclic dinucleotides with anti-PD-L1 antibodies for the treatment of murine non-small cell lung cancer.^[165] This combination therapy not only induced robust CD8⁺ T cell activation through STING stimulation but also reduced T cell inhibition by PD-L1 blockade. Furthermore, a reprogramming of anti-inflammatory macrophages to pro-inflammatory macrophages was induced indicating an anti-tumorigenic phenotype. Another pre-clinical study demonstrated enhanced anti-tumoral immune responses by combining platinum

complex-loaded PC7A-NPs with immune checkpoint blockade.^[166] Nanoparticles released the encapsulated platinum complex pH-dependently in the tumor microenvironment and C7A monomers subsequently acted as adjuvant. By combining this nanovaccine with ICI, CT26 colon tumor growth was strongly inhibited. Similar results were obtained by co-encapsulating the chemotherapeutic drugs paclitaxel and chloroquine with the antigen ovalbumin, the adjuvant CpG ODN as well as anti-PD-L1 antibodies into polymeric nanoparticles.^[167] This combination therapy was efficiently tested in pre-clinical tumor models and induced a long-term immune memory against the encapsulated antigen.

9. Summary and future perspectives

Immunotherapies aim to activate the immune system in a tumor-specific manner and thereby overcome the immunosuppressive features of the tumor microenvironment. Various approaches for preventive and therapeutic vaccination have been tested pre-clinically and in the clinic. Nevertheless, many therapeutic approaches do not achieve complete or long-term tumor remission. Encapsulation of adjuvants, antigens, chemotherapeutic drugs and immune checkpoint inhibitors enhances the activation of dendritic cells. In particular, stimulation of dendritic cells can be achieved by simultaneous delivery of encapsulated antigens and adjuvants, resulting in improved T cell activation. In the future, the combination of nanovaccines and immune checkpoint blockade will provide extensive potential to address the immune system in different ways. In addition, nanocarrier-based vaccine formulations offer the opportunity to personalize cancer therapy by encapsulation of pre-screened neoantigens. Encapsulation of patient-specific tumor peptides or mRNA coding for those peptides is a promising approach to efficiently treat cancer patients and to achieve prolonged overall survival. The functionalization of NP surfaces also offers an opportunity for more specific targeting of antigen-presenting cells such as DCs. Not only mannose functionalization or conjugation of receptor-specific antibodies onto NP surfaces, but also coupling of nanobodies to nanoparticulate carrier systems can be used for this purpose. Since nanoparticles are versatile and modifiable, it will be of particular interest in the future to combine all the knowledge gained so far, so that antigens, adjuvants, ICI and cell targeting are combined in one NP-based vaccine subsequently influencing various mechanisms of the immune system. In addition, the establishment of various NP classes also enables needle-free administration (e.g. oral or intranasal administration), which will also bring advantages in the future, for example, in the vaccination of children or patients with needle phobia. Challenging is in particular the upscaling of different particle formulations. NPs such as micelles, polymer-based NPs and solid lipid NPs are suitable for large-scale production due to their physico-chemical properties, ease of production and stability.^[168-169] However, batch-to-batch variability, sterile

production, and the provision and cleaning of suitable equipment are the main challenges faced by the industry in the future.^[170-171] Additionally, controlling particle size and shape is not possible with every synthesis method used in laboratories for larger-scale approaches.^[171] Nevertheless, methods such as high-pressure homogenization (HPH), hot melt extrusion in combination with HPH, microemulsion techniques, nanoprecipitation, and microchannels enable synthesizing NPs on a large scale.^[169]

Chapter A

Chapter A is a nearly word-to-word reproduction of the publication “*Multicomponent Encapsulation into Fully Degradable Protein Nanocarriers via Interfacial Azide-Alkyne Click Reaction in Miniemulsion Allows the Co-Delivery of Immunotherapeutics*” published in the peer-reviewed journal *Nanoscale Horizons* (2022).

Contribution

Natkritta Hüppe is the main author of this chapter. She synthesized and characterized the protein nanocarriers as well as the azide-transfer agent and crosslinker involved as stated in the experimental part. The surfactant poly((ethylene/butylene)-*block*-(ethylene oxide)) was synthesized by Sabrina Brand. ICP spectroscopy was performed by Michael Steiert, MALDI-TOF was performed by Stephan Türk and horse radish peroxidase activity assay was performed by Marina Machtakova. Natkritta Hüppe performed all degradation and release experiments as well as the analytical and quantification measurements for the degradation and release experiments. Lucas Caire da Silva and Mazarine Houbrechts performed the encapsulation of protein nanocarriers into polymeric vesicles and the degradation experiments. She performed the quantification of resiquimod and muramyl dipeptide. For quantification of polyinosinic:polycytidylic acid, Natkritta Hüppe performed the degradation and release of Poly(I:C) from the protein nanocarrier and the released amount was measured by Beate Müller with HPLC. All electron microscopy measurements were performed by Gunnar Glasser (SEM) and Christoph Sieber (TEM). Sample preparation for SEM was performed by Natkritta Hüppe. Jenny Schunke performed *in vitro* cell culture assays with the adjuvant-loaded protein nanocarriers as well as uptake analyses with fluorescence microscopy.

Multicomponent Encapsulation into Fully Degradable Protein Nanocarriers *via* Interfacial Azide-Alkyne Click Reaction in Miniemulsion Allows the Co-Delivery of Immunotherapeutics

Natkritta Hüppe^a, Jenny Schunke^b, Michael Fichter^{a,b}, Volker Mailänder^{a,b}, Frederik R. Wurm^{a,c*}, Katharina Landfester^{a*}

^a Max Planck Institute for Polymer Research, Ackermannweg 10, 55128 Mainz, Germany

^b Department of Dermatology, University Medical Center Mainz, Langenbeckstraße 1, 55131 Mainz, Germany

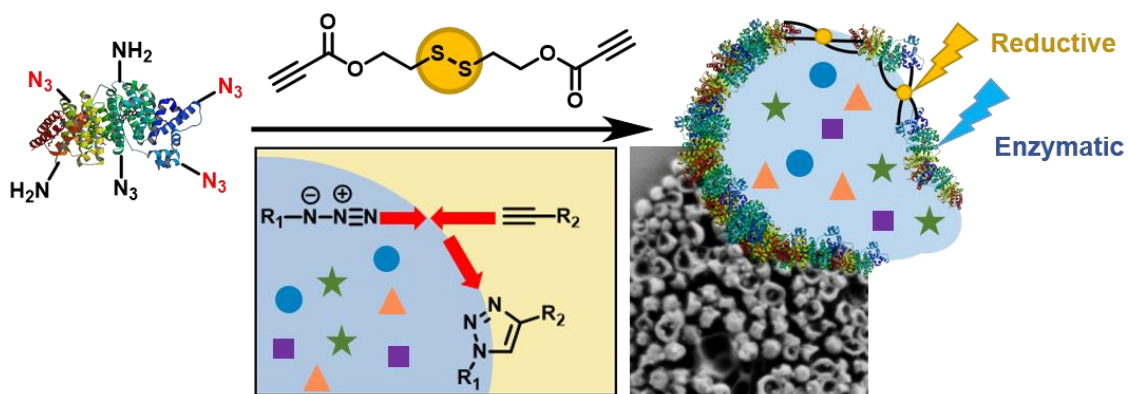
^c Sustainable Polymer Chemistry, Department of Molecules and Materials, Faculty of Science and Technology, MESA+ Institute for Nanotechnology, University of Twente, Drienerlolaan 5, 7522 NB Enschede, The Netherlands

Abstract

Encapsulation of multiple adjuvants along with antigens into nanocarriers allows a co-delivery to antigen-presenting cells for the synergistic induction of robust immune responses. However, loading cargo of different molar mass, polarity, and solubility in high efficiencies remain a challenge. Therefore, we developed a strategy to encapsulate a triple combination of the so-called adjuvants, i.e. with Resiquimod (R848), muramyl dipeptide (MDP) and polyinosinic:polycytidylic acid (Poly(I:C)) into human serum albumin (HSA) nanocarriers. The loading is conducted *in situ* while the nanocarrier is formed by an orthogonal and metal-free click reaction at the interface of an inverse miniemulsion. By this unique approach, high encapsulation efficiency without harming the cargo during the nanocarrier formation process and regardless of their physical properties is achieved, thus keeping their bioactivity. Furthermore, we demonstrated high control over the encapsulation efficiency and varying the amount of each cargo did not influence the efficiency of multicomponent encapsulation. Azide-modified HSA was crosslinked with hexanediol dipropiolate (HDDP) at the interface of a water-in-oil miniemulsion. Varying the crosslinker amount allowed us to tailor the density and degradation rates of the protein shell. Additional installation of disulfide bonds into the crosslinker created redox-responsive nanocarriers, which degraded both by protease and under reducing conditions with dithiothreitol. The prepared HSA nanocarrier were efficiently taken up by dendritic cells and exhibited an additive cell activation and maturation, exceeding

the nanocarriers loaded with only a single drug. This general protocol allows the orthogonal and metal-free encapsulation of various drugs or adjuvants at defined concentrations into the protein nanocarriers.

TOC



Keywords: *Co-delivery, drug delivery, nanomedicine, click chemistry, nanocarrier, vaccine*

Introduction

Biochemical processes in the body rely on a complex interplay of multiple components. If medical therapy aims to mimic or enhance those processes, multiple therapeutic components have to be integrated into one system. For example, in immunotherapy, the biggest challenge is the exhaustion of immune cells due to the immunosuppressive tumor microenvironment.^[172-174] Hence, effective tumor treatment relies on the induction of a strong and durable immune response. Monotherapy proved to be insufficient to overcome these challenges and efforts have to be made to realize a combinatorial treatment with multiple components.^[175-176] True to the motto “The more the merrier”, a combination of multiple components enables additive effects for enhanced treatment efficacy. In vaccination approaches, a combination of multiple adjuvants yields a synergistic effect in dendritic cell-directed T cell stimulation, increasing the vaccination effect.^[148, 177-179]

The key to success is an efficient process for multicomponent encapsulation of cargoes with different physicochemical properties such as molar mass, polarity, and solubility.

Common methods to prepare protein nanocarriers include desolvation, self-assembly or gelation. For example, Abraxane® is a nanoparticle based on albumin-bound paclitaxel, which is commercially used in cancer therapy. Paclitaxel is entrapped into the albumin nanoparticle during the albumin aggregation by a desolvation process. Although efficient entrapment of drugs can be achieved with those methods, there is a lack of control when multiple drugs

should be encapsulated simultaneously into one nanocarrier. Especially when the cargo molecules have different physicochemical properties, such as solubility, controlled and efficient encapsulation of all components is challenging with methods relying on random entrapment.

To design the optimal nanocarrier, several requirements are necessary: 1. simultaneous encapsulation of multiple cargoes, 2. selective reaction for the shell formation without harming the cargo, 3. dense carriers for the transport in the body, and 4. degradation of the carriers at the target site. Combining all requirements in one process proved to be challenging. Our developed process combines all four requirements and enables controlled and efficient multicomponent encapsulation into fully degradable protein nanocarriers (PNCs) *via* azide-alkyne click reaction in inverse miniemulsion.

For the first requirement, an inverse miniemulsion allows the simultaneous encapsulation of different water-soluble cargo molecules into nanocarriers with a defined concentration.^[180] In an inverse miniemulsion, the shell material is crosslinked at the interface of the water-droplets *via* an oil-soluble crosslinker, forming a nanocarrier with a liquid core. The water-soluble cargo molecules are encapsulated inside the nanocarriers during the interfacial shell formation. For the second requirement, click reactions enable selective linkage between shell material and crosslinker without involving the cargo in the shell formation reaction.^[181-182] Previously, protein nanocarriers were prepared by UV-initiated photoclick tetrazole-ene reaction in inverse miniemulsion.^[183] However, UV-light or other harsh initiators, such as metals,^[184] can destroy sensitive cargoes leading to loss of bioactivity. A crosslinker such as hexanediol dipropiolate (HDDP) with an activated alkyne reacts without a catalyst in an azide-alkyne click reaction.^[159, 185] The amount of crosslinker influences the number of links between the shell material and might control the density of the nanocarrier shell for the third requirement. The last requirement is a degradable shell material ensuring the release of the cargo from nanocarriers. Proteins have been widely used as nanocarrier materials, because of their natural biocompatibility and degradability.^[183, 186-188]

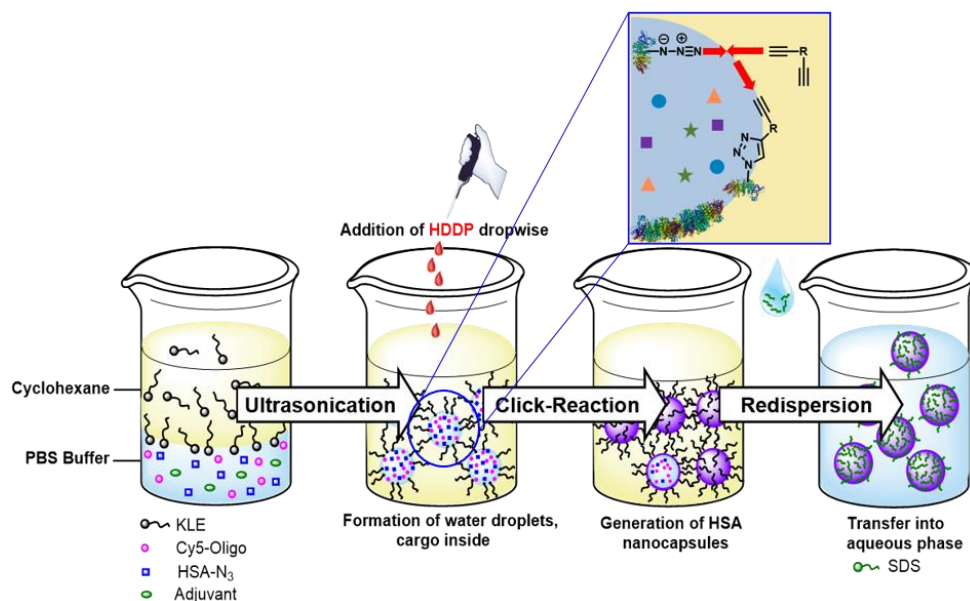


Figure 1. Multicomponent encapsulation into protein nanocarriers through interfacial azide-alkyne crosslinking in inverse miniemulsion

Results and Discussion

For the azide-alkyne click reaction, human serum albumin (HSA) was functionalized at the lysine residue by a metal-free transfer reaction into azide groups using 1-imidazol azide hydrochloride.^[189] After functionalization, the fluorescamine assay showed that about 19-24 amines of the 59 lysine residues per HSA (30-35 accessible lysines) were transformed into azides. The degree of functionalization changed with pH value as lower pH values led to lower nucleophilicity of the amine and less transfer reactions, whereas pH 9.5 gave an optimal balance between yielding high number of transfers and maintaining the protein structure (Table S1). A comparison of the IR spectra of natural and azide-modified HSA showed successful modification as demonstrated by the presence of the characteristic azide signal at 2100 cm^{-1} (Figure 2A). Furthermore, no significant changes in the secondary structure of the protein were observed by CD spectroscopy (Figure S6). Therefore, the modified protein remained highly water-soluble ($> 100\text{ mg/mL}$) further highlighting the mild conditions during the transfer reaction. When the “azidation” was conducted with the horseradish peroxidase (HRP) (Table S2, S17) the enzymatic activity was reduced by 40%, probably due to the high basic pH of 11 during the transfer reaction (Figure S19).

For the formation of protein nanocarriers by azide-alkyne click reaction, we chose the dialkyne hexanediol dipropiolate (HDDP) as a crosslinker of the azide-modified proteins. The carbonyl group located next to the alkyne moiety activates the alkyne by an inductive effect, allowing a click reaction without using a metal catalyst.^[185] Moreover, inserting a disulfide bond into the

chemical structure of HDDP (i.e. to HDDP-SS, cf. Figure 2) created a crosslinker prone to degradation by a reducing agent.^[159]

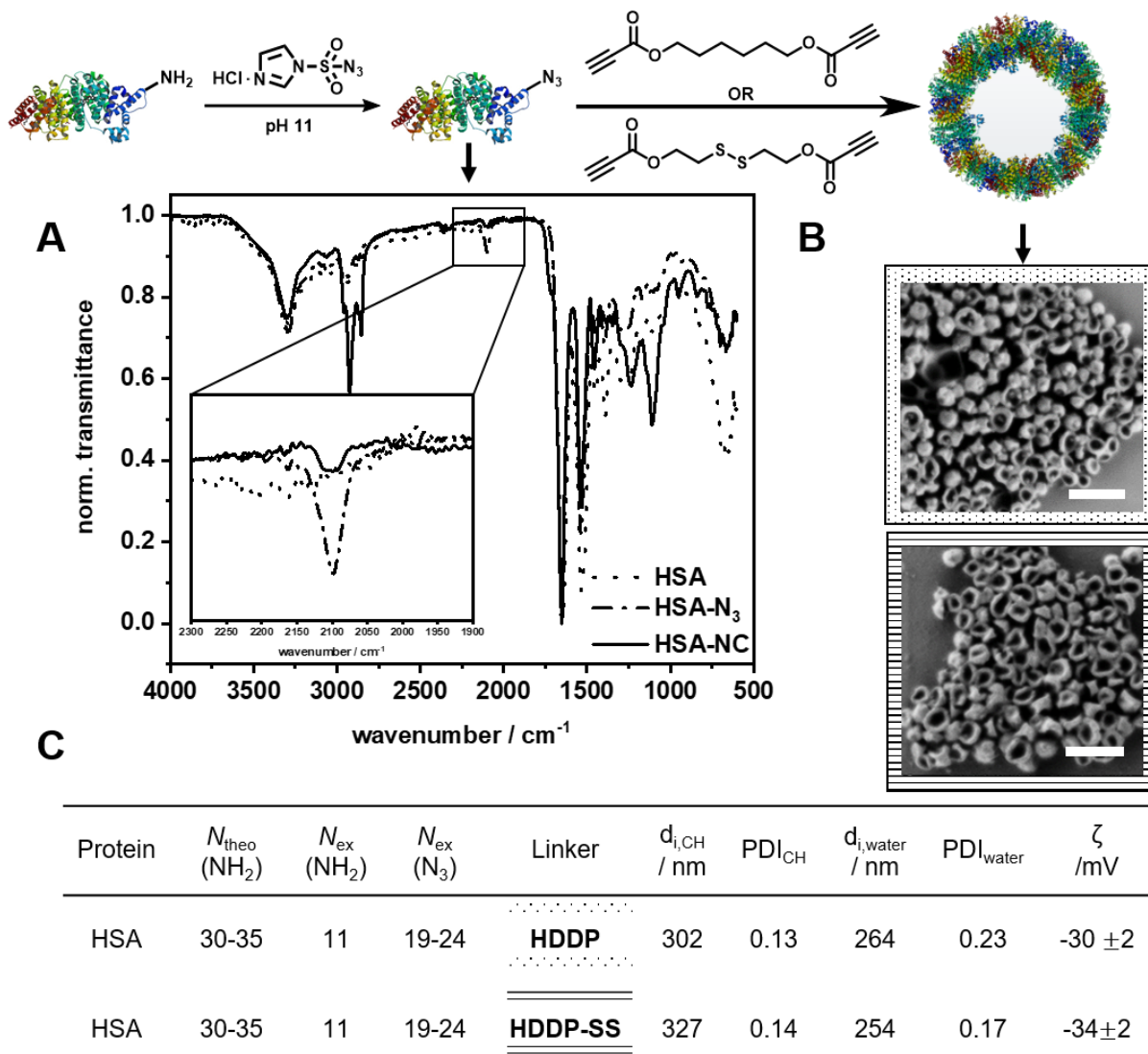


Figure 2. Reaction scheme for the formation of protein nanocarriers through azide-alkyne click reaction (top). A) IR spectra of native (···), azide-functionalized (- - -) and human serum albumin nanocarriers (—). B) SEM images of HSA-NCs using a HDDP (□) and HDDP-SS (□) ratio (Scale bar: 0.5 μm). C) Analytic data of HSA-NCs using HDDP and HDDP-SS.

The PNCs were prepared in an inverse water-in-oil miniemulsion with cyclohexane as the continuous and an aqueous buffer as the dispersed phase (Scheme S2). The aqueous nanodroplets were prepared with high shear forces using ultrasonication and were stabilized by the surfactant P((E/B)-*b*-EO) (KLE).^[190] The protein shell formed through an interfacial crosslinking by click reaction at the water droplet interface after addition of HDDP or HDDP-SS to the inverse miniemulsion. In the IR spectra of the PNCs, the azide signal at 2100 cm^{-1}

decreased due to the formation of the triazol during the click reaction (Figure 2A). The hydrodynamic diameters of the PNCs (d_h) in cyclohexane were determined to be approx. 300 nm by dynamic light scattering (DLS). After redispersion in water using sodium dodecyl sulfate (SDS, 0.02 mM) as the surfactant followed by washing, the diameters decreased to approx. 250 nm with a zeta potential of approx. -30 mV (Figure 2C, Table S4). Scanning electron micrographs and transmission electron micrographs revealed a core-shell morphology of the PNCs (Figures 2B and S8). In addition, the PNCs based on HRP exhibited similar results in size and morphology (Figure S17, S18). This demonstrated the excellent reproducibility and transferability for forming PNCs by the developed protocol. Moreover, the HRP nanocarriers were still enzymatically active, showing approx. 60% of the native enzyme activity (Figure S19).

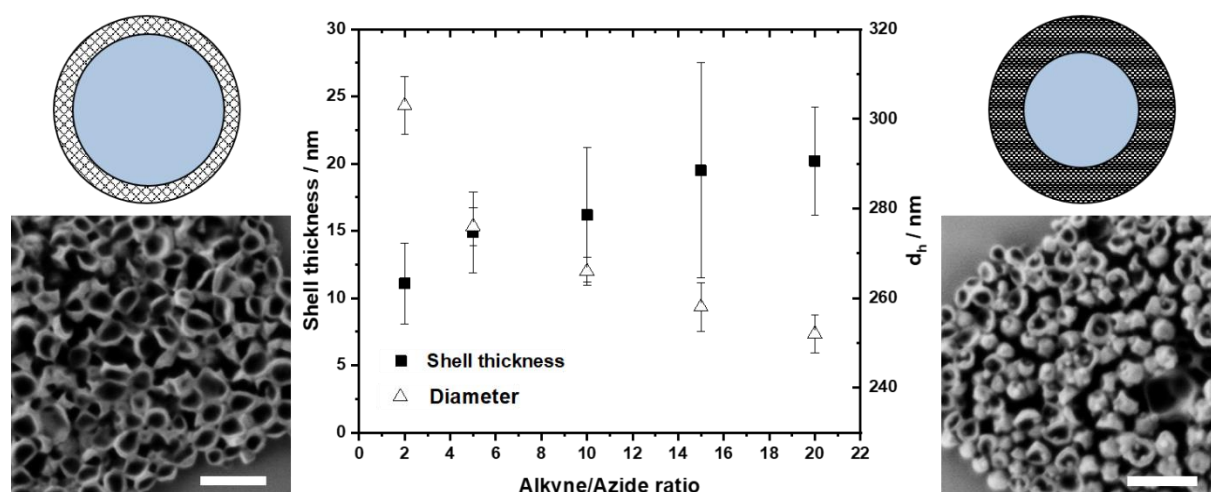


Figure 3. Influence of alkyne:azide ratio on the shell thickness (■) and diameter (△) of protein nanocarriers. Scanning electron micrographs of HSA nanocarriers using a 2:1 (left) and 20:1 (right) ratio (Scale bar: 0.5 μm).

By varying the amount of HDDP crosslinker, shell thickness and size of PNCs could be controlled (Figure 3). When the interfacial crosslinking of azide-modified protein with HDDP was performed with an alkyne:azide ratio of 20:1, PNCs with a $d_h = 250$ nm and approx. 20 nm shell thickness were obtained. With a lower alkyne:azide ratio, the shell thickness decreased, while the diameters increased, probably due to an increased swelling of the softer protein shell (Figure 3). The amount of crosslinker used additionally influenced the encapsulation efficiency after water transfer. The encapsulation efficiency of dextran-sulforhodamine B ($M = 10$ kDa) decreased from 62% to 39% when 20 eq. HDDP or only 2 eq. HDDP were used, respectively, to prepare the PNCs. By encapsulating the low molecular weight dye sulforhodamine-101 ($M = 606.71$ g/mol), a lower crosslinking density was detected, leading to a faster diffusion

through the nanocarrier shell, probably attributed to the thinner and looser shell walls when low amounts of HDDP were used (Figure S12).

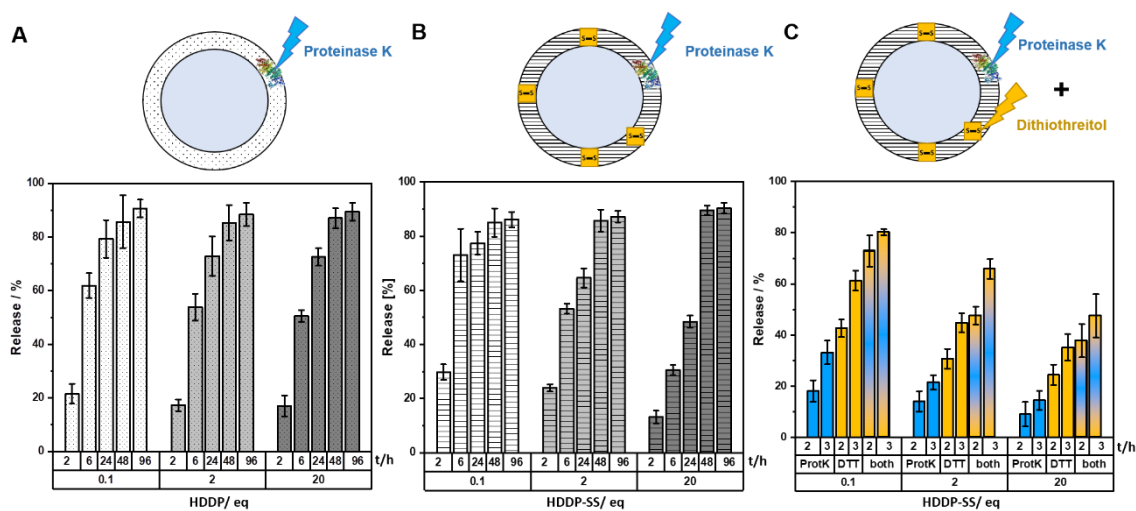


Figure 4. Release kinetics of dextran-rhodamine B (10 kDa) from HSA-NCs prepared with different crosslinking densities as indicated by the ratio of HDDP or HDDP-SS / eq.: A) PNCs crosslinked with HDDP and degraded with proteinase K (5 U/mL), B) PNCs crosslinked with HDDP-SS and degraded with proteinase K (5 U/mL), C) PNCs crosslinked with HDDP-SS and degraded with proteinase K (blue, 5 U/mL) and dithiothreitol (yellow, 3 mM).

The degradation of the PNCs was investigated by monitoring the release of dextran-rhodamine B ($M = 10$ kDa, $\lambda_{em} = 570$ nm) under different conditions. Crosslinking with different amounts of HDDP or HDDP-SS enabled investigating the influence of shell density on the degradation kinetics. The HSA-NCs degraded upon the addition of proteinase K (5 U/mL) and the amount of released dye was detected in the aqueous supernatant. Depending on the time of the degradation experiment, the amount of released dye increased and reached a plateau of approx. 90% dye after 96 h in all cases (Figure 4A). However, the crosslinking density, i.e. the amount of HDDP used during the PNC formation, influenced the degradation rate of the protein shell and thus the release of the dye. Time and crosslinker dependence of dye-release was also observed for the enzymatic degradation of PNCs crosslinked with HDDP-SS (Figure 4B). The HSA-HDDP-SS NCs could be cleaved by proteinase K as well as under reducing conditions, e.g. by adding dithiothreitol (DTT) as a reducing agent. The PNCs crosslinked with different amounts of HDDP-SS were treated with proteinase K (2 U/mL) and DTT (3 mM), respectively, and in combination, and the amount of released dextran-rhodamine B was measured over time, indicating the release kinetics were influenced by the crosslinking degree. The resulting PNCs crosslinked with HDDP-SS obtained the property of dual-degradation by DTT and proteinase K.

The degradation of the PNCs was also visible by the naked eye, as the turbid PNCs dispersion completely cleared up upon DTT addition (Figure S15). DLS was applied to further quantify the degradation rates of PNCs: Following treatment with proteinase K and DTT, respectively, the size of the NCs decreased significantly from 254 nm to 71 nm with a broadening of the polydispersity index to > 0.4 (Figures S13 and 14). Additionally, the derived count rate (DCR) decreased significantly during the degradation experiment, indicating the formation of smaller fragments with lower scattering intensity. The derived count rate was monitored upon DTT treatment and continuously decreased to the lower limit of the DLS apparatus indicating an almost complete degradation of the PNCs (Figure S15).

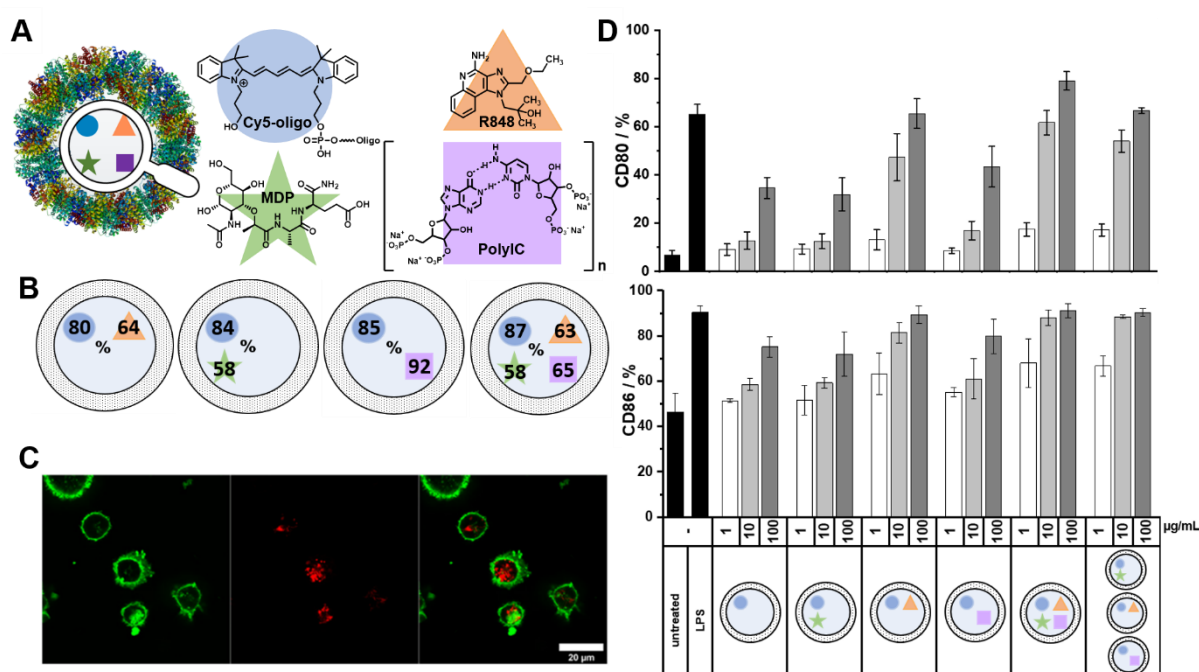


Figure 5. A) Chemical structures of Cy5-oligo dye (●) and adjuvants R848 (▲), MDP (★) and Poly(I:C) (■) encapsulated into HSA-NCs. B) Encapsulation efficiency of cargoes in different combinations into HSA-NCs crosslinked with HDDP in percent. C) Confocal laser scanning microscopy images of bonemarrow-derived dendritic cells (green) and ingested HSA-NCs (red). D) Upregulation of DC maturation markers CD80 and CD86 after stimulation with adjuvant-loaded HSA-NCs with either single loading, triple loading or a mixture of single-loaded NCs. BMDCs (2×10^5 cells/mL) were incubated with differently loaded HSA-NC formulations (1–100 μg/mL) or lipopolysaccharid (LPS) (100 ng/mL) as a positive control for 24 h. Surface expression of CD80 and CD86 of PNC-treated BMDCs was measured by flow cytometry.

Since anti-tumor vaccination still lacks the effective response of immune cells against tumors in most cases of vaccinated patients, the role of nanocarriers for co-delivery of vaccine components needs to step into focus. In the vaccination process, the vaccine, consisting of antigen and adjuvants, is taken up by dendritic cells and the antigens are presented on major histocompatibility complex (MHC) molecules of the DCs to the T cells.^[191-192] Subsequently,

antigen-specific T cells are activated and proliferate to attack cells bearing the tumor-specific antigen eventually leading to tumor cell killing.^[193] Crucial for the success of T cell priming is a strong activation of antigen-presenting cells (e.g. DCs) by adjuvants inducing expression of costimulatory molecules and the release of activating pro-inflammatory cytokines. Choosing the correct type and application route of adjuvants is of great importance for the induction of robust immune responses as each adjuvant binds to distinct receptors triggering different signaling pathways in antigen-presenting cells.^[79, 194] Therefore, a combination of several different adjuvants simultaneously stimulates different receptors, leading to an additive DC activation.^[195] To achieve a high local concentration of adjuvants in one DC, all components must be delivered simultaneously.^[187]

Resiquimod (R848) is a small molecule ($M = 350.8$ g/mol) with low water-solubility (> 1 mg/mL) and acts as an agonist for the toll-like receptors (TLR) 7 and 8.^[85] The water-soluble peptidoglycan muramyl dipeptide (MDP; $M = 492.5$ g/mol) has been shown to be recognized by nucleotide-binding oligomerization domain-containing protein (NOD) 2.^[196] The double-stranded RNA mimic polyinosinic:cytidylic acid (Poly(I:C); 0.2-1 kb) acts as a TLR 3 ligand.^[197] A major challenge is to find a compatible protocol for the multicomponent encapsulation of cargoes with such different properties in terms of solubility and molecular weight. In this study, we combined R848, MDP, and Poly(I:C) and added Cy5-Oligo (5 kDa) as an additional cargo acting as a fluorescent dye (Figure 5A), allowing us to investigate the cellular uptake of PNCs by DCs. All four components were successfully encapsulated into PNCs through the azide-alkyne click reaction in inverse miniemulsion demonstrating the excellent feasibility of developed nanocarrier formation for the encapsulation of multiple components. Even though dimethylsulfoxid (DMSO) was used as a solvent for R848 (14 vol.-% in the disperse phase), stable droplets could be formed with no influence on the interfacial protein shell formation. With such different cargoes, each one needed a specific quantification assay to calculate their EE into the PNCs. The UV-active cargoes, Cy5-Oligo and R848, were quantified through UV/Vis measurements using a standard calibration (Figures S10 and 20). Due to the *N*-acetylglucosamide moiety present within the MDP, a quantification by a modified Morgan-Elson Reaction assay, which was devised for this study, was performed (Figure S21). HPLC was used for the quantification of Poly(I:C) (Figure S22). The PNCs were degraded by proteinase K (30 U/mL, 24 h, 37 °C), filtered, and the amount of each cargo was measured in the supernatant. Comparable EEs were obtained for the small molecules R848, and MDP (up to 65%) and Cy5-Oligo (over 80%) independent from cargo-loading (Figure 5B). Only the EE of the high molecular weight Poly(I:C) decreased significantly from approx. 90% for single-loaded PNCs to approx. 60% for multiple-loaded PNCs. Table S4 summarizes the encapsulation efficiencies and the characterization data for all HSA-NCs prepared herein: In all cases, similar

zeta potentials between -30 and -40 mV were determined, indicating a similar shell formation regardless of the cargo molecule or its charge, i.e. an efficient encapsulation inside of the NCs was achieved. The diameters for all “clicked” NCs were similar and detected between 200-300 nm (after redispersion in water, measured by DLS). To show control over the simultaneous encapsulation of multiple cargo molecules into the crosslinked protein nanocapsules, we varied the amount of each adjuvant and ratios between payloads and quantified the encapsulation efficiency (Table S4). For MDP and Poly(I:C) no significant difference in encapsulation efficiency could be observed when varying their amount, independent if MDP and Poly(I:C) were encapsulated alone or in the triple combination. Only in one case, the encapsulation efficiency of the different cargo molecules were affected. When a high amount of R848 was used, the encapsulation efficiency of all payloads decreased significantly. This could be a result of higher concentration of DMSO in the dispersed phase, which influences the solubility of the payloads in the droplet and thus the encapsulation efficiency. Nevertheless, if the amount of DMSO is kept to a minimum, our developed approach demonstrated high control over the encapsulation efficiency of the multiple payloads and thus control over the concentration and ratios of payload inside the capsules.

Flow cytometric and confocal laser scanning analyses revealed an efficient uptake of the adjuvant-loaded PNCs by the bone marrow-derived dendritic cells (BMDC) *in vitro*, as detected through the fluorescence of Cy5 (Figure 5C + S22). The co-delivery of the adjuvant combination by PNCs was evaluated by the amount of cell surface-expressed activation markers CD80 and CD86 on the BMDCs after incubation with PNCs for 24 h (Figure 5C). Untreated cells served as a negative control whereas cells treated with lipopolysaccharide (LPS), a potent TLR4 agonist inducing high expression of DC maturation, served as a positive control. The expression of CD80 and CD86 increased after treatment with adjuvant-loaded PNCs compared to untreated cells or cells treated with empty PNCs. Among the single-loaded PNCs with either R848, MDP or Poly(I:C), the TLR7/8 ligand R848 yielded the highest stimulation of BMDCs. The expression of the surface markers increased with PNCs loaded with the triple-combination of adjuvants compared to single-loaded PNCs. Moreover, a mixture of single-loaded PNCs with R848, MDP and Poly(I:C), respectively, exhibited a lower expression of surface markers compared to equimolar amounts of all three adjuvants encapsulated into one PNC demonstrating a higher stimulation through co-delivery.

The *in vitro* results underline the importance of simultaneous delivery of cargoes by multicomponent encapsulation into nanocarrier to achieve higher effectivity in nanocarrier-based vaccination approaches. With our developed protein nanocarrier combining all the

nanocarrier design requirements, we could encapsulate and co-deliver multiple components independently of molecular weight (low-high), solubility, or material (also inorganic).

Conclusion

We developed a bioorthogonal protocol for the multicomponent encapsulation and co-delivery of fully-biodegradable protein nanocarriers. For the synthesis of the PNCs, we applied a metal-free protocol to modify the protein's amine groups to azide groups with 1-sulfurylimidazol hydrochloride in water. With an azide-modified protein on hand, human serum albumin nanocarriers were prepared by metal-free azide-alkyne click reaction with activated hexanediol dipropiolate in an inverse miniemulsion. The developed process enabled the simultaneous encapsulation of multiple cargoes with different physicochemical properties such as molecular weights and solubility. A high encapsulation efficiency and a preserved bioactivity of the cargo was obtained. Comparable encapsulation efficiency of each adjuvant was achieved, independent of the amount and ratios of the cargo molecules. Varying the crosslinker amount not only allowed to tailor the density of the shell to entrap different adjuvants, but also the degradation and release rates of the nanocarriers. PNCs were further equipped with disulfide bonds by using HDDP-SS as the crosslinker, which resulted in nanocarriers releasing the cargo enzymatically and under reductive conditions. We demonstrated a successful encapsulation of the adjuvants R848, MDP, and Poly(I:C) into PNCs yielding a higher stimulation of immune cells with co-delivery of all three adjuvants encapsulated into one nanocarrier compared to single-loaded PNCs. In summary, this protocol might be used to develop efficient immunotherapies, which rely on the combination of several drugs and adjuvants with highly different physical properties. Further, the bioorthogonal formation of the nanocarriers with a guaranteed release upon proteolysis might be a powerful tool for the delivery of nucleic acids.

Acknowledgments

This work was funded by the DFG/SFB1066 ('Nanodimensional polymer therapeutics for tumor therapy'). We thank Gunnar Glasser and Christoph Sieber for electron microscopy, Stephan Türk for mass spectrometry, Michael Steiert for ICP-OES and Beate Müller for HPLC measurements. We want to acknowledge Katja Klein and Sabrina Brand for support in synthesis and Marina Machtakova for enzyme activity tests.

Supporting Information

Multicomponent Encapsulation into Fully Degradable Protein Nanocarriers *via* Interfacial Azide-Alkyne Click Reaction Allows the Co-Delivery of Immunotherapeutics

Natkritta Hüppe^a, Jenny Schunke^b, Michael Fichter^{a,b}, Volker Mailänder^{a,b}, Frederik R. Wurm^{a,c}, Katharina Landfester^{a*}*

^a Max Planck Institute for Polymer Research, Ackermannweg 10, 55128 Mainz, Germany.

^b Department of Dermatology, University Medical Center Mainz, Langenbeckstraße 1, 55131 Mainz, Germany

^c Sustainable Polymer Chemistry, Department of Molecules and Materials, Faculty of Science and Technology, MESA+ Institute for Nanotechnology, University of Twente, Drienerlolaan 5, 7522 NB Enschede, The Netherlands

Materials

All chemicals and materials were used as received. Human serum albumin (> 99% purity) was purchased from Sigma Aldrich as well as 1,6-hexanediol (99%), propiolic acid, sulfurylchloride and imidazole. Cyclohexane (HPLC grade) was purchased from VWR. Fluorescamine was purchased from Alfa Aesar. The block copolymer poly((ethylene-co-butylene)-*b*-(ethylene oxide)) P((E/B)-*b*-EO) used as the oil soluble surfactant was synthesized as described in literature and consists of a poly((ethylene-co-butylene) block (NMR: $M_n = 3900$ g/mol) and a poly(ethylene oxide) block (NMR: $M_n = 2700$ g/mol). The anionic surfactant sodium dodecyl sulfate (SDS) was purchased from Sigma Aldrich. Cy5-Oligo was purchased from IBA Lifesciences. Proteinase K from tritirachium album (≥ 30 units/mg) and peroxidase from horseradish (≥ 50 units/mg) was purchased from Sigma Aldrich. Resiquimod (R848), muramyl dipeptide (MDP) and polyinosinic:polycytidylic acid (Poly(I:C) LMW) was purchased from Invivogen. Amicon Ultra-2 centrifugal filter devices were purchased from Merck Millipore (100 kDa) nominal molecular weight limit (NMWL). The magnesium- and calcium- free phosphate-buffered saline, was purchased from Life Technologies. Demineralized water was used for all experiments.

Experiments

1. Synthesis of 1,6-hexandiol dipropiolate (HDDP)

The dialkyne crosslinker was synthesized by esterification following the literature. Briefly, hexandiole (4 g, 33.85 mmol), propiolic acid (9.48 g, 135.39 mmol) and *p*-TsOH (333.33 mg, 5 mol%) were dissolved in 120 mL toluene and stirred at 135 °C under reflux for 3 days using a dean-stark apparatus. Afterwards, the reaction solution was washed twice with 100 mL saturated NaHCO₃ solution and twice with 100 mL water. The solvent was removed and the product purified by column chromatography (PE:EtOAc 10:1). The product was obtained as colorless crystals. Yield: 3.37 g, 45%.

¹H NMR (300 MHz, CD₂Cl₂) δ 4.10 (t, 4H, O-CH₂), 2.87 (s, 2H, HC≡C), 1.61 (m, 4H, CH₂-CH₂-O), 1.32 (m, 4H, CH₂-CH₂-CH₂) ppm. ¹³C NMR (300 MHz, CD₂Cl₂) δ 153, 74.6, 66.6, 28.5, 25.8 ppm.

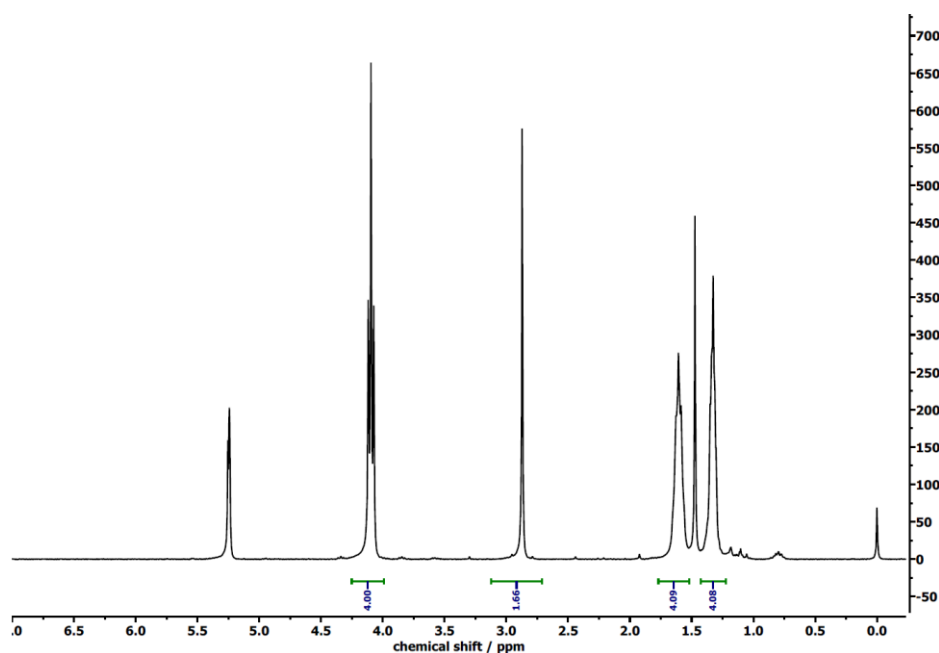


Figure S1. ¹H NMR spectrum of 1,6-hexandiol dipropiolate in CD₂Cl₂.

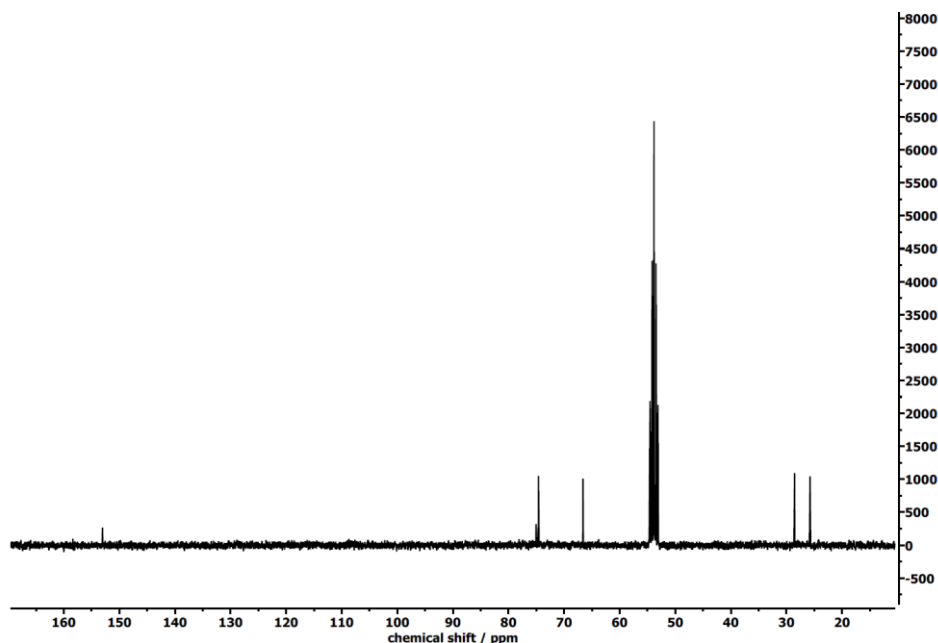


Figure S2. ^{13}C NMR spectrum of 1,6-hexandiol dipropiolate in CD_2Cl_2 .

2. Synthesis of disulfide 1,6-hexanediol dipropiolate (HDDP-SS)

The dialkyne crosslinker was synthesized by esterification following the literature. Briefly, bis(2-hydroxyethyl) disulfide (3.0 g, 19.5 mmol), propiolic acid (5.4 g, 78.0 mmol) and *p*-TsOH (360 mg, 2 mmol) were dissolved in 150 mL benzene and stirred under reflux for 3 days using a dean-stark apparatus. Afterwards, 100 mL saturated NaHCO_3 solution was added to the reaction solution and the organic phase separated. The aqueous phase was washed twice with 100 mL diethylether. The organic phases are combined and dried over Na_2SO_4 . The solvent was removed and the product purified by column chromatography (n-hexane:EtOAc = 3:1). The product was obtained as colorless crystals. Yield: 2.3 g, 46%.

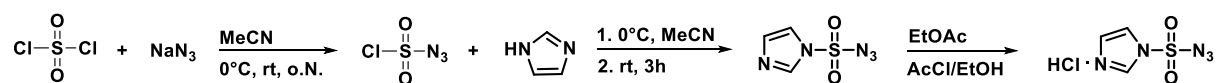
^1H NMR (300 MHz, CDCl_3) δ 4.41 (t, 4H, O- CH_2), 2.96-2.92 (m, 6H, S- CH_2 and $\text{HC}\equiv\text{C}$) ppm.

^{13}C NMR (300 MHz, CD_2Cl_2) δ 152.3, 75.5, 74.3, 74.3, 63.9, 36.7 ppm.

3. Synthesis of 1-imidazole-sulfonyl azide hydrochloride

The azide transfer agent was synthesized according to Goddard-Borger *et al.*^[198] Briefly, sodium azide (1.63 g, 25 mmol) was suspended in 25 mL MeCN and cooled down to 0 °C. Under vigorous stirring sulfonylchloride (3.34 g, 25 mmol) was added dropwise. The reaction solution was slowly brought to room temperature and the reaction carried out at room temperature overnight. Again, the reaction solution is cooled down to 0 °C and imidazole (3.23 g, 47.5 mmol) added in small portions. The reaction is stirred at room temperature for 3 h. Afterwards, 50 mL EtOAc is added and the reaction solution is washed twice with 50 mL saturated NaHCO_3 solution and twice with 50 mL water. The organic phase is dried over

MgSO₄ and filtered. A mixture of AcCl/EtOH is slowly added to the reaction solution at 0 °C. The product is filtered, washed with EtOAc and dried. Yield: 3.13 g.



¹H NMR (300 MHz, D₂O) δ 7.44 (dd, 1H, N-CH=CH), 7.85 (dd, 1H, HC=CH-N), 9.17 (dd, 1H, N=CH-N) ppm. ¹³C NMR (300 MHz, CD₂Cl₂) δ 152.3, 75.5, 74.3, 74.3, 63.9, 36.7 ppm.

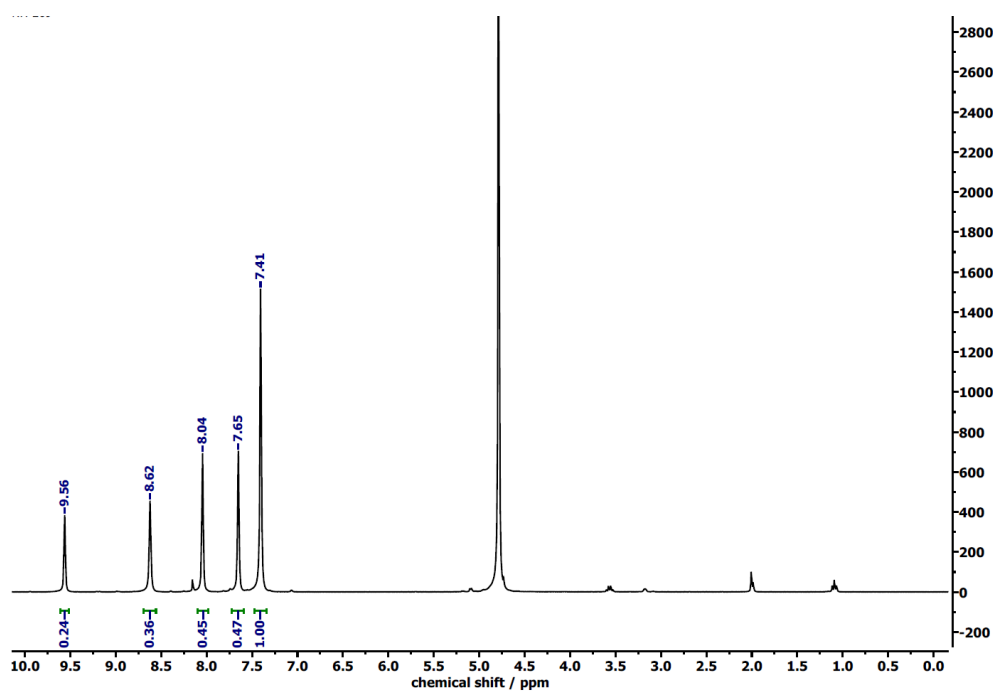


Figure S3. ¹H NMR spectrum of 1-imidazole-sulfonyl azide hydrochloride in D₂O.

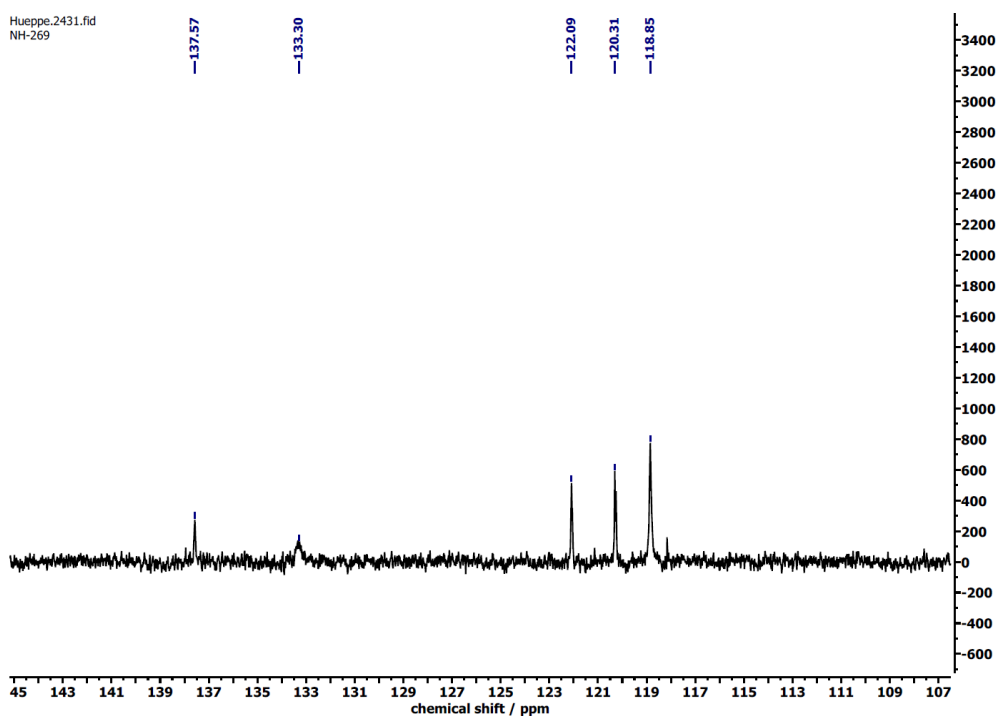


Figure S4. ^{13}C NMR spectrum of 1-imidazole-sulfonyl azide hydrochloride in D_2O .

4. Azidation of proteins with 1-imidazole-sulfonyl azide hydrochloride

The protein (1g) was dissolved in 20 mL K_2CO_3 solution of pH 11. The azide transfer agent (276 mg) was dissolved in 2 mL water and added dropwise to the protein solution. The pH value of the reaction solution was adjusted to pH 11 with 1 M NaOH. The reaction solution was stirred at room temperature for 48 h. The product was purified by dialysis (MWCO 1K) and lyophilized. Yield: 0.93 g. The amount of azide moieties was determined using the fluorescamine assay.

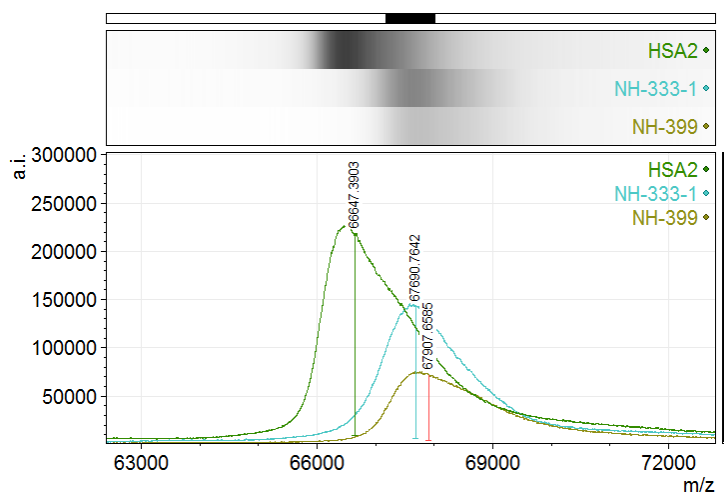


Figure S5. MALDI-TOF of human serum albumin (HSA, green), HSA- N_3 via copper-catalyzed azide-functionalization (blue) and BSA- N_3 via copper-free azide-functionalization.

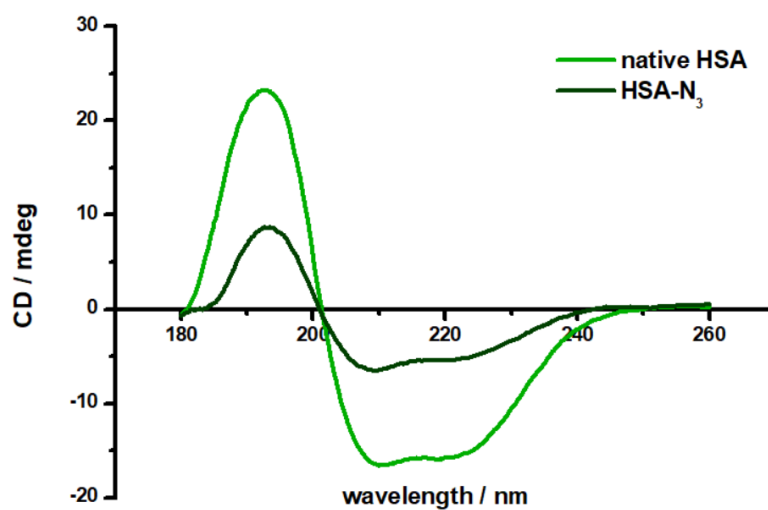
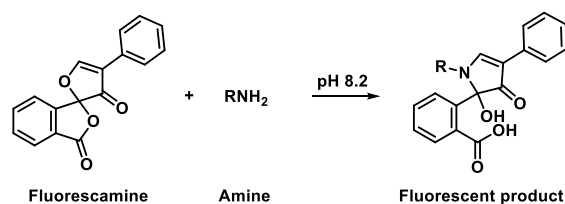


Figure S6. Circular dichroism (CD) spectra of native human serum albumin (HSA) and azide-functionalized HSA.

5. Fluorescamine assay

The quantitative amount of azide groups was determined with the fluorescamine assay in borate buffer at pH 8.2.



Scheme S1. Reaction of fluorescamine with amines to a fluorescent product at pH 8.2.

Glycine was used for the standard calibration curve and lysozyme was used as a reference. A decreased amount of amine groups was determined for the protein after azide-functionalization, indicating a successful reaction.

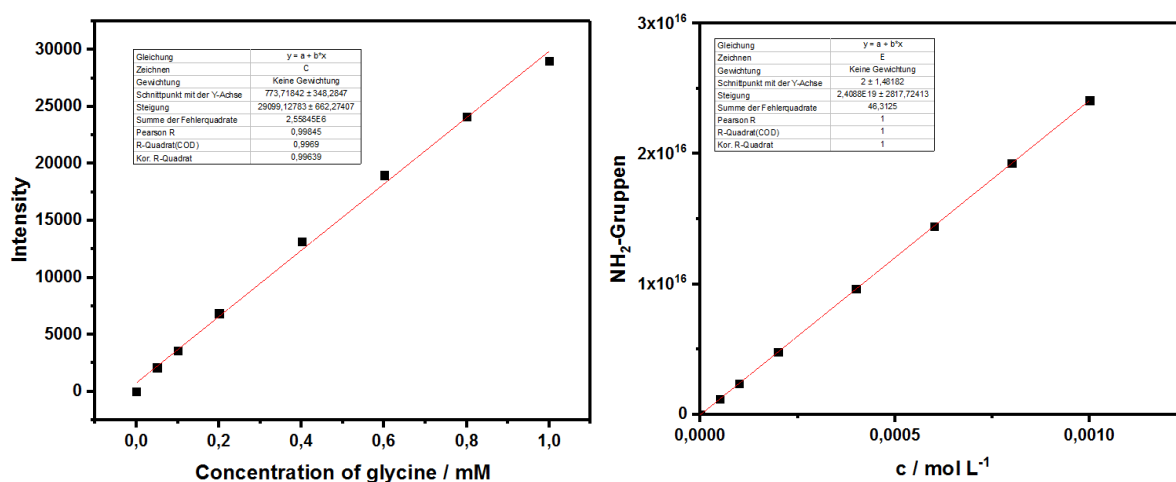


Figure S7. Fluorescamine assay, standard calibration with glycine.

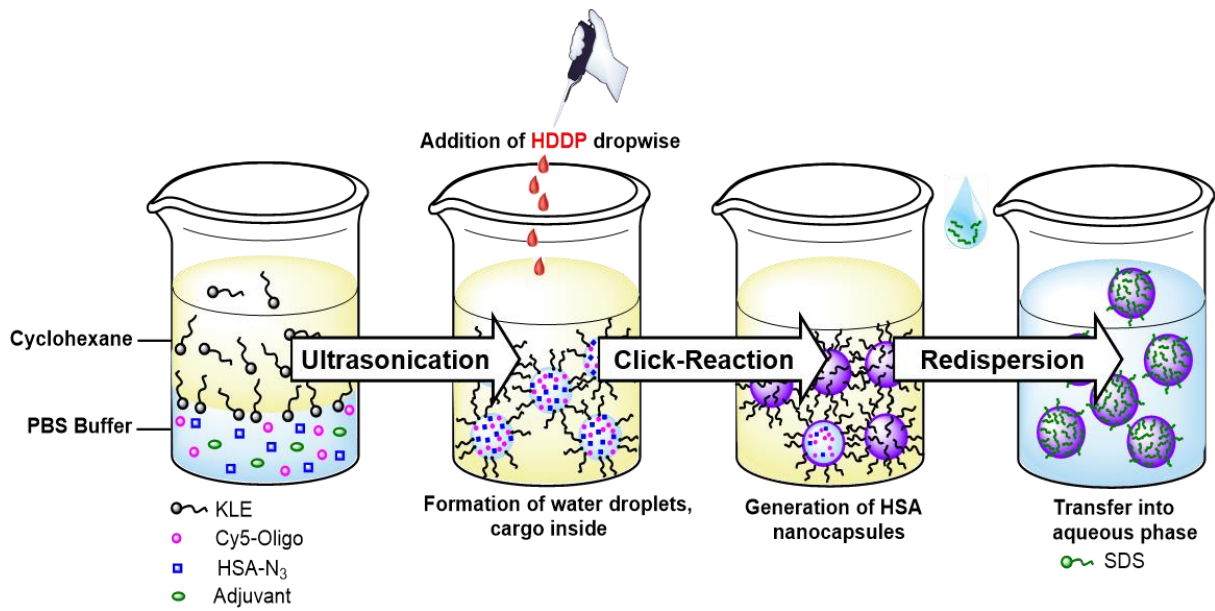
Table 1. Azide-functionalization of human serum albumin at different pH value and time. Number of azide groups ($N_{\text{ex}}(\text{N}_3)$) quantified by the theoretical ($N_{\text{theo}}(\text{NH}_2)$) and experimental ($N_{\text{ex}}(\text{NH}_2)$) number of amines, measured with the fluorescamine assay.

	pH	t/h	$N_{\text{theo}}(\text{NH}_2)$	$N_{\text{ex}}(\text{NH}_2)$	$N_{\text{ex}}(\text{N}_3)$
HSA, nat.	-	-	30-35	35	-
HSA-N ₃		2	-	37	-
HSA-N ₃		4	-	33	2
HSA-N ₃	8.2	8	-	30	5
HSA-N ₃		16	-	29	6
HSA-N ₃		24	-	29	6
HSA-N ₃		48	-	21	14
HSA-N ₃		2	-	28	7
HSA-N ₃		4	-	22	13
HSA-N ₃	9.5	8	-	13	22
HSA-N ₃		16	-	6	29
HSA-N ₃		24	-	5	30
HSA-N ₃		48	-	2	33

HSA-N ₃	2	-	10	16
HSA-N ₃	4	-	3	32
HSA-N ₃	8	-	2	33
	11			
HSA-N ₃	16	-	3	32
HSA-N ₃	24	-	3	32
HSA-N ₃	48	-	2	33

6. Formation of protein nanocarriers

First, the azide-functionalized protein (50 mg) is dissolved in 0.4 mL NaCl solution ($c = 14.4$ mg/mL) and 100 μ L Cy5-Oligo ($c = 0.1$ nmol/ μ L). 35.7 mg of surfactant poly((ethylene/butylene)-*block*-(ethylene oxide)) (P((E/B)-*b*-EO)) were dissolved in 7.5 g of cyclohexane and the mixture was added to the aqueous solution. The two phases were homogenized by ultrasound under ice-cooling (70% amplitude, 3 min, 20 s pulse, 10 s pause). A third solution containing of 10.7 mg P((E/B)-*b*-EO), 35.7 mg crosslinker in 5 g of cyclohexane and was then added dropwise to the stirred miniemulsion at 40 °C. The reaction was carried out at 40 °C for 24 h. Afterwards, the protein nanocarriers were purified by repetitive centrifugation (1500 g, 20 °C) and redispersion in cyclohexane to remove excess of surfactant and crosslinker. For the transfer of the nanocarriers into aqueous media, 500 μ L of concentrated nanocarrier dispersion in cyclohexane is added dropwise to 5 mL 0.1 wt% SDS solution under shaking in an ultrasonication bath for 3 min. Then, the emulsion was stirred open over night to evaporate the organic solvent. The protein nanocarriers in water were purified by repetitive centrifugation and washing in Amicon Ultra-2 centrifugal filters (MWCO 100 kDa).



Scheme S2. Preparation of protein nanocarriers crosslinked with HDDP in inverse miniemulsion and transfer into water.

Table S2. Analytical data of human serum albumin and horse radish peroxidase nanocarriers.

Protein	N_{theo} (NH ₂)	N_{ex} (NH ₂)	N_{ex} (N ₃)	Linker	$d_{i,\text{CH}}$ / nm	PDI_{CH}	$d_{i,\text{water}}$ / nm	$\text{PDI}_{\text{water}}$	ζ /mV
HSA	30-35	11	19-24	HDDP	302	0.13	264	0.23	-30
HSA	30-35	11	19-24	HDDP-SS	327	0.14	254	0.17	-34
HRP	6	2	4	HDDP	424	0.13	231	0.34	-28

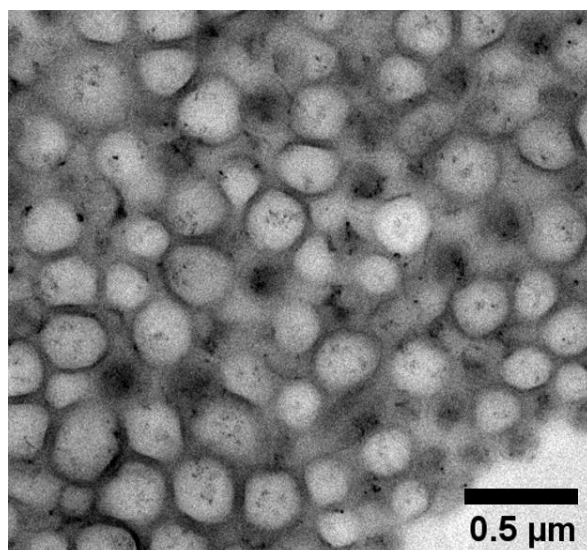


Figure S8. Transmission electron micrograph of human serum albumin nanocarriers.

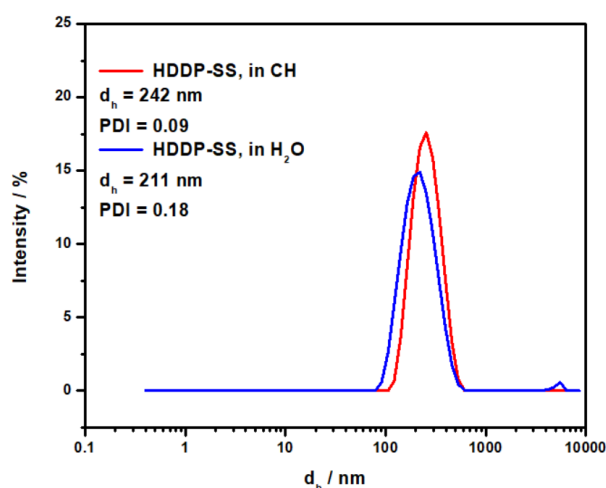


Figure S9. DLS measurement of HSA-HDDP-SS nanocarriers in cyclohexane (red) and water (blue).

7. Characterization of protein nanocarriers

Dynamic light scattering (DLS) was used to determine the average size and size distribution of the nanocarriers. A diluted dispersion (10 μ L sample diluted in 1 mL cyclohexane or 50 μ L sample diluted in 200 μ L H₂O) was measured on a Malvern Zetasizer Nano S (Malvern Panalytical) equipped with a detector at 90° scattering mode at 20 °C. The zeta potential of the nanocarriers were measured in 10⁻³ M potassium chloride solution with a ZetaNanosizer (Malvern Panalytical) at 20 °C. Scanning electron microscopy (SEM) studies were done on a field emission microscope (LEO (Zeiss) 1530 Gemini, Oberkochen, Germany) working at an accelerating voltage of 170 V. The silica wafers are cleaned in the plasma oven prior to use. Then, 2 μ L of a diluted nanocarrier dispersion in cyclohexane or distilled water (concentration similar to samples for DLS) were dropped onto the wafers and dried under ambient conditions

for 15 min. No additional contrast agent was applied. The solid content of the nanocarrier dispersion was measured gravimetrically. The fluorescence intensities for all mentioned experiments were measured using a microplate reader (Infinite M1000, Tecan, Switzerland).

8. Determination of encapsulation efficiency and permeability

The encapsulation efficiency is determined by measuring the fluorescence intensity of using a microplate reader (Infinite M1000 Tecan, Switzerland). The unpurified nanocarrier dispersion after transfer into 0.1 wt% SDS are concentrated in an Amicon centrifuge filter 100 K for 30 min at 500 g. The amount of non-encapsulated dye was measured in the supernatant and the encapsulation efficiency determined in proportion to the fluorescence intensity of the unpurified dispersion. After washing the aqueous dispersion, the permeability of the nanocarrier was measured using the same method. The dispersion was concentrated in an Amicon centrifuge filter at a certain time point and the amount of leaked dye measured in the supernatant.

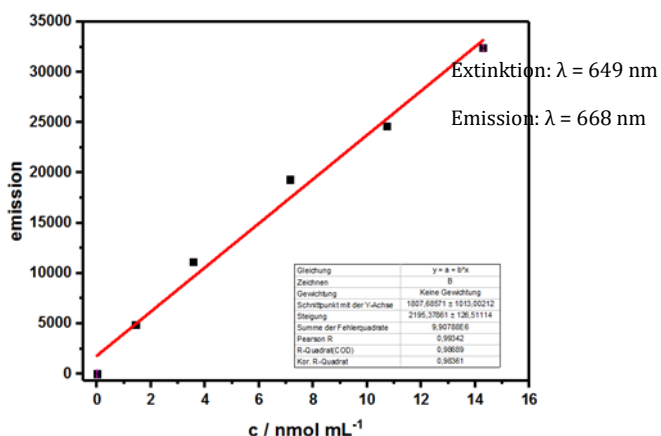


Figure S10. Standard calibration curve of Cy5-Oligo fluorescence.

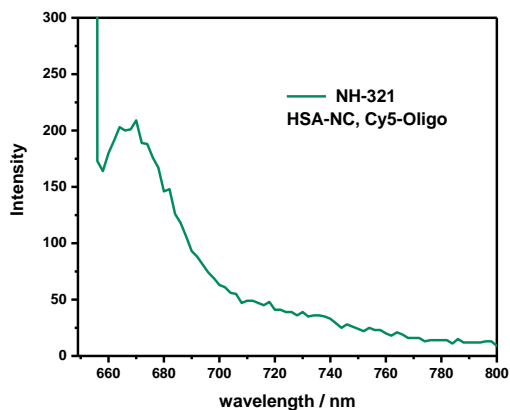


Figure S11. Fluorescence curve of HSA nanocarriers with encapsulated Cy5-oligo.

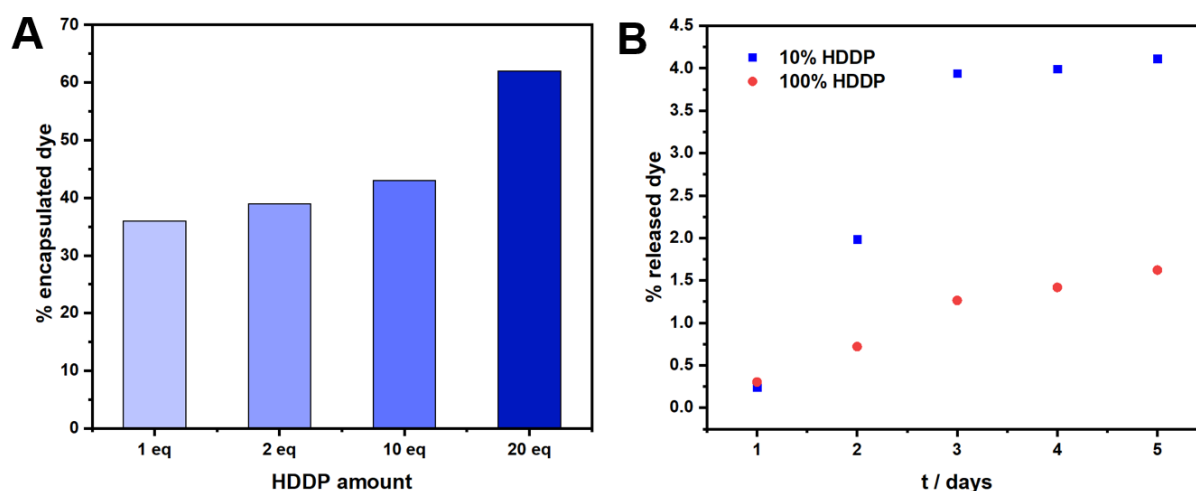


Figure S12. A) Amount of encapsulated dextran-sulforhodamine B ($M = 10$ kDa) after transfer of protein nanocarriers crosslinked with different amount of HDDP to water. Measured by fluorescence. B) Amount of released sulforhodamine 101 upon storage at room temperature measured by fluorescence.

9. Degradability of protein nanocarrier

The enzymatic degradation of the protein nanocapsules were performed with proteinase K and determined by release of Cy5-Oligo. A 0.1 wt% nanocarrier dispersion in PBS buffer was treated with a proteinase K solution (30 U/mL) at 37 °C. After the enzymatic degradation the dispersion is filtered by centrifugation in an Amicon centrifuge filter 3K at 500 g for 30 min and the amount of released dye in the supernatant measured by fluorescence. The degradation of the nanocarriers by proteinase K is also monitored by DLS measurements every 5 min over 10 h. The reduction-responsive properties of HDDP-SS-crosslinked protein nanocarriers were investigated with dithiothreitol (DTT) by release of Cy5-Oligo. A 0.1 wt% nanocarrier dispersion in PBS was treated with a DTT solution (25 mM) at 20 °C. After the reductive degradation, the dispersion is filtered by centrifugation in an Amicon centrifuge filter 3K at 500 g for 30 min and the amount of released dye in the supernatant measured by fluorescence. The degradation of the nanocarriers by DTT is also monitored by DLS measurements every 5 min over 10 h. In both cases, enzymatic and reductive degradation, a sample treated with PBS buffer serves as a control sample and every experiment was performed in triplets.

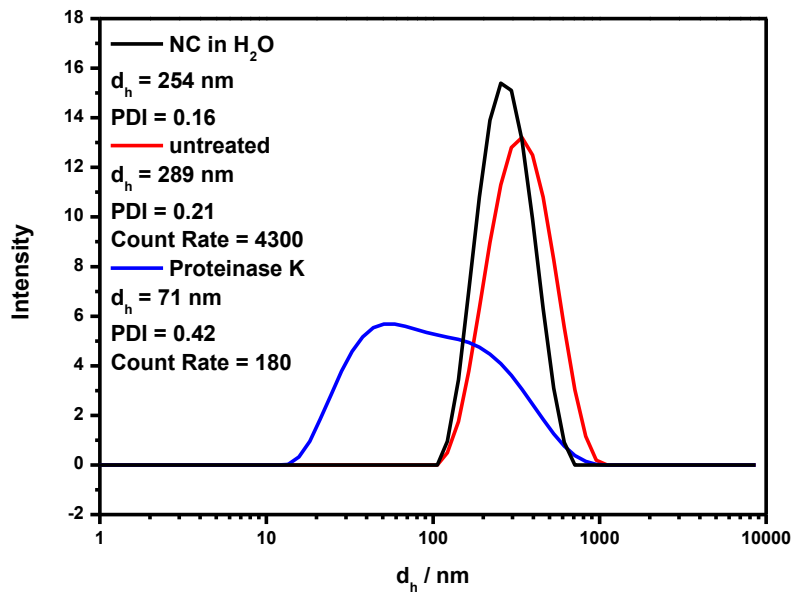


Figure S13. DLS curves of protein nanocarrier before and after treatment with proteinase K.

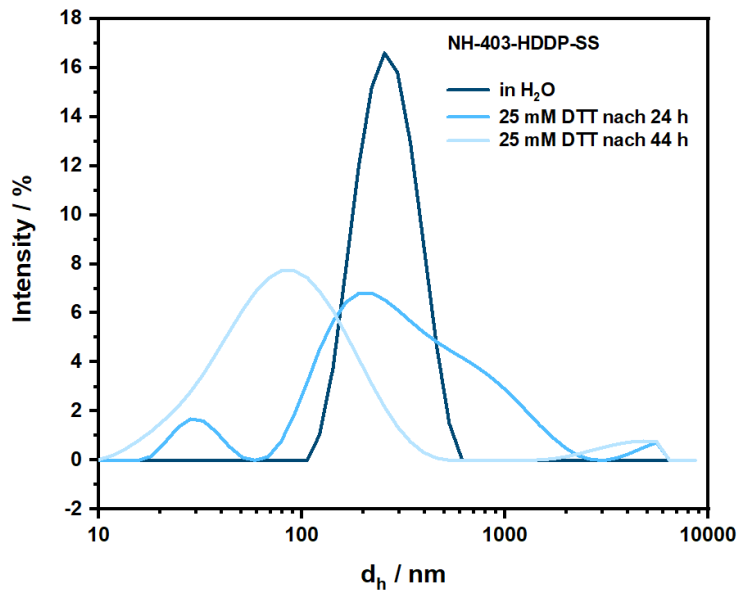


Figure S14. DLS measurement of protein nanocarriers before and after treatment with DTT

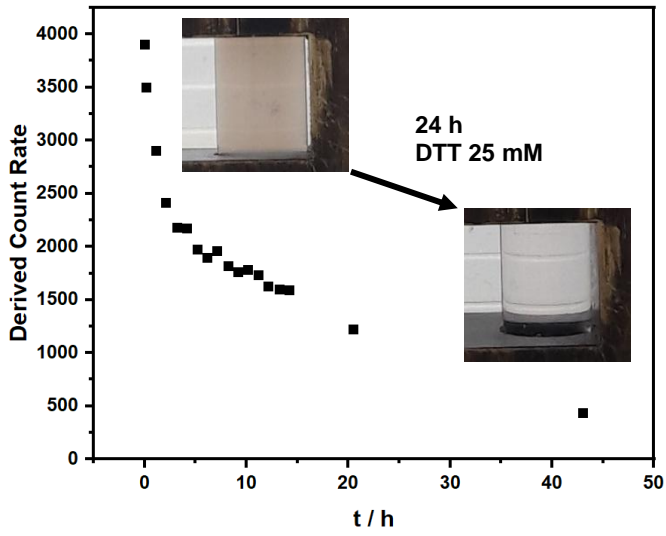


Figure S15. Influence of the derived count rate of human serum albumin nanocarriers crosslinked with HDDP upon treatment of DTT measured by DLS.

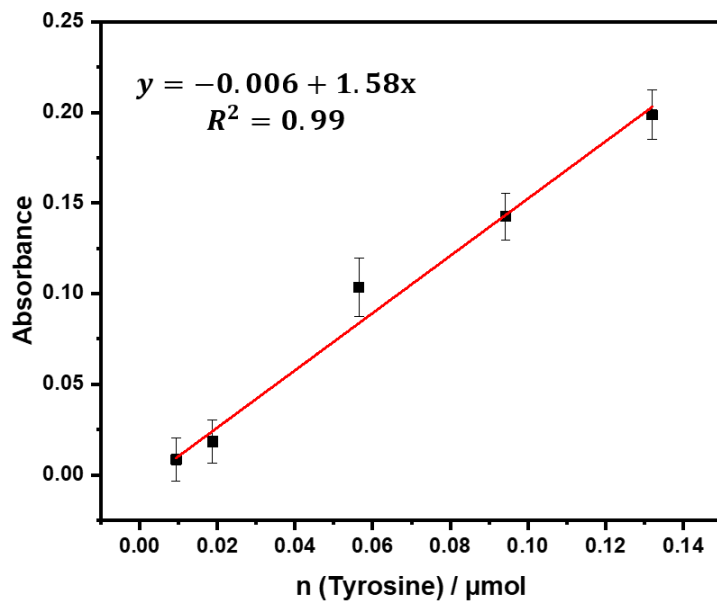


Figure S16. Tyrosine calibration curve for the determination of the enzyme activity of proteinase K.

Table S3. Enzymatic activity assay of proteinase K under the influence of DTT with hemoglobin as substrate. Proteinase K solution incubated with DTT at 37 °C for 10 min, 30 min and 2 h.

Sample	Prot K / UmL ⁻¹	DTT /mmolL ⁻¹	Activity /Umg ⁻¹	Error /Umg ⁻¹	Activity /Umg ⁻¹	Error /Umg ⁻¹	Activity /Umg ⁻¹	Error /Umg ⁻¹
1	0.1	-	62	10	110	27	138	61
2	0.1	1	39	10	110	27	135	75
3	0.1	3	47	11	125	29	138	72
4	0.1	5	45	9	124	6	139	73
5	0.1	25	102	9	161	4	212	84
6	1	-	62	6	51	2	62	6
7	1	1	61	6	52	4	61	6
8	1	3	63	9	52	3	63	9
9	1	5	63	6	52	3	63	6
10	1	25	67	7	53	3	67	7

10. Determination of enzyme concentration in protein nanocarriers

A protein assay with bicinchoninic acid (BCA) was used as the substrate to determine the concentration of the enzyme in the nanocarrier dispersion. Briefly, BCA (100 mg), sodium carbonate (200 mg), sodium hydrogen carbonate (95 mg) and sodium tartrate (16 mg) were dissolved in 10 mL of distilled water and the pH of the solution was adjusted to 11.3 by using 3.0 M NaOH. A solution of CuSO₄ x 5 H₂O (50 mg/mL, 200 µL) in distilled water was added to the substrate solution. 10 µL of protein or nanocarrier dispersion was mixed with 200 µL of metal-containing substrate solution and incubated at 60 °C for 30 min. The absorbance of the sample was measured at 565 nm and the enzyme concentration determined by a standard calibration with native enzyme.

11. Enzymatic activity

The enzymatic activity of HRP and HRP-HDDP nanocarriers were determined using 2,2'-azino-bis(3-ethylbenzothiazoline-6-sulphonic acid) (ABTS) as substrate. Briefly, the substrate was dissolved in 100 mM potassium phosphate buffer (pH 5.0) to a concentration of 5 mg/mL. The enzyme in different stages of the nanocarrier preparation were diluted to a concentration of 0.002 mg/mL protein in a solution of 0.5% Triton X-100 in 40 mM PBS buffer (pH 6.8). The ABTS solution (190 µL) was mixed with the enzyme solution (3.3 µL) in a 96-well plate and the reaction started with addition of 0.3% (w/w) hydrogen peroxide solution (6.6 µL). The absorbance at 405 nm was monitored by a UV/Vis spectrophotometer and the enzyme activity determined by a standard calibration with native HRP.

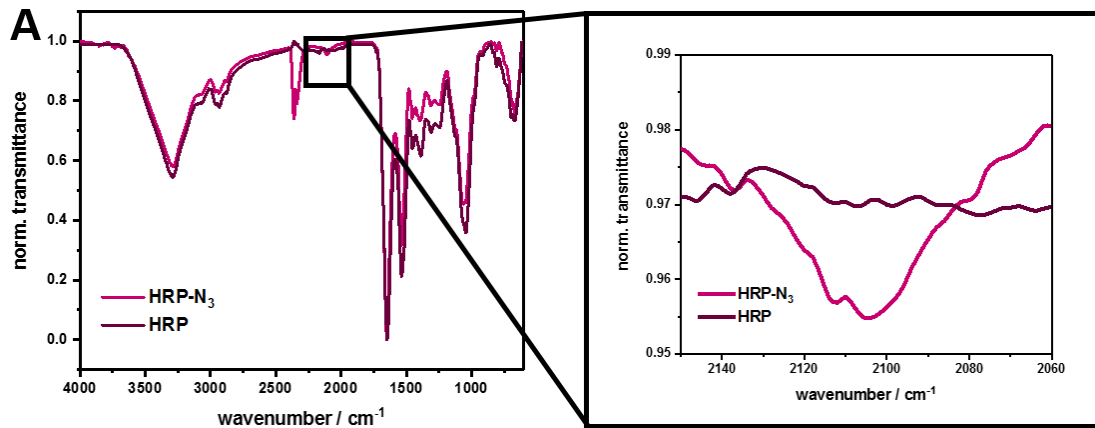


Figure S17. IR spectra of horse radish peroxidase and azide-functionalized HRP.

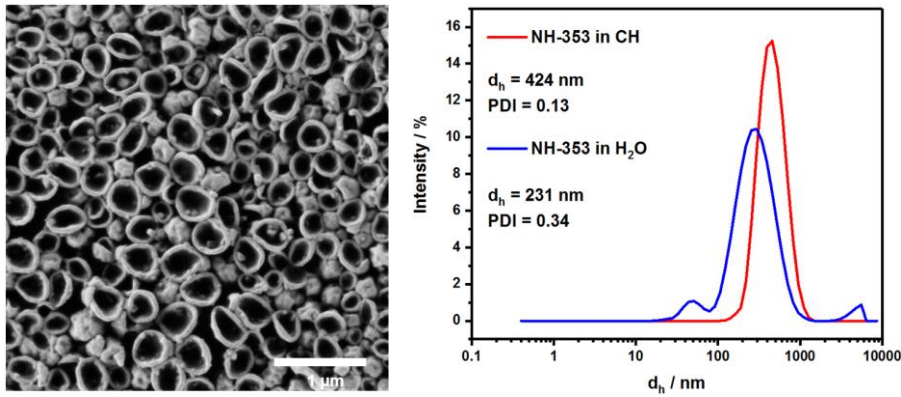


Figure S18. Scanning electron micrograph and DLS measurements of HRP-HDDP nanocarriers in cyclohexane.

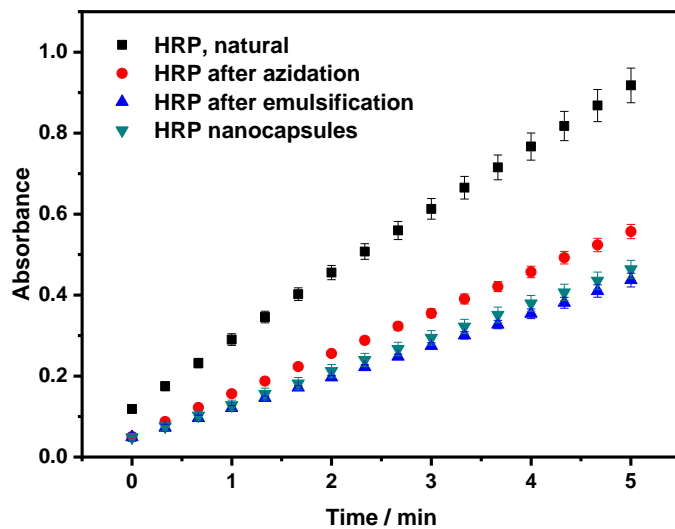


Figure S19. Enzymatic activity of horse radish peroxidase during the preparation of HRP nanocarriers.

12. Quantification of adjuvants in protein nanocarriers

For the quantification of adjuvants in the protein nanocapsules (PNCs), the PNCs were degraded by proteinase K (30 U/mL) at 37 °C overnight. The PNCs remains and the enzyme were separated from the released adjuvants through a centrifuge filter (MWCO 3K, 30 min, 1500 g). The amount of Resiquimod (R848) was determined by fluorescence ($\lambda_{\text{ex}} = 260 \text{ nm}$, $\lambda_{\text{em}} = 360 \text{ nm}$) using a standard calibration curve (Figure S20). Muramyl dipeptide (MDP) was determined from the supernatant using the Morgan-Elson Reaction (Scheme S3). The supernatant (50 μL) was mixed with borate buffer (50 μL , pH 9) and incubated at 100 °C for 3 min. The mixture is cooled to room temperature and DMAB (500 μL) was added to the mixture. The mixture was incubated again at 37 °C for 15 min and afterwards the absorbance measured at 585 nm. The MDP was quantified by a standard calibration (Figure S21). Poly(I:C) was quantified from the full mixture after degradation as it has a too high molecular weight to be separated from the proteins. The full mixture of PNCs after degradation with proteinase K was eluted through a reverse phase HPLC column using a mixture of Acetonitrile, 0.01% formic acid and 0.02 mol/L ammoniumacetate. The Poly(I:C) signal was quantified using a standard calibration curve (Figure S22).

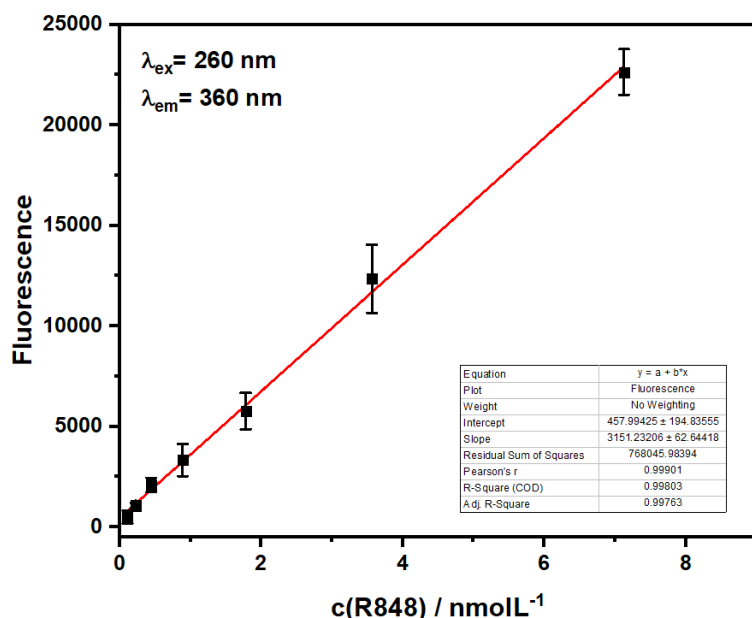


Figure S20. Standard calibration curve of R848 by fluorescence measured at 360 nm.

Scheme S3. Quantification of muramyl dipeptide with Morgan-Elson reaction.

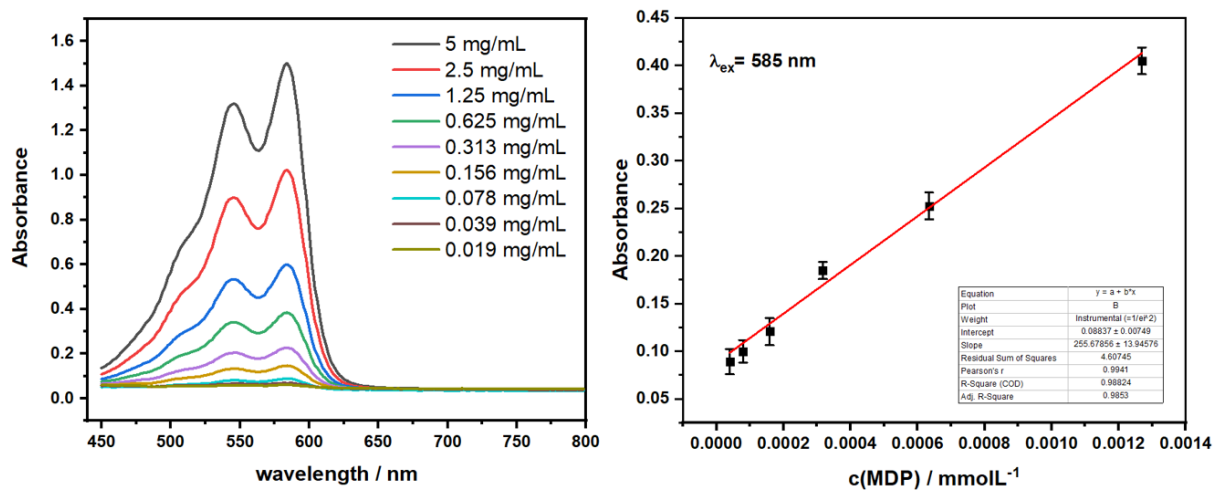
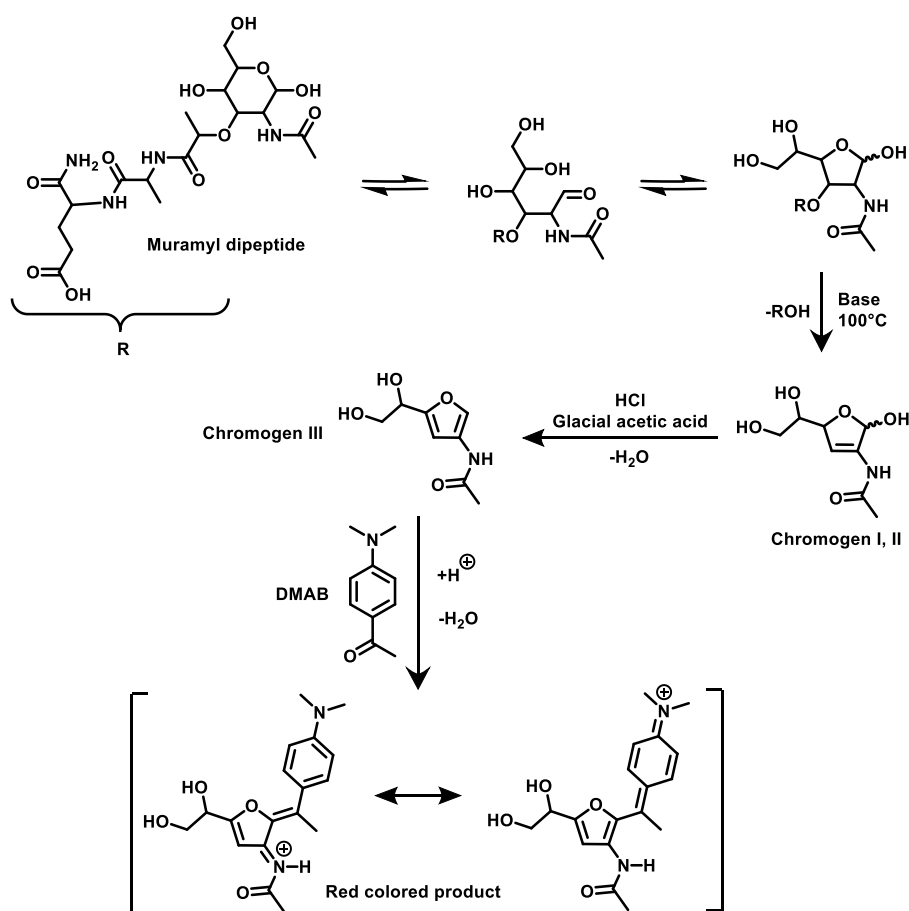


Figure S21. Absorbance measurements of MDP assay via Morgan-Elson reaction with DMAB.

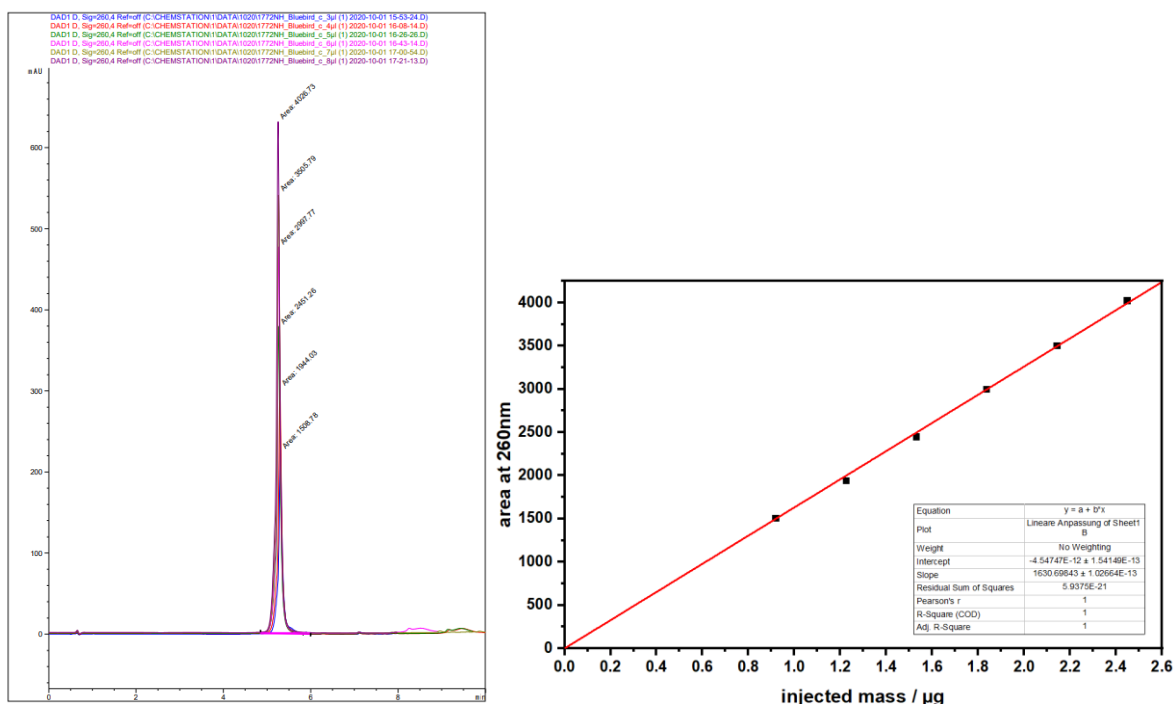


Figure S22. Standard calibration curve of Poly(I:C) measured by HPLC.

Table S4. Encapsulation efficiencies of dye and adjuvants into human serum albumin nanocarriers crosslinked with HDDP or HDDP-SS. Variation of the concentration of R848, MDP and Poly(I:C) in the nanocarriers.

No.	Linker	Adj.	EE _{Cys Oligo} / %	C _{R848,theo} / molL ⁻¹	C _{R848} / molL ⁻¹	C _{R848} / %	C _{MDP,theo} / molL ⁻¹	C _{MDP} / molL ⁻¹	C _{MDP} / %	C _{PolyI:C,theo} / molL ⁻¹	C _{PolyI:C} / molL ⁻¹	C _{PolyI:C} / %	d _{h,H2O} / nm	PDI	ζ / mV
1		-	86	-	-	-	-	-	-	-	-	-	203	0.16	-32
2		R848	80	4.50*10 ⁻⁸	2.88*10 ⁻⁸	64	-	-	-	-	-	-	245	0.17	-40
3		MDP	84	-	-	-	1.02*10 ⁻⁷	5.92*10 ⁻⁸	58	-	-	-	212	0.22	-38
4		PolyI:C	85	-	-	-	-	-	-	2.00*10 ⁻¹⁰	1.84*10 ⁻¹⁰	92	215	0.20	-42
5	HDDP	All 3	85	8.91*10 ⁻⁸	3.15*10 ⁻⁸	35	1.02*10 ⁻⁷	3.73*10 ⁻⁸	37	2.00*10 ⁻¹⁰	5.20*10 ⁻¹¹	26	302	0.25	-34
6		All 3	87	4.50*10 ⁻⁸	2.84*10 ⁻⁸	63	1.02*10 ⁻⁷	5.55*10 ⁻⁸	53	2.00*10 ⁻¹⁰	1.30*10 ⁻¹⁰	65	218	0.21	-38
7		All 3	73	2.23*10 ⁻⁸	1.77*10 ⁻⁸	79	1.02*10 ⁻⁷	5.68*10 ⁻⁸	56	2.00*10 ⁻¹⁰	1.30*10 ⁻¹¹	65	356	0.35	-28
8		All 3	90	4.50*10 ⁻⁸	2.84*10 ⁻⁸	64	5.08*10 ⁻⁸	3.59*10 ⁻⁸	71	2.00*10 ⁻¹⁰	1.46*10 ⁻¹¹	73	366	0.18	-29
9		All 3	91	4.50*10 ⁻⁸	3.05*10 ⁻⁸	69	2.54*10 ⁻⁸	1.86*10 ⁻⁸	73	2.00*10 ⁻¹⁰	1.60*10 ⁻¹¹	80	252	0.07	-32
10		All 3	52	4.50*10 ⁻⁸	3.23*10 ⁻⁸	74	1.02*10 ⁻⁷	7.06*10 ⁻⁸	69	5.00*10 ⁻¹¹	4.65*10 ⁻¹¹	93	194	0.27	-31
11		-	57	-	-	-	-	-	-	-	-	-	258	0.16	-34
12	HDDP-SS	R848	57	4.50*10 ⁻⁸	3.34*10 ⁻⁸	75	-	-	-	-	-	-	254	0.14	-33
13		All 3	73	4.50*10 ⁻⁸	2.93*10 ⁻⁸	65	1.02*10 ⁻⁷	6.43*10 ⁻⁸	63	2.00*10 ⁻¹⁰	1.22*10 ⁻¹⁰	61	304	0.19	-32

13. *In vitro* experiments with BMDCs

Bone marrow-derived dendritic cells (BMDC) were differentiated from bone marrow progenitors (BM cells) of 8- to 10-week-old C57BL/6J mice. Briefly, the bone marrow was obtained by flushing the femur, tibia, and hip bone with Iscove's Modified Dulbecco's Medium (IMDM) containing 5% FCS (Sigma-Aldrich) and 50 μ M β -mercaptoethanol (Roth, Karlsruhe, Germany). For the analysis of DC maturation and nanocarrier uptake/binding and degradation via flow cytometry the BM cells (2×10^5 cells/1.25 mL) were seeded in 12 well suspension culture plates (Greiner Bio-One, Frickenhausen, Germany) with culture medium (IMDM with 5% FCS, 2 mL-glutamine, 100 U/mL penicillin, 100 μ g/mL streptomycin [all from Sigma-Aldrich], and 50 μ M β -mercaptoethanol), supplemented with 10 ng/mL GM-CSF. On day 3, 500 μ L of the same medium was added into each well. On day 6, 1 mL of the old medium was replaced with 1 mL fresh medium per well. Before usage, all nanoparticle solutions were checked for endotoxin contaminations by limulus amoebocyte lysate (LAL) assay (Thermo Fisher Scientific) according to the manufacturer's instructions.

14. Confocal imaging

Uptake of PNCs containing fluorescent Cy5-Oligo (red) was monitored by Confocal Laser Scanning Microscopy (cLSM). To this end, BMDC (3×10^5 cells) on day 7 of culture were seeded in chamber slides (Thermo Fisher Scientific) and treated with 150 μ g/mL PNCs for 3 h at 37 °C. After that, the chamber slides were washed, and the samples were incubated with DAPI (Sigma-Aldrich) to stain the cell nuclei (blue). Unbound dye was washed off. Samples were assayed using a Zeiss LSM710 (Carl Zeiss) and analyzed using ImageJ (NIH, Bethesda, USA) and ZEN 2009 (Carl Zeiss) software.

15. Flow cytometry assay

To detect cell-nanocarrier-interaction and to analyze the expression of surface markers, cells were harvested and washed in staining buffer (phosphate buffer saline [PBS]/2% FCS). To block Fc receptor-mediated staining, cells were incubated with rat anti-mouse CD16/CD32 Ab (clone 2.4G2) for 15 min at room temperature. After that, cells were incubated with eFluor450-conjugated Ab specific for MHC class II I-Ab,d,q/I-Ed,k(cloneM5/114.15.2), fluorescein isothiocyanate (FITC)-labeled Ab directed at CD80 (clone 16-10A1), phycoerythrin (PE) anti-CD86 (clone GL-1), PE-Cy7-labeled anti-CD11c (clone N418), for 30 min at 4 °C. Dead cells were stained by incubation with fixable viability dye (FVD) eFI506 for 30 min at room temperature in the dark. Samples were measured with a BD FACSCanto II flow cytometer equipped with BD FACSDiva software (BDBiosciences). Data were generated based on defined gating strategies and analyzed using FlowJo software (FlowJo, Ashland, USA).

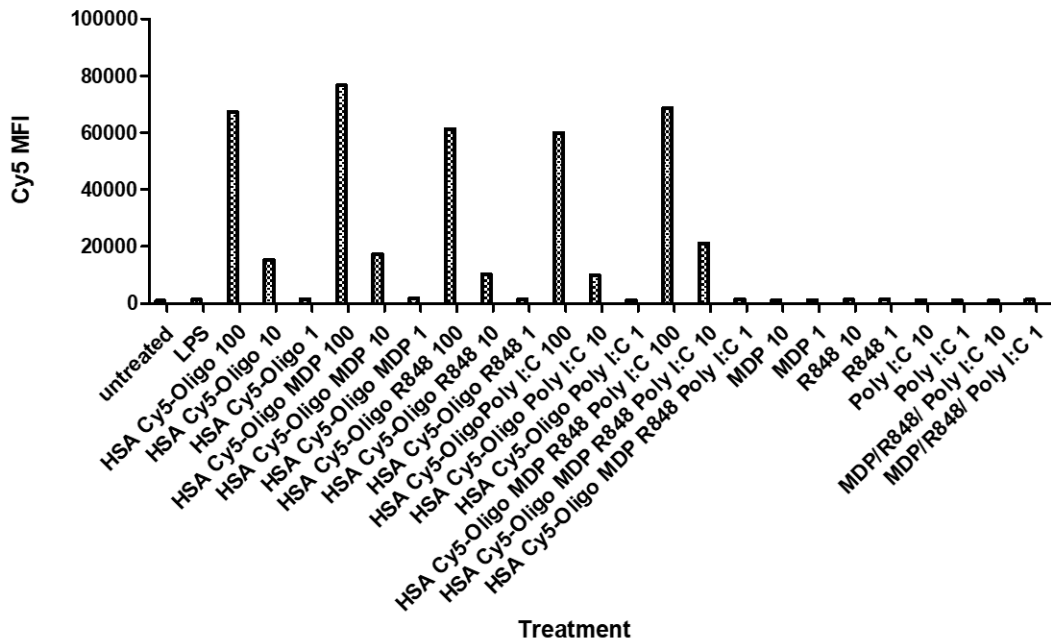


Figure S23. Cell binding/uptake into BMDC of loaded HSA-HDDP nanocarrier and free adjuvants measured by flow cytometry.

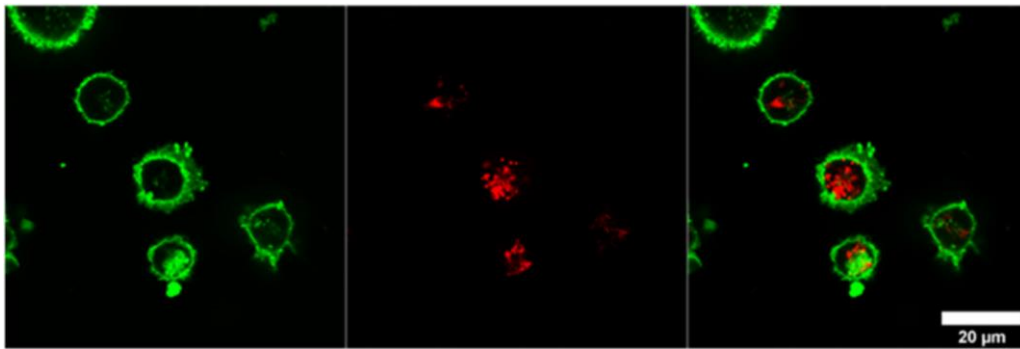


Figure S24. Confocal image of bone marrow-derived dendritic cells (green) and uptaken human serum albumin nanocarriers (red).

Chapter B

Results presented in Chapter B are based on data previously discussed in the publication “*Multicomponent encapsulation into fully degradable protein nanocarriers via interfacial azide-alkyne click reaction in miniemulsion allows the co-delivery of immunotherapeutics*” by Hüppe *et al.* (Nanoscale Horizons, 2022) in Chapter A. The following experiments were designed to establish adjuvant-loaded OVA-NCs for the co-administration of tumor antigens and adjuvants for melanoma treatment and are briefly discussed in the overall context of this work.

Contribution

Chapter B was written by Jenny Schunke. Adjuvant-loaded OVA-NCs were synthesized by Dr. Natkritta Hüppe. Biological assays *in vitro* were performed by Jenny Schunke. *In vivo* tumor studies were conducted by Jenny Schunke with support by Dr. Michael Fichter.

Adjuvant-loaded ovalbumin-based nanocarriers for the induction of DC-mediated anti-melanoma immune responses

1. Material and Methods

Materials and methods are described in detail in Chapter C. Supplementary methods are listed below. The description is based on material and methods of Chapter C and was adapted and supplemented.

1.1 Encapsulation efficiency of Cy5-Oligo and adjuvants

Nanocapsules (NCs) were transferred into 0.1wt% SDS. Afterwards, the unpurified dispersion containing the NCs was centrifuged at 500 x g for 30 min using an Amicon Ultra-2 centrifugal filter (MWCO 100 kDa). The encapsulation efficiency was determined after measuring the amount of free Cy5-Oligo in the supernatant using a microplate reader (Infinite M1000, Tecan, Switzerland), in proportion to the fluorescence intensity of the unpurified dispersion. The same procedure was applied to measure the permeability of the NCs after washing the aqueous dispersion and quantification of leaked dye.

To determine the amount of encapsulated adjuvants, the OVA-NCs were degraded using proteinase K (30 U/mL, 37 °C; Sigma Aldrich, United States) overnight. Released adjuvants and degraded NCs were separated from the enzyme via centrifugation using an Amicon Ultra-2 centrifugal filter (MWCO 3K, 30 min, 1,500 x g). The amount of encapsulated Cy5-Oligo and

the TLR7/8 agonist resiquimod (R848) was determined by fluorescence measurements using a microplate reader (Infinite M1000, Tecan, Switzerland) (Cy5: $\lambda_{\text{ex}} = 649 \text{ nm}$, $\lambda_{\text{em}} = 668 \text{ nm}$; R848: $\lambda_{\text{ex}} = 260 \text{ nm}$, $\lambda_{\text{em}} = 360 \text{ nm}$). Encapsulation efficiency of muramyl dipeptide (MDP) was determined from sample flow-through with the Morgan-Elson reaction. 50 μL of sample supernatant was mixed with borate buffer (50 μL , pH 9), incubated at 100 °C for 3 min and 500 μL dimethylaminoborane (DMAB) were added at room temperature. After further incubation at 37 °C for 15 min, absorbance measurements at 585 nm were performed and MDP amounts were quantified by standard calibration. To quantify the amounts of encapsulated Poly(I:C), NCs were degraded with proteinase K and subsequently eluted through a reverse phase HPLC column (Acetonitrile, 0.01% formic acid, 0.02 mol/L ammoniumacetate). Poly(I:C) signal was finally quantified using a standard calibration curve. A reproducible encapsulation efficiency for all cargos from batch to batch could be observed. All adjuvants were purchased from InvivoGen (United States).

1.2 T cell proliferation *in vitro*

Immature DCs (10^6 cells/mL) were incubated with OVA-NC formulations in 12 well- plates for 24 h. Treatment with LPS [100 ng/mL] served as positive control. Afterwards, NC-pretreated BMDCs were harvested and washed. Splenic OT-I and OT-II T cells were isolated with the CD4⁺ or CD8a⁺ T Cell Isolation Kit according to manufacturer's instruction (Miltenyi.Biotec, Germany). Both, CD4⁺ and CD8⁺ T cells (5×10^4) were co-cultured with serially diluted BMDCs (starting with 10^4) in triplicates with culture medium ($V = 200 \mu\text{L}$) in 96 well-plates (Greiner Bio-One, Germany) for four days. Genomic incorporation of ³H thymidine (0.25 $\mu\text{Ci}/\text{well}$, last 16 h of incubation) was used to assess T cell proliferation. A liquid scintillation counter (1205 Betaplate, LKB Wallac, Finland) was used to measure radioactivity after harvesting of cells onto glass fiber filters (Perkin Elmer, United States).

2. Results and Discussion

Nanovaccines not only offer the advantage of protected adjuvant transport to dendritic cells (DCs) but also of co-delivery of immunomodulatory molecules in combination with antigens. Using a tumor antigen as nanocarrier (NC) shell material increases the encapsulation capacity of NCs and enables encapsulation of greater amounts of adjuvants. To develop an immunotherapeutic vaccine consisting of an antigen-based shell and an adjuvant-containing aqueous core, ovalbumin (OVA), an established model antigen, was selected for NC synthesis. OVA is biocompatible, biodegradable and commonly used as antigen in immunological studies. In order to evaluate the NC-mediated antigen-specific T cell activation and subsequent cancer

cell recognition as well as tumor cell killing, MDP and R848 alone or in combination with Poly(I:C) were encapsulated into OVA-NCs.

Treatment of bone marrow-derived dendritic cells (BMDCs) with 100 $\mu\text{g/ml}$ of non-loaded OVA-NCs already triggered a slight upregulation of CD80 expression indicating DC maturation (Fig. 1). This effect was significantly enhanced by the encapsulation of MDP, R848 or Poly(I:C). BMDC treatment with either 100 $\mu\text{g/ml}$ MDP/R848-loaded or 100 $\mu\text{g/ml}$ MDP/R848/Poly(I:C)-loaded OVA-NCs resulted in approx. 4-fold increased CD80 expression compared to untreated cells (Fig. 1). Co-delivery of both adjuvant combinations induced CD80 expression already at a concentration of 1 $\mu\text{g/ml}$. Therefore, both NC formulations represent interesting vaccine candidates for further evaluation of T cell activation *in vitro* and *in vivo*. Since there were no significant differences between the co-delivery of MDP/R848 alone or in combination with Poly(I:C) observed, the focus was further set on MDP/R848-loaded NCs (Fig. 1).

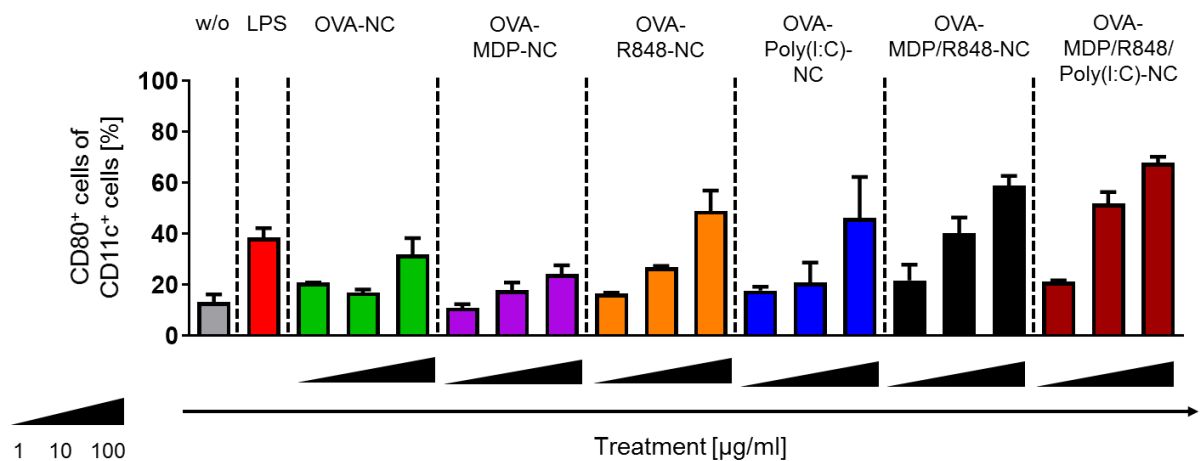


Figure 1. 2×10^5 cells were seeded into 12-well plates and treated with 1 - 100 $\mu\text{g/ml}$ adjuvant-loaded OVA-NCs for 24 h. Non-treated cells (w/o), treatment with non-loaded OVA-NCs and LPS-treated cells [100 ng/mL] served as controls. Cells were harvested and analyzed for their expression levels of CD80 via flow cytometry ($n = 3$). Data represent mean \pm SD.

Additionally experiments were performed with a separate batch of OVA-MDP/R848-NCs. This revealed a dose-dependently increased uptake of Cy5-loaded OVA-NC formulations by BMDCs (Fig. 2).

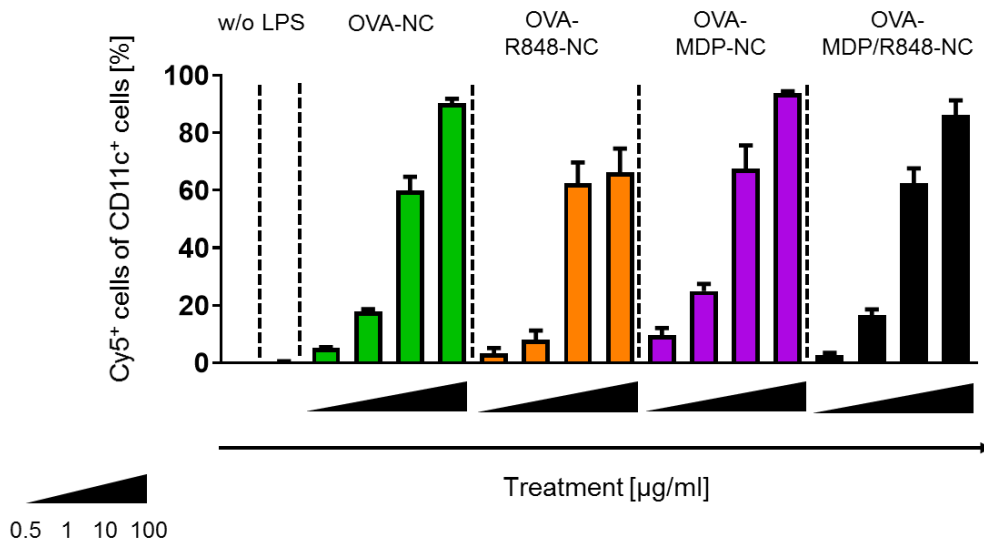


Figure 2. Uptake of Cy5-Oligo-labelled OVA-NCs by BMDCs *in vitro*. 2×10^5 cells ($V_{\text{total}} = 1$ mL) were seeded into 12-well plates and co-incubated with 1 – 100 µg/mL OVA-NCs for 24 h. Treatment with LPS [100 ng/mL], non-treated cells (w/o), and treatment with non-loaded NCs served as controls. BMDCs were harvested and uptake was determined by flow cytometry ($n = 3$). Data represent mean \pm SD.

Furthermore, previous results of OVA-NC-induced DC maturation marker expression could be reproduced (Fig. 3).

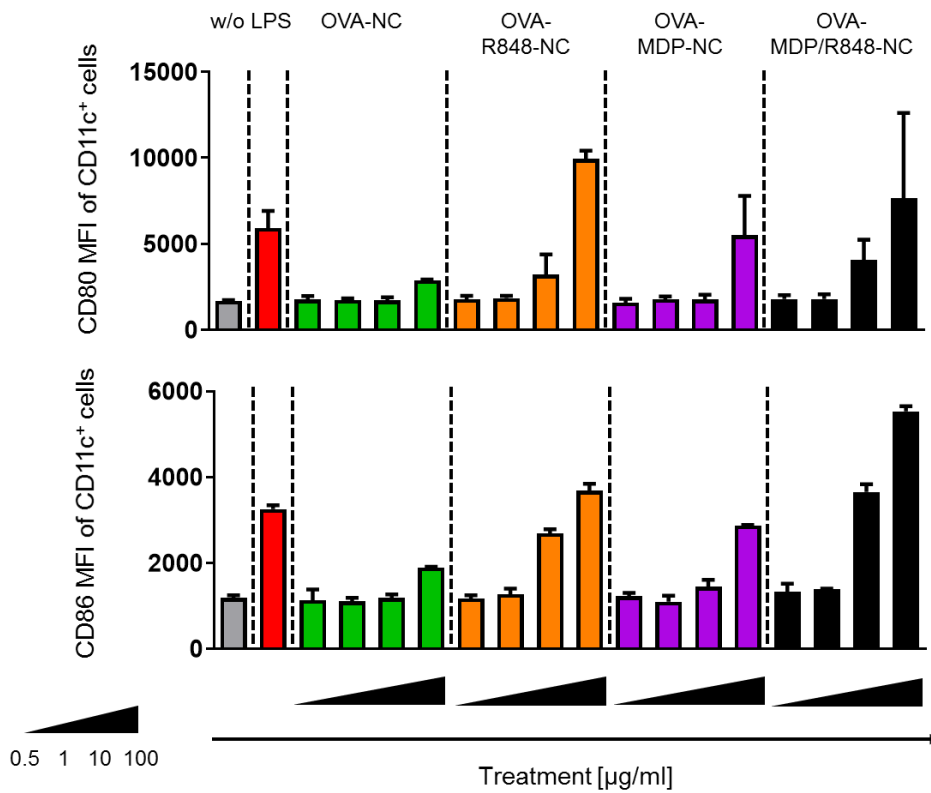


Figure 3. 2×10^5 BMDCs were seeded into 12-well plates and treated with 0.5 - 100 $\mu\text{g}/\text{mL}$ adjuvant-loaded OVA-NCs for 24 h. Non-treated cells (w/o), treatment with non-loaded NCs, and LPS treatment [100 ng/mL] served as controls. Cells were harvested and analyzed for their expression levels of CD80 and CD86 via flow cytometry ($n = 3$). Data represent mean \pm SD.

Combined encapsulation of MDP and R848 triggered superadditive secretion of the pro-inflammatory cytokines IFN- γ , IL-6, and TNF- α starting at a concentration of 5 $\mu\text{g}/\text{ml}$ compared to single adjuvant-loaded OVA-NC formulations (Fig. 4). OVA-MDP-NCs did not induce IFN- γ or IL-6 production, whereas TNF- α secretion was triggered after the application of 10 $\mu\text{g}/\text{ml}$ (Fig. 4). R848-loaded OVA-NCs elicited secretion of all three cytokines.

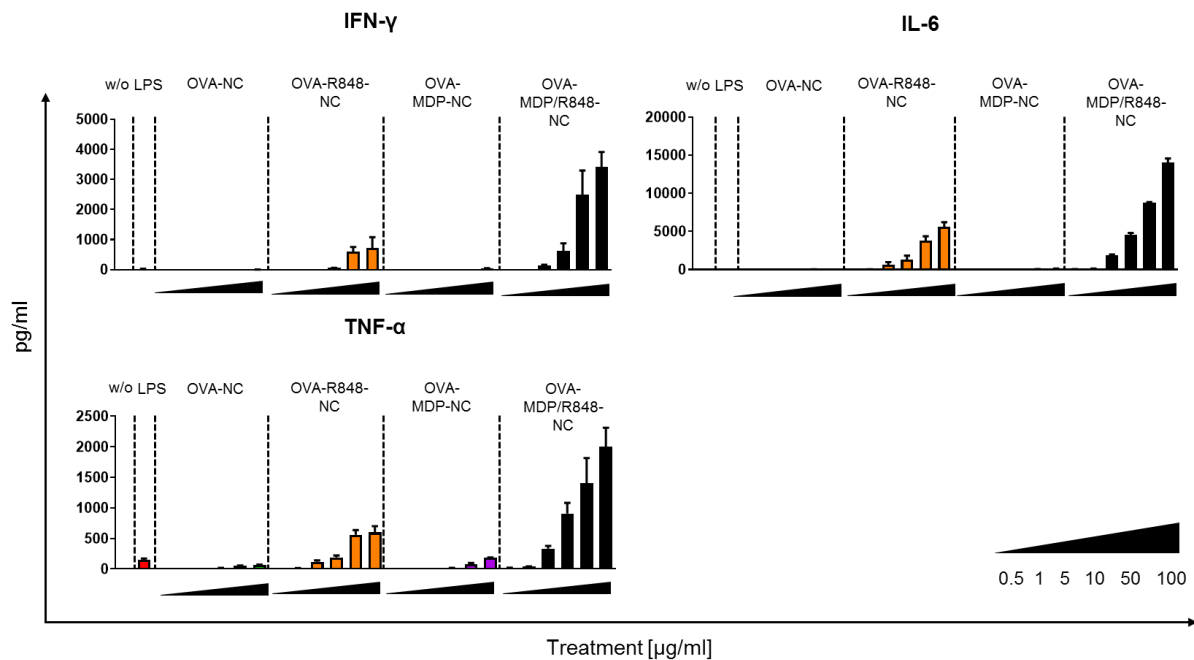


Figure 4. Secretion of pro-inflammatory cytokines by splenocytes *in vitro*. 2×10^5 cells were seeded into 12-well plates and treated with adjuvant-loaded OVA-NC formulations [0.5 – 100 $\mu\text{g}/\text{mL}$] for 24 h ($n = 3$). Non-treated cells (w/o), treatment with non-loaded NCs, and LPS treatment [100 ng/mL] served as controls. The production of the pro-inflammatory cytokines IFN- γ , IL-6 and TNF- α was quantified using a bead-based immunoassay. Data represent mean \pm SD.

Having demonstrated successful encapsulation of adjuvants into OVA-NCs and an advantage of combined encapsulation of MDP and R848 with respect to DC maturation, DC-mediated OVA-specific priming of T cells was subsequently investigated. For this purpose, CD4 $^+$ T cells isolated from OT-II mice, recognizing OVA residues bound to MHC class II molecules, and CD8 $^+$ T cells isolated from OT-I mice, recognizing peptides presented via MHC class I molecules, were co-cultured with NC-pretreated DCs. A ^3H -thymidine incorporation assay was performed in order to quantify adjuvant- and antigen-based proliferation of CD4 $^+$ and CD8 $^+$ T cells. Pretreatment with double adjuvant-loaded OVA-NCs triggered the strongest proliferation of CD4 $^+$ and CD8 $^+$ T cells *in vitro* demonstrating that the epitopes required for T cell activation remain intact despite crosslinking of OVA during the for shell formation process (Fig. 5).

Moreover, the proliferation of CD8⁺ T cells implied DC cross-presentation of OVA peptides resulting in a broad T cell response induced by NC administration.

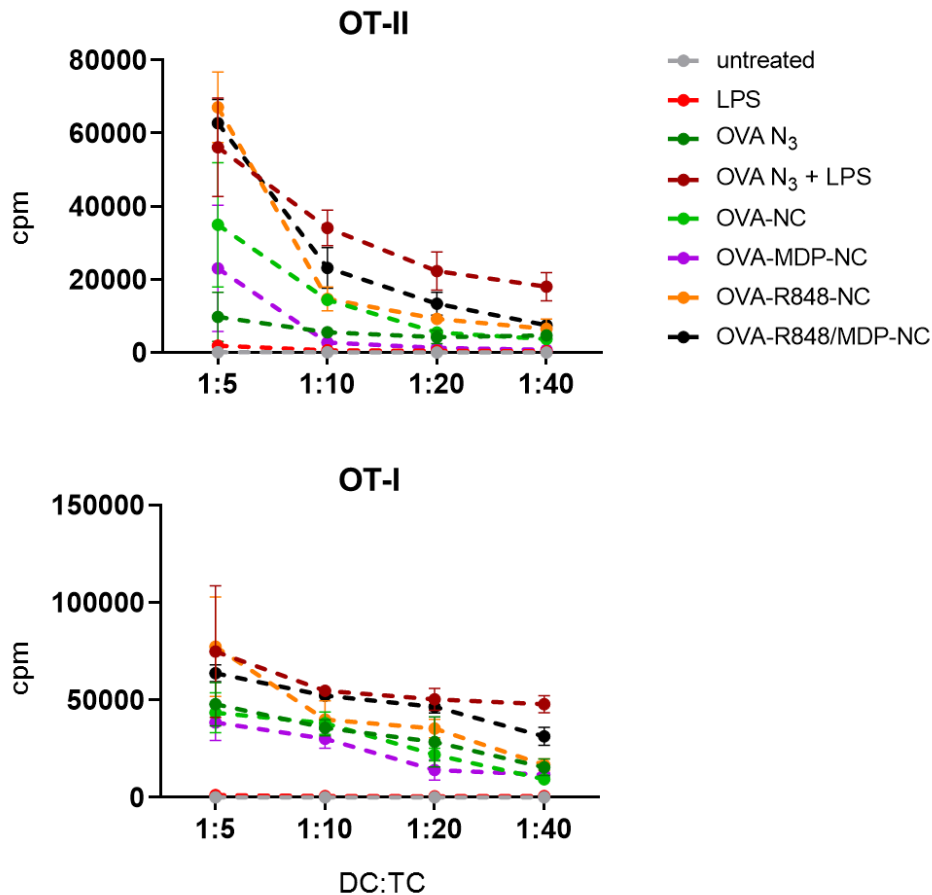


Figure 5. Adjuvant-loaded OVA-NCs induce antigen-specific DC-mediated T cell proliferation. BMDCs (10^6 cells/mL) were incubated with different OVA-NC formulations [$10 \mu\text{g/mL}$] in 12-well plates ($V = 1 \text{ mL}$) for 24 h. Treatment with LPS [100 ng/mL] served as control. Titrated numbers of BMDCs (starting with 10^5 cells/mL) were co-cultured with OVA peptide-specific T cells isolated from spleens derived from OT-II or OT-I mice (5×10^5 cells/mL) in triplicates in 96 well plates. After 3 days, T cell proliferation was measured by ^3H -thymidine incorporation. Data represent mean \pm SD.

Since the immune system is a complex network of different immune cells and stimulating molecules, the potential of adjuvant-loaded OVA-NCs to elicit anti-tumor immune responses against OVA-expressing B16/F10 melanoma was investigated *in vivo*. Treatment of B16/F10-OVA melanoma-bearing mice with non-loaded OVA-NCs, OVA-MDP-NCs, and OVA-R848-NCs reduced the tumor growth and prolonged the overall survival by up to 8 to 12 days (Fig. 6, Fig. 7, Fig. 8). No significant differences in survival compared to the treatment with non-loaded OVA-NCs combined with soluble adjuvants could be observed (Fig. 6, Fig. 7, Fig. 8). Enhanced anti-tumoral immune responses which strongly reduced B16/F10-OVA tumor growth, were triggered by vaccination with MDP/R848-loaded OVA-NC formulation (Fig. 6, Fig.

7). This NC therapy approx. doubled the survival time of melanoma-bearing mice, with one individual exhibiting complete tumor remission (Fig. 8).

However, complete tumor remission was not induced by administration of MDP/R848-loaded OVA-NCs. Therefore, a combination of the Toll-like receptor 7/8 agonist R848 with the potent stimulator of interferon genes (STING) agonist diamidobenzimidazole (compound 3) was tested in subsequent experiments for its potential to induce stronger anti-tumor immune responses *in vitro* and *in vivo* (see Chapter C).

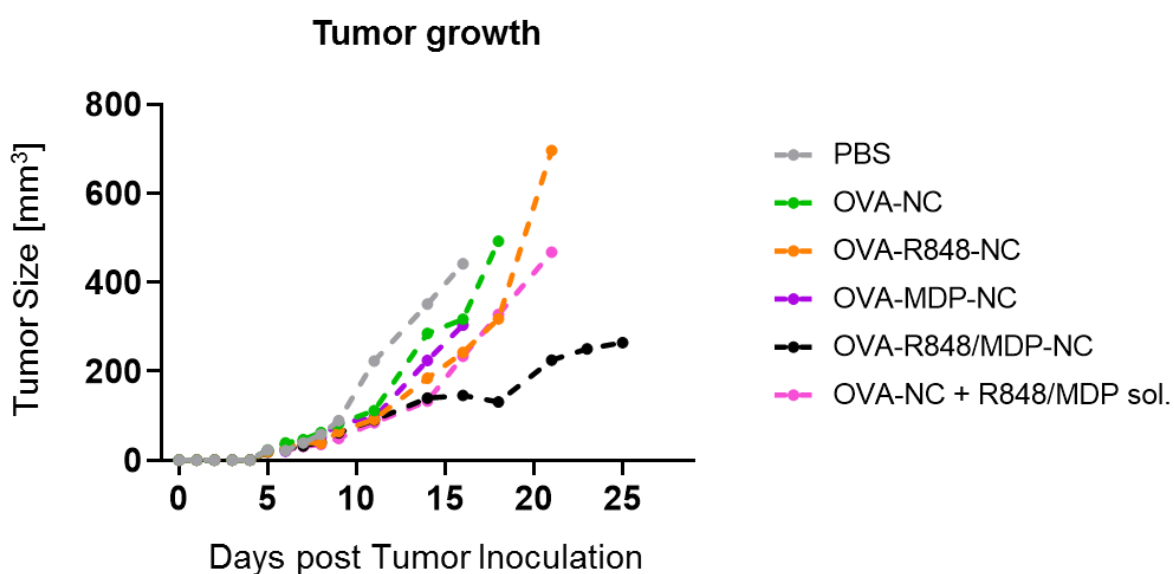


Figure 6. B16/F10-OVA tumor growth following treatment with 3x 500 μ g adjuvant-loaded OVA-NCs or non-loaded OVA-NCs in combination with soluble adjuvants. Treatment with PBS and non-loaded OVA-NCs served as controls (n = 5). Data represent mean only.

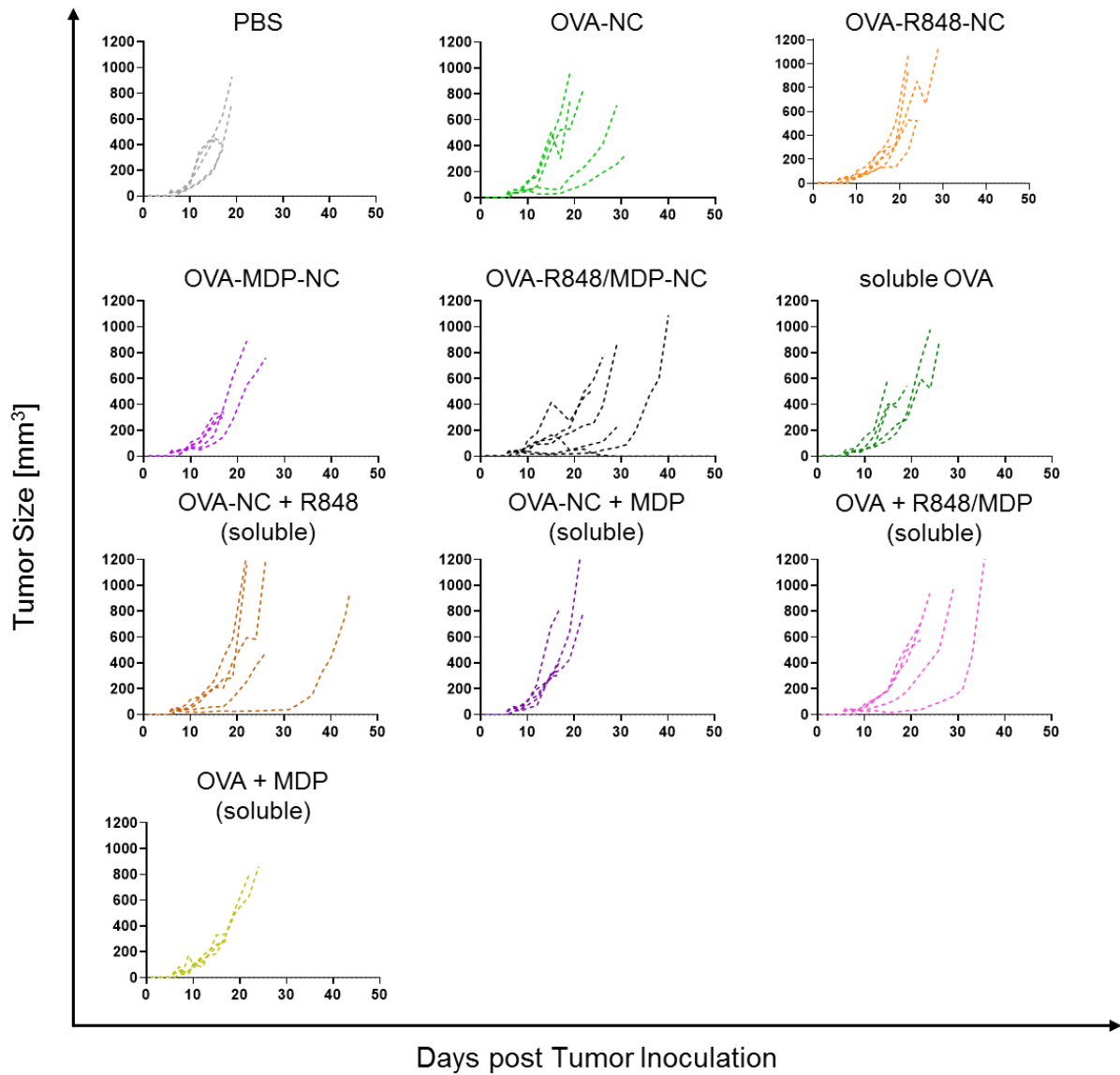


Figure 7. B16/F10-OVA tumor growth curves of individual mice of different treatment groups. C57BL/6J mice were injected with 5×10^5 B16/F10-OVA cells subcutaneously and treated at a tumor size of 25 to 50 mm³. Adjuvant-loaded OVA-NCs as well as non-loaded OVA-NCs and soluble adjuvants were injected subcutaneously at days 6, 13 and 20 post tumor cell inoculation ($3 \times 500 \mu\text{g}$). Treatment with PBS and non-loaded OVA-NCs served as controls ($n = 5$).

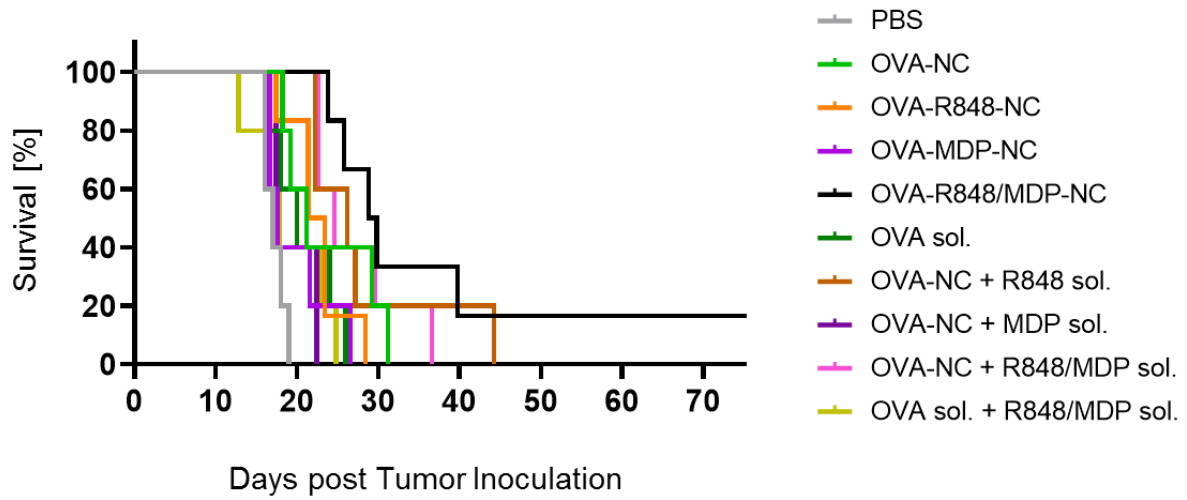


Figure 8. Overall survival for each group of NC treated B16/F10-OVA melanoma-bearing mice (n = 5).

Acknowledgement

This work was supported by the Deutsche Forschungsgemeinschaft (DFG) through the CRC1066 in subproject Q2 and Q6.

Chapter C

Chapter C is a nearly word-to-word reproduction of the submitted paper “*Co-delivery of STING and TLR7/8 agonists in antigen-based nanocapsules to dendritic cells enhances CD8⁺ T cell-mediated melanoma remission*” in the peer-reviewed journal *Advanced Materials*. Figures were created with BioRender.com.

Contribution

Chapter C was written by Jenny Schunke. Adjuvant-loaded OVA-NCs were synthesized by Dr. Natkrittta Hüppe and Katja Klein. Biological assays *in vitro* were performed by Jenny Schunke. *In vivo* tumor studies were conducted by Jenny Schunke with support by Dr. Michael Fichter. Nicole Mangazeev performed *in vitro* assays with monocyte-derived dendritic cells under guidance of Jenny Schunke. Kai R. Speth conducted the protein corona analyses. Tanja Klaus, Vanessa Bolduan, Dr. Michael Kuske and Paul Schneider assisted Jenny Schunke with the dissection of organs from mice as well as the preparation of the cell suspensions.

Co-delivery of STING and TLR7/8 agonists in antigen-based nanocapsules to dendritic cells enhances CD8⁺ T cell-mediated melanoma remission

Jenny Schunke^a, Natkrittta Hüppe^b, Nicole Mangazeev^a, Kai R. Speth^{a,b}, Tanja Klaus^a, Vanessa Bolduan^a, Michael Kuske^a, Paul Schneider^a, Stephan Grabbe^a, Katharina Landfester^{b,*}, Volker Mailänder^{a,b,*}, Michael Fichter^{a,b}

^a Department of Dermatology, University Medical Center Mainz, Langenbeckstraße 1, 55131 Mainz, Germany

^b Max Planck Institute for Polymer Research, Ackermannweg 10, 55128 Mainz, Germany

* Corresponding authors: mailaend@mpip-mainz.mpg.de, landfest@mpip-mainz.mpg.de

Abstract

Insufficient efficacy of tumor vaccines still represents a major challenge due to poor adjuvant potency. Combining antigen and adjuvants of different classes bears the potential to induce a broad spectrum of anti-tumor immune responses. Here we demonstrate a novel nanocarrier (NC)-based vaccine combining the type I interferon-triggering STING agonist diamidobenzimidazole (diABZI) compound 3 and the well-established TLR7/8 agonist resiquimod (R848). Encapsulation of both adjuvants into polymeric nanocapsules enables the simultaneous transport of immunostimulatory molecules with tumor antigens. Thereby achieved co-delivery further improved DC stimulation and subsequent anti-tumor immune responses.

Combined encapsulation of R848 and diABZI enhanced DC activation and induced stronger antigen-specific T cell responses compared to the single adjuvant NC treatment or using soluble forms of antigens and adjuvants *in vitro* and *in vivo*. This was determined by the vigorous expression of CD80, CD83, and CD86. Furthermore, the dual adjuvant therapy initiated the highest secretion levels of different pro-inflammatory cytokines and chemokines.

Moreover, a substantial antigen-specific T cell proliferation led to robust tumor remission in a murine B16/F10 melanoma model. Subcutaneous administration of R848/diABZI-loaded NCs induced enhanced infiltration of CD4⁺ and CD8⁺ T cells as well as neutrophils in tumor-draining lymph nodes (LN) and tumor tissue. Encapsulating the melanoma-specific antigenic peptide of TRP-2 into the adjuvant-loaded NCs reduced the growth of B16/F10 melanoma and prolonged the overall survival. The herein presented novel anti-tumor vaccination strategy avoids the use of structural compounds, increases the antigen load of dendritic cells, uses a fixed combination of antigen and two potent adjuvants and bears the potential to overcome the immunosuppressive tumor microenvironment inducing vigorous antigen-specific anti-cancer immunity.

1. Introduction

The aim of vaccination in the context of cancer therapy is to activate the immune system in a tumor-specific manner and thus, to induce tumor cell killing and remission. For this purpose, the specific capability of antigen-presenting cells (APCs), in particular dendritic cells (DCs), to take up and process antigens and activate T cells can be exploited.^[199-200] In addition, the administration of adjuvants to induce a strong and directed immune response is required in order for DCs to be activated. As components of an adjuvant-based therapeutic vaccination, stimulator of interferon genes (STING) agonists and ligands of Toll-like receptors (TLRs) can be used for vigorous DC activation and maturation.^[107, 201] Both pathways of stimulation should

be additive or even synergistic in the best scenario. Induction of the cGas-STING pathway leads to an effective activation of the immune system against viral infections via production of type I interferons (IFN).^[202-203] TLRs belong to the family of pattern recognition receptors and play an important role in the endogenous defense against pathogens. The binding of Pathogen Associated Molecular Patterns (PAMPs) to their specific receptor, such as STING or TLRs, induces acute inflammatory immune responses accompanied, among others, by the secretion of pro-inflammatory cytokines, representing a prerequisite for effective tumor therapies. Furthermore, both, TLR and STING signaling are important for the initiation of the adaptive immune system, involving of T and B lymphocytes.^[204] This is based on the expression of co-stimulatory molecules, such as CD80 and CD86, and the migration of mature DCs to draining lymph nodes following antigen uptake, subsequently priming T lymphocytes by antigen presentation via MHC molecules and affecting different immune cells by cytokine secretion.^[200-201] Of particular interest for cancer immunotherapies are plasmacytoid DCs (pDCs) and conventional DCs type I due to their capability to cross-present exogenous antigens on MHC class I molecules and thereby activating CD8⁺ T cells. It has been shown, that high type I interferon levels within various solid tumors are associated with a better outcome *in vivo*^[108]. Both DC subtypes produce substantial amounts of type I interferons upon activation and can initiate a pro-inflammatory anti-tumor immune response.^[205-206]

A strong and targeted activation of the immune system to fight cancer is explicitly necessary, since numerous tumor escape mechanisms decrease the response to immunotherapies. These include the loss of tumor-specific antigens, reduced or absent expression of MHC class I molecules by tumor cells, and downregulation of T cell activity via immune checkpoint receptors.^[207-209] These factors lead to a reduced activation of T cells and subsequently to a decreased infiltration rate into tumor tissues. Patients with so-called cold tumors, characterized by a pronounced immunosuppressive tumor microenvironment, respond poorly to many immunotherapies.^[210] In contrast, it was shown, that patients with high numbers of infiltrating T cells (especially CD3⁺/CD8⁺ T cells) and high levels of intra-tumoral pro-inflammatory cytokines (hot tumors) often respond to immunotherapies resulting in a better survival prognosis. This is specifically true for melanoma tumors.^[211] To convert cold tumors into hot tumors, DC-based immunotherapies have been developed.^[210] TLR ligands or STING agonists are often used in this therapeutic approach due to their potential to trigger pro-inflammatory immune responses.^[212-214] This is characterized by the production of cytokines, such as IL-12 or type I interferons (IFN- α , IFN- β). In general, DCs offer versatile options to generate an extensive antigen-specific immune response in the context of tumor therapy.

Adjuvant-loaded antigen-based nanocapsules provide an effective and combined delivery of both, antigens and adjuvants, to dendritic cells in a protected and coordinated manner. This prevents non-specific activation of other immune cells, the concomitant delivery of antigen and adjuvants and ensures hereby effective and enhanced antigen presentation by each DC. In particular, biodegradable protein-based nanocapsules are of relevance with regard to subsequent application in humans. Herein, we report tremendous DC activation *in vitro* and *in vivo* with combined delivery of TLR7/8 agonist R848, STING agonist (diABZI compound 3), and tumor antigen in bio-orthogonally crosslinked ovalbumin nanocapsules (OVA-NCs). The effective DC maturation following NC uptake was evaluated by upregulation of co-stimulatory molecules and secretion of pro-inflammatory cytokines as well as the resulting antigen-specific T cell activation *in vitro* and *in vivo*. Additionally, we show that vaccination with adjuvant-loaded OVA-NCs induced side effect-free tumor remission in the B16/F10 mouse model and the generation of a long-term immune memory determined by tumor cell re-challenge of cured mice.

2. Materials and Methods

2.1 Azidation of ovalbumin (with 1-imidazole-sulfonyl azide hydrochloride)

The azidation of ovalbumin was performed as previously described by Hüppe *et al.* [156] Briefly, 1 g ovalbumin (Sigma Aldrich, United States) was dissolved in 20 mL K_2CO_3 solution (pH 11). 1-imidazole-sulfonyl azide hydrochloride (276 mg) was dissolved in 2 mL water and added dropwise to the ovalbumin solution. NaOH (1 M) was used to adjust the pH of the solution to pH 11 and the solution was stirred at room temperature for 48 h. The azidized ovalbumin was purified by dialysis (MWCO 1 kD) and subsequently lyophilized with a yield of 0.78 g. The number of azide groups was quantified by fluorescamine assay (Alfa Aesar, United States) in borate buffer at pH 8.2.

2.2 Synthesis of ovalbumin nanocapsules

The synthesis of ovalbumin nanocapsules was performed in line with the previously described method by Hüppe *et al.* [156] Briefly, the azide-functionalized ovalbumin (50 mg) was dissolved in 0.4 mL NaCl solution ($c = 14.4$ mg/mL) or aqueous solution containing adjuvants and 100 μ L Cy5-Oligo ($c = 0.1$ nmol/ μ L; IBA Lifesciences, Germany) was added. 35.7 mg of the surfactant poly((ethylene/butylene)-block-(ethylene oxide)) (P((E/B)-b-EO)) were dissolved in 7.5 g of cyclohexane (VWR, United States) and the mixture was added to the aqueous solution. The two phases were homogenized by ultrasound under ice cooling (70% amplitude, 3 min, 20 s pulse, 10 s pause) to form a miniemulsion. In a third step, 10.7 mg P((E/B)-b-EO) and 35.7 mg 1,6-hexanediol dipropionate (HDDP) crosslinker was dissolved in 5 g of cyclohexane,

added dropwise to the miniemulsion and the reaction proceeded at 40 °C for 24 h while stirring. Subsequently, the ovalbumin nanocapsules (OVA-NCs) were purified by centrifugation (3x, 1,500 x g, 20 °C) and washing with cyclohexane in order to remove excess surfactant and crosslinker. The nanocapsules (500 µL) were transferred to aqueous media by dropwise adding to 5 mL of a 0.1wt% sodium dodecyl sulfate (SDS; Sigma Aldrich, United States) solution under shaking in an ultrasonication bath for 3 min (35 kHz, 20 °C). The dispersion was stirred open overnight in order to evaporate the cyclohexane. Finally, nanocapsules were purified by centrifugation (3x, 500 x g, 30 min, 20 °C) in Amicon Ultra-2 centrifugal filters (MWCO 50 kDa; Merck Millipore, United States) and washed with water.

2.3 Encapsulation efficiency of Cy5-Oligo and adjuvants

Nanocapsules (NCs) were transferred into 0.1wt% SDS. Afterwards, the unpurified dispersion containing the NCs was centrifuged at 500 x g for 30 min using an Amicon Ultra-2 centrifugal filter (MWCO 100 kDa). The encapsulation efficiency was determined after measuring the amount of free Cy5-Oligo in the supernatant using a microplate reader (Infinite M1000, Tecan, Switzerland), in proportion to the fluorescence intensity of the unpurified dispersion. The same procedure was applied to measure the permeability of the NCs after washing the aqueous dispersion and quantification of leaked dye.

To determine the amount of encapsulated adjuvants, the OVA-NCs were degraded using proteinase K (30 U/mL, 37 °C; Sigma Aldrich, United States) overnight. Released adjuvants and degraded NCs were separated from the enzyme via centrifugation using an Amicon Ultra-2 centrifugal filter (MWCO 3K, 30 min, 1,500 x g). The amount of encapsulated Cy5-Oligo, TLR7/8 agonist resiquimod (R848; InvivoGen, United States) and STING agonist diABZI (Selleckchem, United States) was determined by fluorescence measurements using a microplate reader (Infinite M1000, Tecan, Switzerland) (Cy5: $\lambda_{\text{ex}} = 649 \text{ nm}$, $\lambda_{\text{em}} = 668 \text{ nm}$; R848: $\lambda_{\text{ex}} = 260 \text{ nm}$, $\lambda_{\text{em}} = 360 \text{ nm}$; diABZI: $\lambda_{\text{ex}} = 260 \text{ nm}$, $\lambda_{\text{em}} = 400 \text{ nm}$). A reproducible encapsulation efficiency for all cargos from batch to batch could be observed.

2.4 Physicochemical characterization of nanocapsules

Adjuvant-loaded OVA-NCs were physicochemically characterized as previously described by Hüppe *et al.*^[156]. Briefly, size determination, zeta potential measurement, and SEM were performed as follows.

2.4.1 Dynamic light scattering (DLS)

To determine the average NC size and size distribution, either 10 μL of NCs were diluted in 1 mL cyclohexane. Samples were measured using a Malvern Zetasizer Nano S (Malvern Panalytical, United Kingdom) with the 90° scattering mode at 20 °C.

2.4.2 Zeta potential

Zeta potential of NCs in a 10^{-3} M potassium chloride solution was measured utilizing the ZetaNanosizer (Malvern Panalytical, United Kingdom) at 20 °C.

2.4.3 Scanning electron microscopy (SEM)

The morphology of nanocapsules was analyzed via scanning electron microscopy using a field emission microscope (LEO 1530 Gemini, Zeiss, Germany) with an accelerating voltage of 170 V. 2 μL of nanocapsule dispersion in cyclohexane were added to silica wafers (pre-cleaned in the plasma oven) and air-dried for 15 min and subsequently analyzed.

2.4.4 Confocal laser scanning microscopy

Confocal laser scanning microscopy was performed in order to visualize the uptake of Cy5-Oligo-loaded OVA-NCs with a Zeiss LSM 710 NLO (Zeiss, Germany). 3×10^5 BMDCs were cultured in 8-well chamber slides (#80827, ibidi, Germany) at 37 °C overnight after adding 10 $\mu\text{g}/\text{mL}$ OVA-NCs to each well. 4 mg/mL CellMask™ Orange (Life Technologies, United States) were added to the cells for cell membrane staining 5 min prior to analysis.

2.5 Animals

6-week-old C57BL/6J mice were obtained from Charles River Laboratories (Germany). OT-IxLy5.1 and OT-IxLy5.1 mice were bred and kept for experimental procedures at the University Medical Center Mainz (Germany) or at the animal facility of the Translational Animal Research Center (TARC), University Medical Center Mainz with food and water supply ad libitum according to the “Guide for Care and Use of Laboratory Animals”. The described experiments were approved by the local animal welfare authority (“Landesuntersuchungsamt Rheinland-Pfalz”).

2.6 Cultivation of BMDCs and splenocytes

GM-CSF bone marrow-derived dendritic cells (BMDCs) were generated and cultured as previously described by Bros *et al.*^[215] Briefly, bone marrow (BM) from 8- to 12-week-old C57BL/6J mice was harvested from femur and tibia, erythrocytes were lysed with 1 mL Gey's Red Cell Lysis Buffer for 1 min (155 mM NH_4Cl , KHCO_3 , EDTA 100 μM , pH 7.4), and BM cells were seeded in 12-well plates (2×10^5 – 4×10^5 cells/mL; Sarstedt, Germany). BMDCs were

differentiated from BM progenitor cells by culturing for 7 to 8 days with GM-CSF-supplemented (10 ng/mL) culture medium (IMDM containing 5% FCS, 2mM L-glutamine, 100 U/mL penicillin, 100 µg/mL streptomycin, 50 µM β-mercaptoethanol). Medium and supplements were purchased from Sigma Aldrich (United States) and Thermo Fisher Scientific (United States). FBS was purchased from PAN-Biotech (Germany). Cell culture medium was changed on days 3 and 6. Splenocytes were isolated from dissected spleens of C57BL/6J mice. A single-cell suspension was obtained by grinding the dissected spleens through 40 µm-cell strainers (Sarstedt, Germany). For culturing, cells were adjusted to a concentration of 2×10^6 splenocytes/mL using cell culture medium (see above) and seeded in 12-well plates ($V = 1$ mL) or 96-well plates ($V = 200$ µL).

2.7 Generation of human monocyte-derived dendritic cells

Peripheral blood mononuclear cells (PBMCs) were isolated from buffy coats, received from healthy donors upon informed consent (Blood Bank of the University Medical Center Mainz) as previously described by Fichter *et al.*^[216]. Briefly, PBMCs were separated from other blood cells by centrifugation for 20 min at 900 x g and room temperature through Histopaque-1077 density gradient media (Sigma Aldrich, United States). PBMCs were extracted from the interphase, washed with PBS, and CD14⁺ monocytes were isolated using magnetic cell separation via CD14 MicroBeads (MACS, Miltenyi Biotec, Germany). The received cells were then washed and cultured at a concentration of 10^6 in 6-well plates (Greiner, Austria) in IMDM medium supplemented with 10% FBS, 1% GlutaMAX, 1% beta-mercaptoethanol, 1% non-essential amino acids, 1 mM sodium pyruvate, 100 U/mL penicillin and 100 g/mL streptomycin. Lastly, GM-CSF (200 U/mL) and IL-4 (200 U/mL) were added to each well. Cells were cultured for 6 days at 37 °C and 5% CO₂ with addition of 1 mL fresh medium containing GM-CSF (600 U/mL) and IL-4 (600 U/mL) at days 2 and 4. Cytokines were purchased from PeproTech (Thermo Fisher Scientific, United States).

2.8 Incubation of OVA-NCs and soluble adjuvants *in vitro*

Immature BMDCs were treated with soluble adjuvants or adjuvant-loaded OVA-NCs after preliminary removal of the culture medium at days 7 or 8 of culturing. Both splenocytes and BMDCs were treated with non-loaded and adjuvant-loaded OVA-NCs at concentrations of 0.1 µg/mL to 100 µg/mL in a total volume of either 1 mL or 200 µL cell culture medium (see section 2.6) in 12-well or 96-well plates, respectively. 10^{-4} µg/mL to 10 µg/mL of soluble adjuvants were added to the cell culture. Additionally, LPS (0.1 µg/mL, Merck Millipore, United States) was added to the cell culture as a positive control for stimulation. Cells were cultured at 37 °C and 7.5% CO₂ for 24 h, and analyzed for NC uptake and expression of surface markers via flow

cytometry (2.10.1). To analyze cytokine and chemokine secretion, culture supernatants were collected after 24 h of incubation and further processed as described below (2.9).

Human monocyte-derived dendritic cells (moDCs) were seeded into 96-well plates after 6 days of culturing at a concentration of 10^6 cells/mL. OVA-NC formulations were added at concentrations of 10^{-3} $\mu\text{g/mL}$ to 100 $\mu\text{g/mL}$ in a total volume of 200 μL . Cells were further cultured at 37 °C and 7.5% CO_2 for 24 h, and analyzed for NC uptake and expression of surface markers via flow cytometry (2.10.1). To analyze cytokine and chemokine secretion, culture supernatants were collected after 24 h of incubation and further processed as described below (2.9).

2.9 Cytokine Assay

The cytokine secretion of cultivated and pretreated cells as well as cytokine levels in murine sera were quantified using a multiplex bead-based immunoassay (LEGENDplex Mouse Anti-Virus Response Panel (13-plex), LEGENDplex Human Anti-Virus Response Panel (13-plex, BioLegend, United States) in accordance with manufacturer's instructions. Data analysis was performed using LEGENDplex v8.0 software (BioLegend, United States).

2.10 Flow Cytometry and Antibodies

Flow cytometric analyses were performed using the Attune NxT Flow cytometer (Thermo Fisher Scientific, United States) and measurements were analyzed with the Attune NxT software v3.2.1 (Thermo Fisher Scientific, United States).

2.10.1 NC-mediated DC maturation

BMDCs and splenocytes were harvested 24 h after treatment with 0.1 to 100 $\mu\text{g/mL}$ OVA-NCs (adjuvant-loaded and non-loaded) or 10^{-4} to 10 $\mu\text{g/mL}$ soluble adjuvants, seeded in 96-well v-bottom plates and incubated with rat anti-mouse CD16/CD32 Ab (clone 2.4G2) diluted 1:100 in PBS, supplemented with 2% FBS and 2 mM EDTA, to block Fc receptor-mediated staining for 10 min at room temperature. Thereafter, the cells were stained with antibodies specific for CD11c (PE-Cy7, clone N418), MHC class II-A^{b,d,q/l-Ed} (eFluor450, clone M5/114.15.2), CD80 (PE, clone 16-10A1) and CD86 (FITC, clone GL1) in a total volume of 100 μL for 20 min at 4 °C. All antibodies were purchased from Thermo Fisher Scientific (United States). Dead cells were discriminated from living cells by adding 100 μL Fixable Viability Dye (eFluor™ 506, ThermoFisher) diluted 1:1000 in PBS for 25 min at 4 °C.

MoDCs were incubated with a Fc receptor-blocking antibody (BD Biosciences, United States) diluted 1:100 in PBS, supplemented with 2% FBS and 2 mM EDTA, for 15 min at room temperature. Afterwards, cells were stained with antibodies specifically binding to HLA-ABC

(BB700, clone: G46-2.6), HLA-DR (BV711, clone: G46-6), CD11c (FITC, clone: B-ly6), CD14 (APC-Cy7, clone: MP ϕ 9), CD80 (BV421, clone: L307.4), CD83 (PE), and CD86 (PE-Cy7, clone: FUN-1) in a total volume of 100 μ L for 30 min at 4 °C. All antibodies were purchased from BD Biosciences (United States). Dead cells were discriminated from living cells by adding 100 μ L Fixable Viability Dye (eFluor™ 506; Thermo Fisher Scientific, United States) diluted 1:1000 in PBS for 25 min at 4 °C.

2.10.2 Analysis of infiltrating immune cells

Murine tumors were dissected and tumor cell suspensions were generated using the Tumor Dissociation Kit, mouse (Miltenyi Biotec, Germany) according to manufacturer's instructions. Cells from inguinal lymph nodes were obtained by grinding through 40 μ m-cell strainers and resuspended in PBS supplemented with 2% FBS and 2 mM EDTA, for further use.

Organ- and tumor tissue-infiltrating immune cells were identified via staining with antibodies specific for CD3 (PE-CF594, clone 145-2C11/ APC, clone REA641), CD4 (eFluor450, clone RM4-5), CD8 (APC-Cy7, clone 53-6.7), CD25 (FITC, clone PC61.5.3), CD62L (APC, clone DX5), CD69 (BV11, clone HK1.4), CD44 (PE, clone IM7), NK1.1 (PE, clone PK136), CD11b (PE-Cy7, clone M1/70), Ly6C (eFluor450, clone HK1.4), Ly6G (PE-eFluor610, clone RB6-8C5), PD-1 (BV711, clone 29F.1A12), and TIM-3 (BB700, clone 5D12/TIM-3). Dead cells were stained as previously described with Fixable Viability Dye (see section 2.10.1). Antibodies and Fixable Viability Dye were purchased from Thermo Fisher Scientific (United States).

2.10.3 DC subpopulations

To distinguish DC subpopulations and to exclude other immune cells, splenocytes were stained with antibodies specific for CD3 (FITC, clone 145-2C11), CD19 (FITC, clone MB19-1), CD14 (FITC, clone rmC5-3), NK1.1 (FITC, clone PK136), Ly6G (FITC, clone REA526), CD11c (PE-CF594, clone N418), CD11b (BV711, clone M1/70), MHC-II (PerCP-Cy5.5, clone M5/114.15.2), Siglec-H (APC, clone 551), CD8a (APC-Cy7, clone 53-6.7), CD172a (PE-Cy7, clone P84) and XCR1 (BV421, clone ZET). Dead cells were stained as previously described with Fixable Viability Dye (see section 2.10.1). Antibodies and Fixable Viability Dye were purchased from Thermo Fisher Scientific (United States).

2.11 Analysis of OVA-NC protein corona

2.11.1 Protein corona preparation

Aliquots of the nanocapsule formulations accounting for a particle surface area of 0.05 m² in a total volume of 300 μ l LC-MS grade water (Biosolve, France) were incubated with 1 mL of murine citrate plasma (Innovative Research, USA) for 1 h at 37 °C and 300 rpm shaking.

Afterwards, nanocapsules were pelleted by centrifugation (10,000 x g) for 1 h at 4 °C and subsequently washed with 1 mL PBS. This washing procedure was repeated three times. Protein corona proteins were eluted from nanocapsule surfaces by resuspension in 100 µL desorption buffer (2% sodium dodecyl sulfate, 62.5 mM Tris-HCl) and heating up to 95 °C for 5 min and subsequent centrifugation at 10,000 x g and 4 °C. Remaining supernatant was subjected to protein quantification using a Pierce™ assay (Thermo Fisher Scientific, United States) and protein analysis using liquid chromatography coupled to mass spectrometry (LC-MS).

2.11.2 In-solution digestion

Proteins were digested as previously described^[217-218].

Briefly, Pierce™ detergent removal columns (Thermo Fisher Scientific, United States) were used to remove SDS. Protein precipitation was achieved using the ProteoExtract® Protein Precipitation Kit (Merck Millipore, United States) according to the manufacturer's instruction. Precipitated proteins were resuspended with an 50 mM ammonium bicarbonate buffer supplemented with RapiGest™ SF (Waters Cooperation, United States) and incubated for 15 min at 80 °C shaking at 300 rpm. Protein reduction was achieved by incubation with 5 mM dithiothreitol (DTT; Sigma Aldrich, United States) for 45 min at 56 °C shaking at 300 rpm, followed by alkylation with iodoacetoamide (15 mM, Sigma Aldrich, United States) for 60 min at room temperature. Proteins were enzymatically degraded using trypsin (protein:trypsin ratio: 50:1) for 17 h at 37 °C shaking at 300 rpm. The reaction was stopped by adding 2 µL hydrochloric acid (Sigma Aldrich, United States) and subsequent incubation for 45 min at 37 °C shaking at 300 rpm.

2.11.3 Liquid chromatography coupled to mass spectrometry (LC-MS)

For absolute protein quantification, the reference peptide standard Hi3 E.coli (Waters Cooperation, United States) was spiked into all peptide samples at a concentration of 50 fmol/µL.^[219]

Analyses were performed using a nanoACQUITY ultra-performance liquid chromatography (UPLC) coupled to a Synapt G2-Si mass spectrometer (Waters Cooperation, United States) with settings as described previously by our group^[220]. Briefly, ionization was carried out with a NanoLockSpray source in positive ion mode and the Synapt G2-Si was operated in resolution mode performing data-independent acquisition experiments. MassLynx 4.1 and Progenesis QI (2.0) was used for data analysis. The murine proteome as well as the sequence for ovalbumin (accession no.: P01012) as reference data for peptide identification was downloaded from Uniprot (Swiss-Prot reviewed). Protein quantification was carried out based on the TOP3/Hi3

approach providing the absolute amount of each protein in fmol.^[221] The relative amount of the most abundant proteins in each sample was calculated. Complete lists with all identified proteins are provided in the ESI.

2.12 Tumor cell culture

B16/F10 and B16/F10-OVA-Luc cells (provided from TRON, Mainz, Germany) were cultured in DMEM (Dulbeccos's Modified Eagle's Medium, 4,500 mg/L glucose; Sigma Aldrich, United States) supplemented with 10% FBS (heat-inactivated), 1% GlutaMAX as well as 100 U/mL penicillin/100 g/mL streptomycin in T-175 flasks (Sarstedt, Germany) at 37 °C and 7.5% CO₂. For tumor inoculation, B16/F10 cells were harvested at 70% confluence with trypsin-EDTA (0.05% trypsin, 0.02% EDTA; Sigma Aldrich, United States) for 3 min at 37 °C.

2.13 Tumor cell inoculation and immunization with OVA-NCs

B16/F10 cells were harvested and adjusted to a concentration of 5x10⁶/mL with sterile PBS (Sigma Aldrich, United States). 100 µL (5x10⁵ cells) were injected subcutaneously into the right flank of shaved mice. Tumor size was determined by caliper measurement and tumor volume was calculated (longest dimension x perpendicular dimension x perpendicular dimension / 2). First OVA-NC injection was performed at a tumor size between 25 to 50 mm³. Tumor-bearing mice were immunized three times weekly with either as follows: (i) PBS, (ii) OVA-NC, (iii) OVA-R848-NC, (iv) OVA-diABZI-NC, (v) OVA-R848-diABZI-NC, (vi) OVA-NC + soluble (sol.) R848, (vii) OVA-NC + sol. diABZI, (viii) OVA-NC + sol. R848/diABZI, (ix) sol. OVA + sol. R848/diABZI. Mice received 50 µg – 500 µg OVA-NCs per injection. Soluble adjuvants were applied in equimolar doses compared to the adjuvant-loaded nanocapsule formulations.

In order to analyze DC maturation *in vivo*, nanocapsule formulations were injected subcutaneously into the tail base and immune cells of inguinal lymph nodes were isolated 24 h following injection. Cells were stained for flow cytometry according to section (see section 2.10.1).

2.14 NC biodistribution and *in vivo* Imaging

350 µg of Cy5-Oligo-loaded (i) OVA-NC, (ii) OVA-R848-NC, (iii) OVA-diABZI-NC and (iv) OVA-R848/diABZI-NC were injected subcutaneously into the tail base of shaved mice. PBS and soluble Cy5-Oligo were injected as controls. After 24 h, inguinal lymph nodes (LN) were dissected, cell suspensions were generated and used for flow cytometric analyses of DC maturation. Therefore, cells were stained with antibodies specific for DC maturation markers (see section 2.10.1).

2.15 T cell proliferation assay *in vivo*

350 µg of (i) OVA-NC, (ii) OVA-R848-NC, (iii) OVA-diABZI-NC, (iv) OVA-R848/diABZI-NC, and soluble ovalbumin in combination with 10 µg CpG (ODN-1826) serving as positive control were subcutaneously injected into C57BL/6J mice. 24 h afterwards, naïve CD8⁺ T cells and CD4⁺ T cells were isolated from either OT-Ix Ly5.1 or OT-IIxLy5.1 mice via magnetic cell separation with the Naïve CD4⁺/CD8⁺ T cell isolation kit (Miltenyi Biotec, Germany) in accordance to manufacturer's instructions. Thereafter, isolated T cells were stained with Cell Trace Violet (Thermo Fisher Scientific, United States) accordingly to manufacturer's instructions and 1x10⁶ cells of each T cell subtype were injected intravenously into the pretreated mice. After 72 h, spleen and inguinal lymph nodes were dissected and single-cell suspensions were generated for flow cytometric analyses (see sections 2.6). Cells were stained with antibodies specific for CD3 (PE, clone 145-2C11), CD4 (PE-Cy7, clone RM4-5), CD8 (APC-Cy7, clone 53-6.7), and Ly5.1/CD45.1 (APC, clone A20). Antibodies were purchased from Thermo Fisher Scientific (United States). Heparinized murine blood samples were collected via cardiac puncture and centrifuged at 2,000 x g for 10 min at 4 °C. Plasma was used for cytokine and chemokine analyses using a bead-based immunoassay (LEGENDplex mouse anti-virus panel, BioLegend, United States) and stored at -80 °C until further use.

3. Results and Discussion

3.1 Synthesis of adjuvant-loaded ovalbumin nanocapsules

Ovalbumin nanocapsules (OVA-NCs) were synthesized via azide-alkyne click reaction under basic conditions using an inverse water-in-oil miniemulsion as described by Hüppe *et al.*^[156] By addition of HDDP to the inverse miniemulsion, the formation of protein shells through interfacial crosslinking could be initiated.^[159] A core-shell morphology was revealed by scanning electron microscopy. Furthermore, the NCs were characterized by dynamic light scattering (DLS), which displayed a NC diameter of 280 to 350 nm and a zeta potential of -30 to -45 mV. The amount of encapsulated Cy5-Oligo, TLR 7/8 agonist resiquimod (R848) and STING agonist diABZI was determined by fluorescence measurements. A reproducible encapsulation efficiency for all cargos was observed (Tab. 1).

Table 1. Physico-chemical characterization data of Cy5-labelled non-loaded and adjuvant-loaded ovalbumin nanocapsules (PDI: polydispersity index, ζ = zeta potential, EE: encapsulation efficiency).

	m(adjuvant) /mg (per mg OVA)	d_h (CH) /nm	PDI	ζ /mV	EE (Cy5%)	EE (R848/%)	EE (diABZI/ %)
OVA-NC	-	302	0.3	-32	65	-	-
OVA-R848-NC	0.014	327	0.27	-40	70	62	-
OVA-diABZI- NC	0.0148	340	0.38	-44	74	-	90
OVA- R848/diABZI- NC	0.014; 0.0148	288	0.53	-38	72.5	47	38

3.2 Combining soluble R848 and diABZI triggers vigorous DC maturation *in vitro*

Dendritic cells are the most important immune cells with regard to anti-tumor vaccination approaches due to their ability to orchestrate tumor antigen-specific immune responses.^[174, 200]

In order to evaluate, whether combined treatment with R848 and diABZI results in increased DC activation *in vitro* compared to single adjuvant treatment, splenocytes were co-incubated with different concentrations of soluble adjuvants. Both TLR7/8 agonists and STING agonists are known to induce strong activation of DCs and consequently CD8⁺ T cells.^[222-223]

The effect of dual adjuvant treatment was verified by determining the amount of secreted pro-inflammatory cytokines in the cell culture medium. A strongly increased production of the pro-inflammatory cytokines IFN- α , IFN- β , IFN- γ , IL-6, IL-12, and TNF- α (Fig. 1, SI Fig. 3) as well as the chemokines CCL5 and CXCL10 (SI Fig. 3) was measured in a concentration-dependent manner. A synergistic effect on cytokine production was achieved with the combined administration of R848 and diABZI for all cytokines and chemokines. Similar findings were also reported by Bhatnagar *et al.*, who investigated synergistic effects on the amount of secreted IL-6, IL-12 and TNF- α by BMDCs combining DMXAA (STING agonist) and 522 (TLR7/8 agonist).^[213] However, DMXAA failed in phase III clinical trials due to weak downstream type I interferon secretion, in contrast to the use of diABZI.^[224-226] Clearly, the combination even of the soluble adjuvants shows a very promising cytokine production. *In vivo* this can only work if both adjuvants together with the antigen end up in the same dendritic cell.

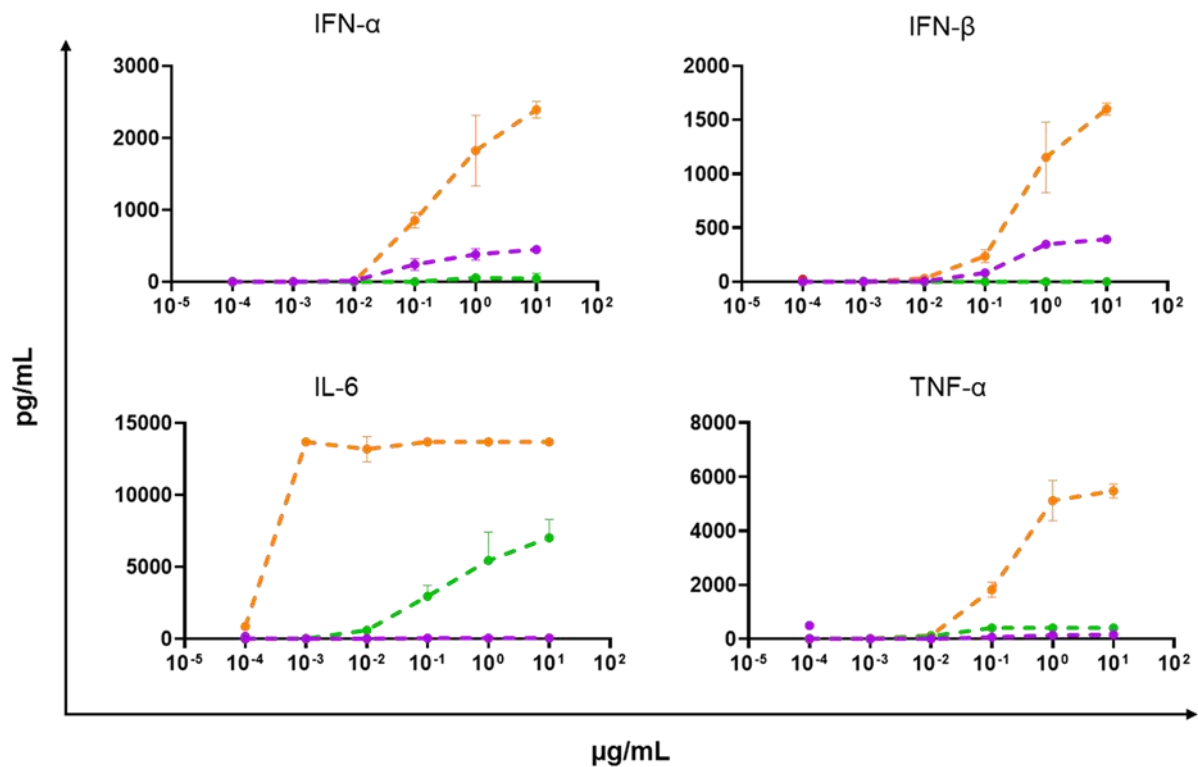


Figure 1. Secretion of pro-inflammatory cytokines by splenocytes *in vitro*. 4×10^5 cells were seeded into 96-well plates and treated with soluble R848 and diABZI compound 3 [10^{-4} to $10 \mu\text{g/mL}$] for 24 h ($n = 3$). LPS [100 ng/mL] served as positive control. The production of the pro-inflammatory cytokines IFN- α , IFN- γ , IL-6 and TNF- α was quantified using a bead-based immunoassay. Data represent mean \pm SD.

3.3 Uptake and toxicity of OVA-NCs

Particulate vaccines allow protected transport of antigens and adjuvants to DCs preventing non-specific uptake and elimination by other immune cells.^[227] To ensure the combined uptake of R848 and diABZI, both adjuvants were encapsulated into polymeric OVA-NCs. In order to evaluate the uptake of Cy5-Oligo-labelled OVA-NCs by DCs, flow cytometric and microscopic analyses of pretreated BMDCs were performed. Flow cytometry displayed a concentration-dependent amount of $\text{CD11c}^+/\text{Cy5}^+$ cells after 24 h with a maximum of approx. 75% at a treatment concentration of $100 \mu\text{g/mL}$ (Fig. 2 A). Confocal laser scanning microscopy measurements additionally verified the uptake of Cy5-labelled NCs into the cells (Fig. 2 B). The toxicity of non-loaded and adjuvant-loaded OVA-NCs in different concentrations was evaluated by staining pretreated BMDCs with Fixable Viability Dye followed by flow cytometric quantification of dead cells. In comparison to PBS-treated cells, serving as negative control, a slight increase in the percentage of dead cells was detectable after co-incubation with both diABZI-loaded NC formulations after 24 h, which can be explained by vigorous cell activation (SI Fig. 1). The amount of dead DCs was not increased after the treatment with non-loaded and R848-loaded OVA-NCs (SI Fig. 1).

3.4 OVA-R848/diABZI-NCs induce strong maturation of dendritic cells *in vitro*

The ability of adjuvant-loaded OVA-NCs to induce the maturation of splenic DCs *in vitro* was determined by the expression level of the maturation markers CD80 and CD86. Furthermore, the levels of secreted pro-inflammatory cytokines and chemokines were quantified. A concentration-dependent effect on maturation of splenic DCs was shown with adjuvant-loaded OVA-NCs, whereby the strongest expression levels of CD80 and CD86 were obtained with the administration of OVA-R848/diABZI-NCs (Fig. 2 C). In comparison, non-loaded OVA-NCs did not trigger DC maturation or cytokine production. At a concentration of 10 µg/mL or lower, the expression of CD80 and CD86 surpassed the levels triggered by the positive control (100 ng/mL LPS). Additionally, synergistic effects of R848 and diABZI in combination could be detected regarding the production of IFN- α , TNF- α , CCL5, and CXCL10 at concentrations starting from 10 µg/mL and 30 µg/mL, respectively. Treatment with 10 µg/mL to 30 µg/mL R848-loaded NCs induced a saturation of IL-6 and TNF- α production at approximately 2,300 pg/mL and 400 pg/mL (Fig. 2 D, SI Fig. 6). Stronger secretion levels could only be achieved by combined encapsulation with diABZI. Both single adjuvant-loaded NCs induced saturated production of CCL5 and CXCL10 starting from 10 µg/mL of approx. 500 pg/mL to 1,000 pg/mL, respectively (SI Fig. 6). Furthermore, R848-loaded NCs triggered the strongest IFN- γ secretion with approx. 600 pg/mL, 9-fold higher compared to the treatment with dual adjuvant-loaded NCs at a NC concentration of 100 µg/mL (Fig. 2 D). This observation can in part be explained by the 1.5-fold higher encapsulation rate of R848 in single adjuvant-loaded NCs in comparison to dual adjuvant-loaded NCs (see Table 1). Similar results regarding the secretion of pro-inflammatory cytokines and chemokines were observed for the treatment of GM-CSF and Flt3-L BMDC cultures. The highest secretion level of IL-12, IL-6, TNF- α , IFN- α , and IFN- β were elicited by dual adjuvant-loaded OVA-NCs in GM-CSF-supplemented BMDC culture (SI Fig. 4). Superadditive effects concerning the secretion levels of IFN- α , IFN- β , IFN- γ , IL-6, TNF- α , and CCL5 were induced with R848/diABZI-loaded NCs in Flt3-L BMDC cultures. The production of IL-12, CXCL1 as well as CCL2 could only be induced by the dual adjuvant-NCs (SI Fig. 5).

Treating human moDCs with diABZI- and R848/diABZI-loaded OVA-NCs resulted in dose-dependently increased expression of DC maturation markers CD80, CD83, and CD86 (SI Fig. 7). DC maturation was not triggered by the treatment with non-loaded or R848-loaded NCs (SI Fig. 7). Analyses of cytokine and chemokine production revealed similar effects of all NC formulations on DC maturation. Secretion of IL-6, IL-12p70, TNF- α , IFN- γ , and IFN- λ 1 was dose-dependently increased by the treatment with both diABZI-containing OVA-NC

formulations however, not through the administration of non-loaded and R848-loaded NCs (SI Fig. 8).

In order to determine possible effects of different protein corona compositions upon OVA-NC uptake by dendritic cells liquid chromatography-mass spectrometry (LC-MS) measurements were performed. The analysis of the most abundant corona proteins show mainly albumin adsorption on NC surfaces while there were no significant differences between OVA-NC formulations indicating no influence on NC uptake (SI Fig. 2). Due to degradation of OVA-NCs during corona preparation a high abundance of ovalbumin was found.

It has been shown that R848 and diABZI trigger a complementary cytokine secretion.^[224] Combining both adjuvants enables a versatile induction of pro-inflammatory and anti-tumoral immune responses. Additionally, not only additive but superadditive synergistic effects of the dual adjuvant-loaded NCs with respect to DC maturation could be observed, which can be explained by the simultaneous uptake of R848 and diABZI by DCs and subsequent stimulation via two signaling pathways. Superadditive synergistic effects on DC maturation by combined encapsulation of MDP (NOD2 agonist), R848 (TLR7/8 agonist) and Poly(I:C) (TLR3 agonist) in protein nanocapsules have already been reported by Paßlick *et al.*^[187] However, the production of type I interferons, necessary for an effective anti-tumor vaccination, was lacking. The importance of intratumoral and intranodal IFN- α and IFN- β secretion was also demonstrated in the context of melanoma therapy.^[212, 228]

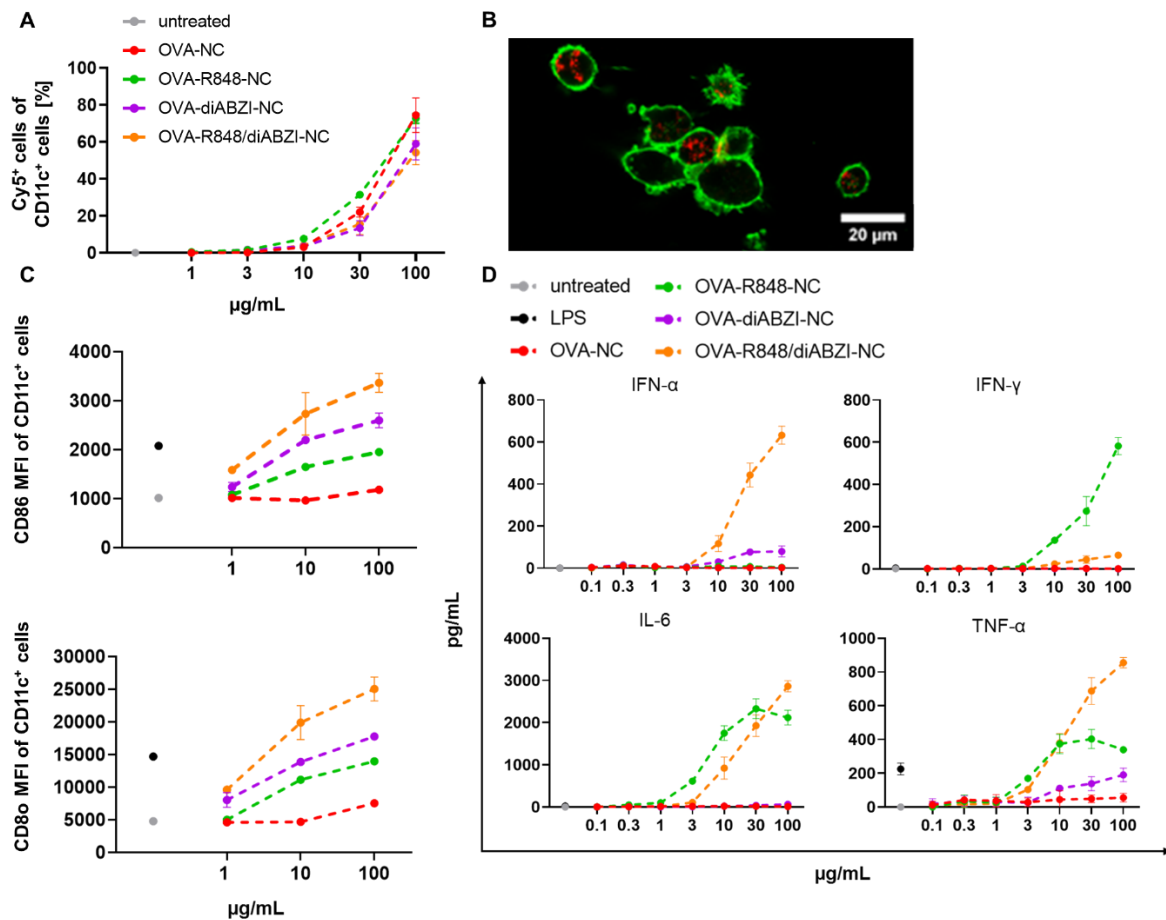


Figure 2. (A) Uptake of Cy5-Oligo-labelled OVA-NCs by BMDCs *in vitro*. 2×10^5 cells ($V_{\text{total}} = 1$ mL) were seeded into 12-well plates and co-incubated with 1 – 100 µg/mL OVA-NCs for 24 h. BMDCs were harvested and uptake was determined by flow cytometry ($n = 3$). (B) Confocal laser scanning imaging of OVA-NC (red) uptake by BMDCs (green). 3×10^5 BMDCs were treated with Cy5-loaded OVA-NCs (10 µg/mL) overnight. Plasma membrane was stained with CellMask™ Orange. (C) 2×10^5 cells were seeded into 12-well plates and treated with 1 - 100 µg/mL adjuvant-loaded OVA-NCs for 24 h. Non-loaded NCs and LPS [100 ng/mL] served as controls. Cells were harvested and analyzed for their expression levels of CD80 and CD86 via flow cytometry ($n = 3$). (D) 2×10^6 splenocytes were seeded into 12-well plates and co-incubated with 0.1 – 100 µg/mL OVA-NCs for 24 h. To quantify the secretion levels of pro-inflammatory cytokines, culture supernatants were analyzed with a bead-based assay. Data represent mean \pm SD.

3.5 Subcutaneous OVA-NC injection induced B16/F10-OVA melanoma remission *in vivo*

After these promising *in vitro* results we set out to test our approach in an *in vivo* mouse tumor model. Multiple reports have already shown the induction of DC activation *in vitro* and *in vivo* by combined encapsulation of different adjuvants or cytokines, as well as the subsequent activation of $CD4^+$ and $CD8^+$ T cells.^[156, 179, 213] Yet, many adjuvant combinations do not show sufficient efficacy to enable long-term tumor remission *in vivo*. This demonstrates that *in vitro* results of T cell activation can be surrogate markers, but need verification by *in vivo* experiments.

To verify whether NC-based DC maturation leads to a targeted anti-tumoral and long-lasting immune response *in vivo*, B16/F10-OVA melanoma-bearing mice were treated with adjuvant-loaded NCs in a prime-boost-boost regimen (Fig. 3 A). Treatment with diABZI-loaded OVA-NCs elicited complete tumor remission in 60% of mice and vaccination with R848/diABZI-loaded OVA-NCs resulted in complete tumor remission in 80% of mice after the second NC injection (Fig. 3 B, SI Fig. 9). Tumor antigen-specific activation of T cells and subsequent cancer cell killing was shown to be dependent of host type I interferon production, which could be increased by STING agonist application.^[224] Injection of non-loaded and R848-loaded OVA-NCs decelerated tumor growth compared to PBS-treated mice but did not result in long-term survival (Fig. 3 B, SI Fig. 9). Furthermore, the encapsulation of both adjuvants triggered a significantly stronger anti-tumor immune response compared to the treatment with non-loaded OVA-NCs in combination with soluble adjuvants. Additionally, using OVA-NC formulations, rather than soluble antigens for the vaccination approach, led to a stronger tumor growth reduction. In summary, encapsulation of the adjuvants as well as the protected transport via antigen-based NC to each DC and the orchestrated co-delivery of antigen and adjuvants enables an effective treatment of OVA-expressing B16/F10 tumors. The combined encapsulation of R848 and diABZI was therefore tested. Administration of R848- and diABZI-loaded OVA-NCs resulted in an increased overall survival from 20% to 60% in the observation period of 90 days compared to the treatment with diABZI-loaded OVA-NCs alone (Fig. 3 C). This can be explained by the observed stronger DC maturation by application of the dual adjuvant NCs.

In order to evaluate the lowest effective dose with respect to the induction of full tumor remission at day 30, a titration study with NC doses of 50 μg , 200 μg , 350 μg , and 500 μg per injection was performed (Fig. 3 D). A reduction in the amount of injected NCs to 350 μg still led to full eradication of B16/F10-OVA melanoma *in vivo* at day 30 in all animals, while lower doses did not achieve long-lasting tumor growth inhibition (Fig. 3 D). This indicates that a certain amount of antigen and adjuvants is crucial for the generation of sufficiently strong antigen-specific immune responses and complete tumor remission.

To achieve the strongest possible treatment effect, subcutaneous (s.c) NC injection was compared to intravenous NC injection *in vivo*. S.c. injection of dual adjuvant-loaded NCs induced full tumor remission and thus, a prolonged overall survival (Fig. 3 E, Fig. 3 F, SI Fig. 10), whereas intravenous (i.v.) injection solely reduced tumor growth (Fig. 3 E, SI Fig. 10). With s.c. application into the tail base, locally and systemically occurring DCs can be reached and the proximity to the tumor-draining lymph node allows rapid activation of T cells. S.c.-administered proteins can be transported directly to lymph node-resident DCs via the lymphatic

system and are additionally taken up and processed by cutaneous DCs.^[229] These can subsequently migrate to draining lymph nodes to prime and activate antigen-specific T cells.^[230] Comparing both injection routes when administering proteins, it was shown that a greater number of DCs took up and processed the proteins via s.c. injection, whereas with i.v. injection, mainly B lymphocytes were responsible for the uptake.^[229] Clinical trials for the treatment of breast cancer showed, that the bioavailability of subcutaneous treatment was not inferior to intravenous treatment.^[231]

To prove, whether the DC-mediated anti-tumor immune response was antigen-specific, B16/F10-OVA melanoma- as well as B16/F10 melanoma-bearing mice were treated with OVA-R848/diABZI-NCs in comparison (Fig. 3 G). Treating mice with OVA-expressing B16/F10 melanoma resulted in tumor remission, while the growth of B16/F10 tumors was only reduced (Fig. 3 H, SI Fig. 11). Herewith, the antigen-specific activation of T cells by activated DCs was proven. However, the treatment with adjuvant-loaded NCs triggered a general anti-tumoral activation of the murine innate immune system, since untreated B16/F10 tumors grew significantly faster. Cytokine-secreting DCs trigger the activation of innate immune cells, including NK cells, which in turn can destroy tumor cells.^[232] However, our vaccination approach based on adjuvant-loaded OVA-NCs demonstrated the necessity of tumor cell-killing antigen-specific T cells for tumor remission.

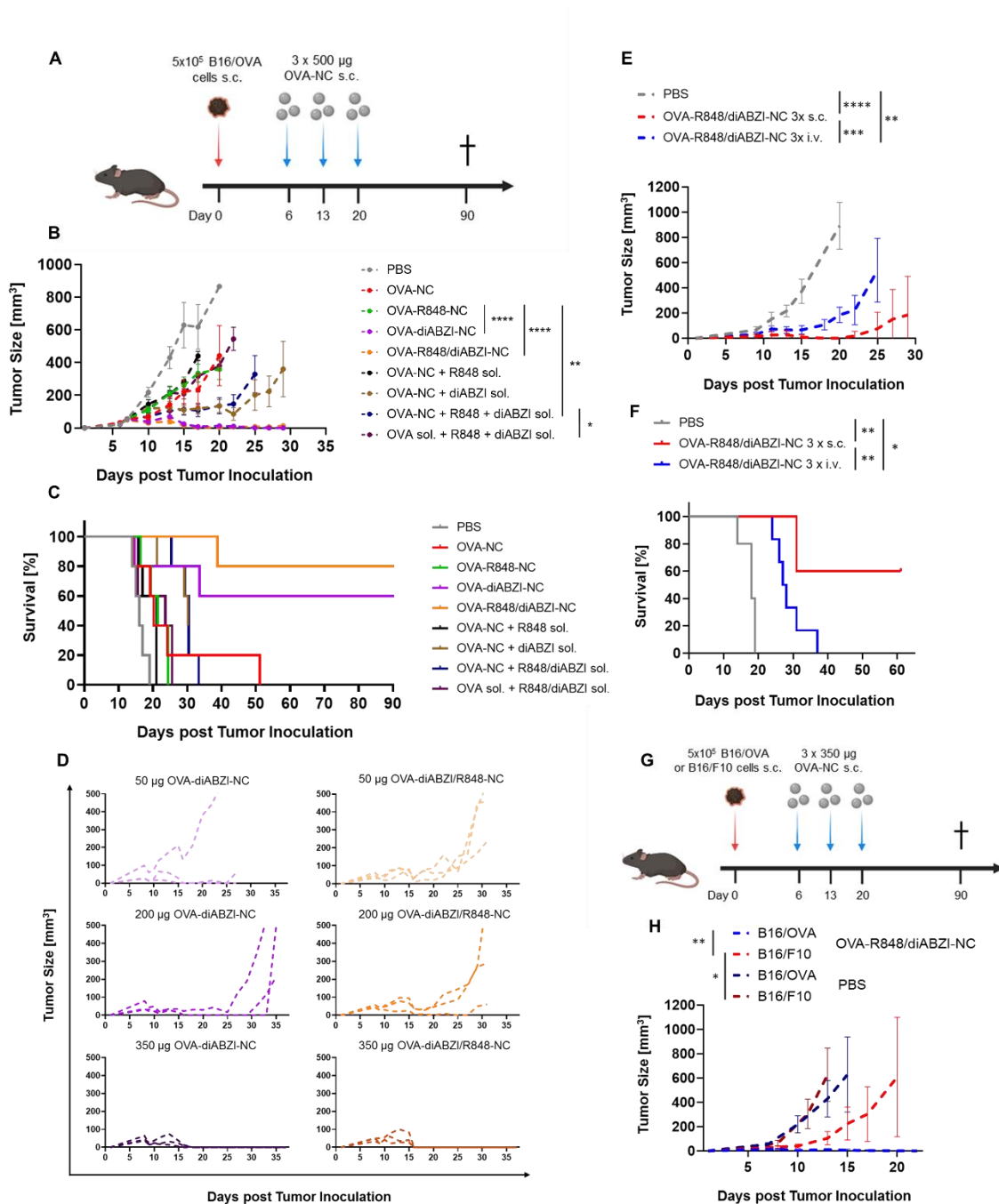


Figure 3. (A) Treatment scheme of B16/F10-OVA-bearing mice with adjuvant-loaded OVA-NCs. C57BL/6J mice were injected with 5×10^5 B16/F10-OVA cells subcutaneously and treated at a tumor size of 25 to 50 mm³. Mice were treated at days 6, 13 and 20 post tumor cell inoculation. **(B)** B16/F10-OVA tumor growth following treatment with $3 \times 500 \mu\text{g}$ adjuvant-loaded OVA-NCs or non-loaded OVA-NCs in combination with soluble adjuvants. Treatment with PBS and non-loaded OVA-NCs served as controls ($n = 5$). **(C)** Overall survival for each group ($n = 5$). **(D)** B16/F10-OVA tumor growth curves of individual mice treated 3x with either 50 μg , 200 μg or 350 μg diABZI- or R848/diABZI-loaded OVA-NCs per injection ($n = 3$). **(E)** Tumor growth curves comparing subcutaneous OVA-NC injection with intravenous OVA-NC injection ($n = 5$). Mice were injected 3x with 350 μg R848/diABZI-loaded OVA-NCs subcutaneously or intravenously. PBS served as negative control. **(F)** Overall survival for each group ($n = 5$). **(G)** Treatment scheme of B16/F10 melanoma-bearing mice with $3 \times 350 \mu\text{g}$ R848/diABZI-loaded OVA-NCs. C57BL/6J mice were injected with 5×10^5 B16/F10-OVA cells or B16/F10 cells subcutaneously and treated at a tumor

size of 25 to 50 mm³. PBS served as negative control. **(H)** Tumor growth curves of individuals in different treatment groups (n = 4-6). Data represent mean \pm SD. Statistical analyses were performed using Ordinary one-way ANOVA and Tukey's post hoc test and significance was given with *p < 0.05, **p < 0.01, ***p < 0.001, ****p < 0.0001.

3.6 OVA-R848/diABZI-NCs induce immune cell infiltration and activation

To further analyze the effects of adjuvant-loaded OVA-NC treatment on immune cells, C57BL/6J mice were subcutaneously injected with 350 μ g NCs and DCs were isolated from inguinal lymph nodes after 24 h. Their expression level of maturation markers was evaluated by flow cytometric analyses. The frequency of CD80⁺ DCs was increased from 25% in untreated mice to approx. 65% after application of OVA-diABZI-NCs and approx. 75% after injection of dual adjuvant OVA-NCs (Fig. 4 A). This effect was even more pronounced with respect to the expression of CD86, which was increased 10-fold as a result of diABZI-loaded NC treatment (Fig. 4 A). Overall expression of CD83 appeared minute; nevertheless, it was increased 3-fold by applying diABZI-loaded OVA-NCs and 7.5-fold following injection of OVA-R848/diABZI-NCs (Fig. 4 A). The expression of CD80 and CD86 is particularly important for the successful priming of naïve T cells, further leading to cancer cell destruction.^[233]

In order to characterize and quantify infiltrating immune cells into lymph nodes and tumor tissue, cell suspensions were generated 5 days after NC-vaccination of tumor-bearing mice, stained for immune cell type-specific surface markers, and analyzed via flow cytometry. Neutrophils play an ambiguous role in the context of anti-tumor immunity. Human neutrophils mediate cancer cell killing via the expression of TNF-related apoptosis-inducing ligand. Furthermore, they can exhibit an antigen-processing cell-like phenotype and cross-present antigens to naïve T cells.^[234-236] Injection of R848/diABZI-loaded NCs resulted in significantly increased density of neutrophils in inguinal lymph nodes compared to untreated mice and those treated with non-loaded NCs in combination with soluble STING agonist (Fig. 4 B). This trend was comparable but not as pronounced for the treatment with diABZI-loaded OVA-NCs. CD8⁺ T cells are in the focus of immunotherapy research due to their ability to specifically destroy mutated cells. Following DC-mediated priming against antigens they kill target cells by releasing granules containing granzymes, perforin, cathepsin C, and granulysin. They can further bind to Fas receptors on cancer cells and virus-infected cells and hereby initiate the activation of caspases and endonucleases, leading to DNA-fragmentation of targeted cells.^[165, 233] By administering both diABZI-containing OVA-NCs, the density of CD8⁺ T cells in lymph nodes and tumor tissue was significantly augmented (Fig. 4 B).

To evaluate the activation level of the tumor-infiltrated CD8⁺ T cells, flow cytometric analyses of CD69 and CD25 expression levels were performed (Fig. 4 C). The treatment with diABZI- and dual adjuvant-loaded OVA-NCs increased the amount of CD69⁺/CD25⁻-expressing CD8⁺ T cells 14-fold and 19.5-fold, respectively and of CD69⁺/CD25⁺-expressing T cells 5.5-fold to

6-fold in comparison to PBS application. Furthermore, the density of CD69⁺/CD25⁺ T cells was 2-fold higher and of CD69⁺/CD25⁻ T cells approx. 1.5-fold higher after the treatment with encapsulated adjuvants compared to the treatments with equimolar amounts of soluble adjuvants. Non-loaded OVA-NCs and R848-loaded NCs did not trigger T cell activation. These observations explain the OVA-diABZI-NC- and OVA-R848/diABZI-NC-induced tumor remission *in vivo*. CD69 is an early T cell activation marker whose expression increases 3 hours after T cell activation following T cell receptor (TCR) binding to the antigen/MHC complex. After 24 hours, the expression of CD69 is downregulated again.^[237-239] CD25, the alpha chain of the IL-2 receptor, is expressed within 24 hours after TCR-mediated T cell activation for a few days. This activation marker is important for the responsiveness to IL-2 and IL-2 secretion, playing an important role in lymphocyte activation, proliferation and inducing pro-inflammatory cytokine production.^[237, 240-241] Flow cytometric analyses of tissue-infiltrating CD8⁺ T cells revealed a continuous activation of cytotoxic T cells even six days after the first vaccination with diABZI- and dual adjuvant-loaded OVA-NCs.

Furthermore, the treatment of both diABZI-containing NC formulations led to a significantly reduced expression of programmed cell death 1 (PD-1) by tumor-infiltrating CD8⁺ T cells compared to untreated mice whereas T cell immunoglobulin and mucin domain-containing protein 3 (TIM-3) expression was significantly increased compared to untreated mice (SI Fig. 12). The percentage of PD-1-expressing CD8⁺ T cells of PBS-treated mice in the tumor tissue was 3.5-fold higher compared to diABZI- and dual adjuvant-loaded NCs and approx. 2-fold higher compared to the treatment with non-loaded OVA-NCs in combination with soluble diABZI and both adjuvants. PD-1 is an inhibitory receptor expressed by T cells whose binding to its ligand PD-L1 leads to impaired T cell function.^[242] The lower expression levels upon treatment with diABZI- and diABZI/R848-loaded OVA-NCs conclude that a high percentage of tumor-infiltrating CD8⁺ T cells leads to effective melanoma cell killing and explain the observed complete tumor remission in both groups. However, a 5.5-fold higher expression of TIM-3 was detected following treatment with both diABZI-containing OVA-NC formulations as well as a 3-fold to 4-fold higher percentage induced by the treatment with non-loaded OVA-NCs with soluble adjuvants. TIM-3 acts as an immune checkpoint and is mainly expressed by CD4⁺ and CD8⁺ T cells as well as other immune cells. It plays an important role in inhibitory signaling upon anti-tumoral and anti-viral T cell activity.^[243] Studies have shown a correlation of TIM-3 signaling and the cGAS-STING pathway.^[244] The blockade of TIM-3 led to an amplified endocytosis of extracellular DNA, which in turn triggered type I interferon production via STING signaling. Vice versa, the diABZI-triggered production of type I interferons through STING could lead to the observed, significantly increased TIM-3 expression by T cells to prevent an overshooting immune response.

Moreover, the antigen-specific activation of CD4⁺ and CD8⁺ T cells was proven by analyzing the amount of proliferating cells *in vivo* via flow cytometry. The treatment with OVA-R848/diABZI-NCs triggered significantly increased OVA-specific T cell proliferation of OT-I and OT-II T cells *in vivo* compared to untreated mice (SI Fig. 14).

Immunizing B16/F10-OVA-bearing mice with diABZI- and R848/diABZI-loaded OVA-NCs induced a vigorous secretion of IL-6, IFN- α , IFN- γ , CXCL10, CCL2, CCL5, and CXCL1 (SI Fig. 13). Secretion levels of those cytokines and chemokines were significantly higher in comparison to untreated mice as well as compared to mice treated with non-loaded NCs in combination with soluble adjuvants (SI Fig. 13).

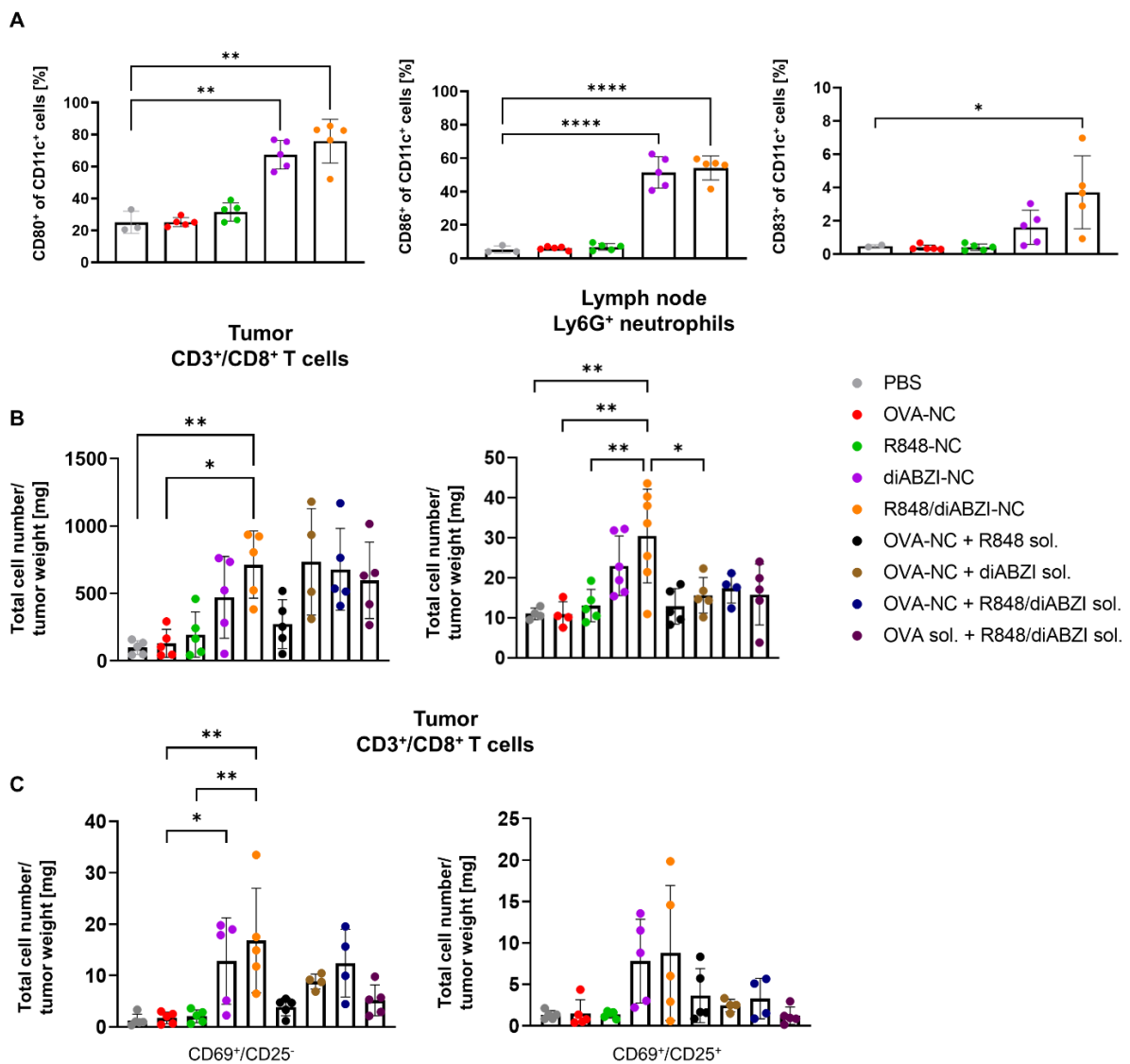


Figure 4. (A) Maturation of dendritic cells *in vivo* triggered by uptake of adjuvant-loaded NCs. C57BL/6J mice were injected subcutaneously with 350 μ g OVA-NCs into the tail base ($n = 5$). After 5 days, inguinal lymph nodes were dissected and expression of CD80, CD83, and CD86 by DCs was analyzed by flow cytometry. (B) Infiltration density of CD8⁺ T cells in tumor tissue and neutrophils into draining lymph nodes ($n = 4-5$). Tumors and lymph nodes were dissected 5 days after injection of 350 μ g OVA-NCs. Cell suspensions were generated and stained for immune cell-

specific surface markers for flow cytometric analyses. **(C)** Activation state of tumor tissue-infiltrating CD8⁺ T cells. B16/F10-OVA melanoma-bearing mice were treated with 350 µg OVA-NCs. Cell suspensions were generated from tumor tissue and analyzed for infiltrating activated T cells via flow cytometry. Cells were stained with antibodies against CD69 and CD25. Data represent mean ± SD. Statistical analyses were performed using Ordinary one-way ANOVA and Tukey's post hoc test and significance was given with *p < 0.05, **p < 0.01, ***p < 0.001, ****p < 0.0001.

3.7 Encapsulation of TRP2 reduces B16/F10 tumor growth significantly

After proving the efficacy of our STING and TLR7/8 agonist-based NC vaccine, we encapsulated the melanoma-specific antigen tyrosinase-related protein 2 (TRP2) for further tumor therapy studies. TRP2 has already been effectively used for immunotherapeutic vaccination approaches *in vivo*.^[245-247] To investigate, whether the treatment of ovalbumin-independent B16/F10-bearing mice with adjuvant-loaded NCs induces tumor remission, TRP2 peptide (SI Fig. 15) was encapsulated into OVA-NCs and tested *in vivo*. Injection of both diABZI-containing OVA-NCs decreased tumor growth significantly in comparison to the adjuvant-free and R848-loaded OVA-NCs (Fig. 5 A, SI Fig. 15). TLR7/8 agonist-loaded NCs tended to result in a slower tumor growth compared to adjuvant-free OVA-NCs, however, no significant effect could be observed (Fig. 5 A, SI Fig. 15). Mice treated with dual adjuvant-containing OVA-NCs showed the longest overall survival (Fig. 5 B, SI Fig. 15). The presumably lower amount of antigen in the NCs compared to the ovalbumin-based tumor model may be causal for the reduced efficacy of the therapy. Nevertheless, also in this model it could be shown, that the simultaneous transport of antigen and adjuvants by each NC is crucial for a potent anti-tumor immune response.

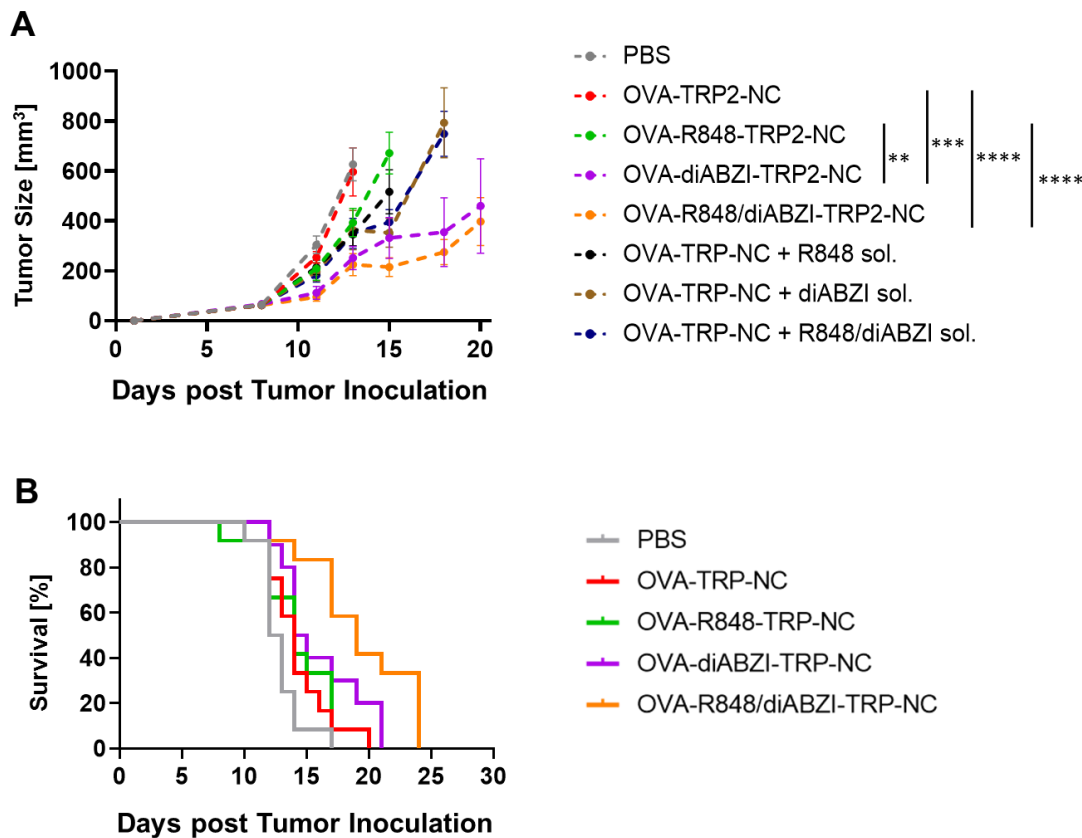


Figure 5. (A) B16/F10 tumor growth curves after treatment with different OVA-NC formulations. C57BL/6J mice were injected with 5×10^5 B16/F10 cells subcutaneously and treated at a tumor size of 25 to 50 mm³. Mice were treated with 3×350 μ g adjuvant-loaded and TRP2-containing OVA-NCs at days 7, 14 and 21. OVA-NCs were subcutaneously injected into the tail base. PBS, non-loaded OVA-NCs and OVA-NCs in combination with soluble adjuvants served as controls ($n = 12$). **(B)** Overall survival for each treatment group ($n = 12$). Data represent mean \pm SD. Statistical analyses were performed using Ordinary one-way ANOVA and Tukey's post hoc test and significance was given with * $p < 0.05$, ** $p < 0.01$, *** $p < 0.001$, **** $p < 0.0001$.

4. Conclusion

In conclusion, the encapsulation of TLR7/8 agonist R848 and STING agonist diABZI (compound 3) into biodegradable ovalbumin nanocapsules enabled the effective maturation of dendritic cells and triggered an antigen-specific T cell response against B16/F10 melanoma, resulting in full tumor remission and long-lasting immune memory. The uptake of adjuvant-loaded OVA-NCs led to potent secretion of pro-inflammatory cytokines in addition to vigorous expression of co-stimulatory molecules, such as CD80 and CD86, *in vitro* and *in vivo*. Moreover, subcutaneous injection of adjuvant-loaded OVA-NCs increased the infiltration and activation of antigen-specific CD8⁺ T cells in tumor tissue and draining lymph nodes. In addition, tumor-specific antigens were successfully encapsulated and induced anti-tumor immune responses *in vivo*. This novel adjuvant-based nanocapsule formulation bears the potential for the development of effective and personalized anti-tumor vaccines.

Acknowledgement

This work was supported by the Deutsche Forschungsgemeinschaft (DFG) through the CRC1066 in subproject Q2 and Q6.

Supplementary Information

Co-delivery of STING and TLR7/8 agonists in antigen-based nanocapsules to dendritic cells enhances CD8⁺ T cell-mediated melanoma remission

Jenny Schunke^a, Natkritta Hüppe^b, Nicole Mangazeev^a, Kai R. Speth^{a,b}, Tanja Klaus^a, Vanessa Bolduan^a, Paul Schneider^a, Michael Kuske^a, Stephan Grabbe^a, Katharina Landfester^{b,*}, Volker Mailänder^{a,b,*}, Michael Fichter^{a,b}

^a Department of Dermatology, University Medical Center Mainz, Langenbeckstraße 1, 55131 Mainz, Germany

^b Max Planck Institute for Polymer Research, Ackermannweg 10, 55128 Mainz, Germany

* Corresponding authors: mailaend@mpip-mainz.mpg.de, landfest@mpip-mainz.mpg.de

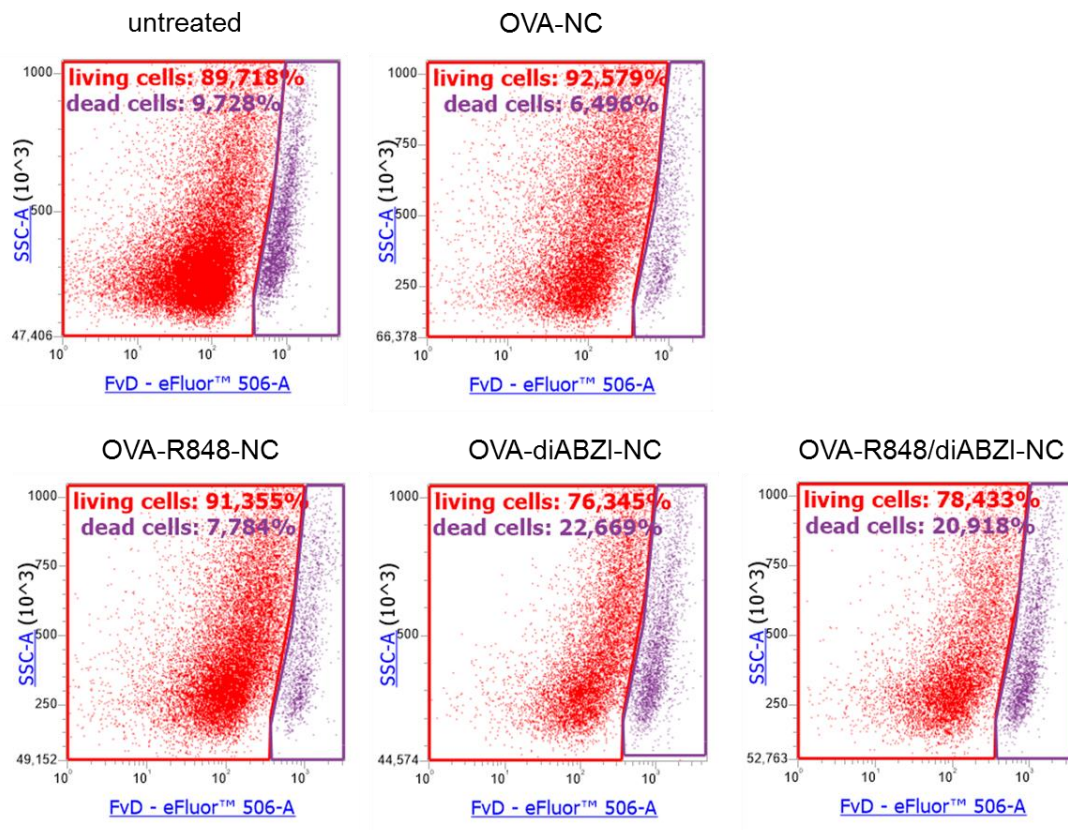


Figure 1. Flow cytometric determination of dead BMDCs after OVA-NC uptake (representative measurement). BMDCs were harvested 24 h after treatment with 100 µg/mL OVA-NCs (adjuvant-loaded and non-loaded). Dead

Chapter C

cells were discriminated from living cells by adding 100 μ L Fixable Viability Dye (eFluor™ 506, ThermoFisher) diluted 1:1000 in PBS for 25 min at 4 °C.

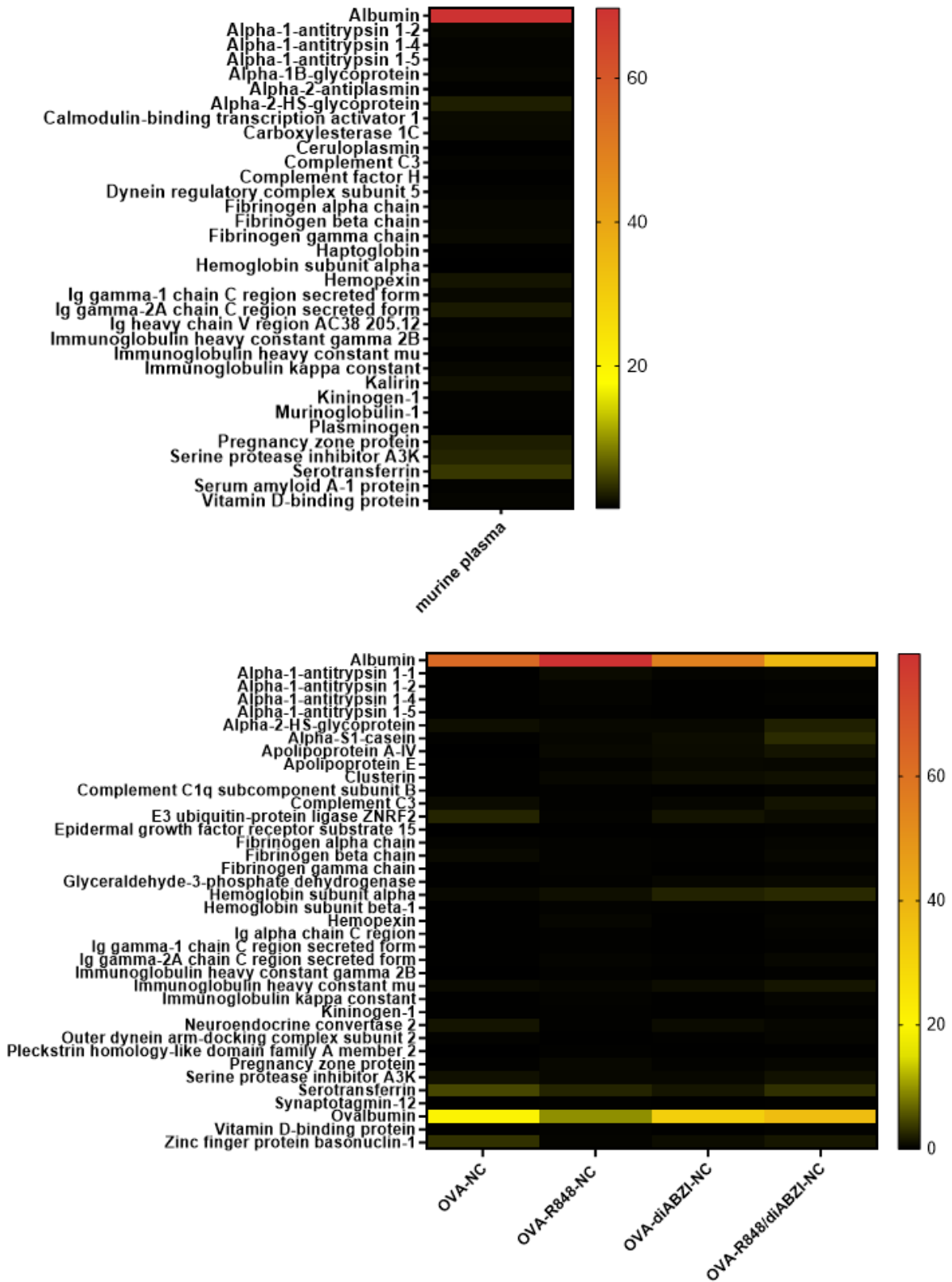


Figure 2. LC-MS analysis of protein corona formation on different OVA-NC formulations. OVA-NCs were incubated in murine citrate plasma for 1 h at 37 °C and corona proteins were subsequently desorbed and analyzed. Heat maps show the most abundant proteins of pure murine plasma (top) or of corona proteins (bottom). The relative amount of each protein in % is calculated based on the total amount of all identified proteins determined in fmol.

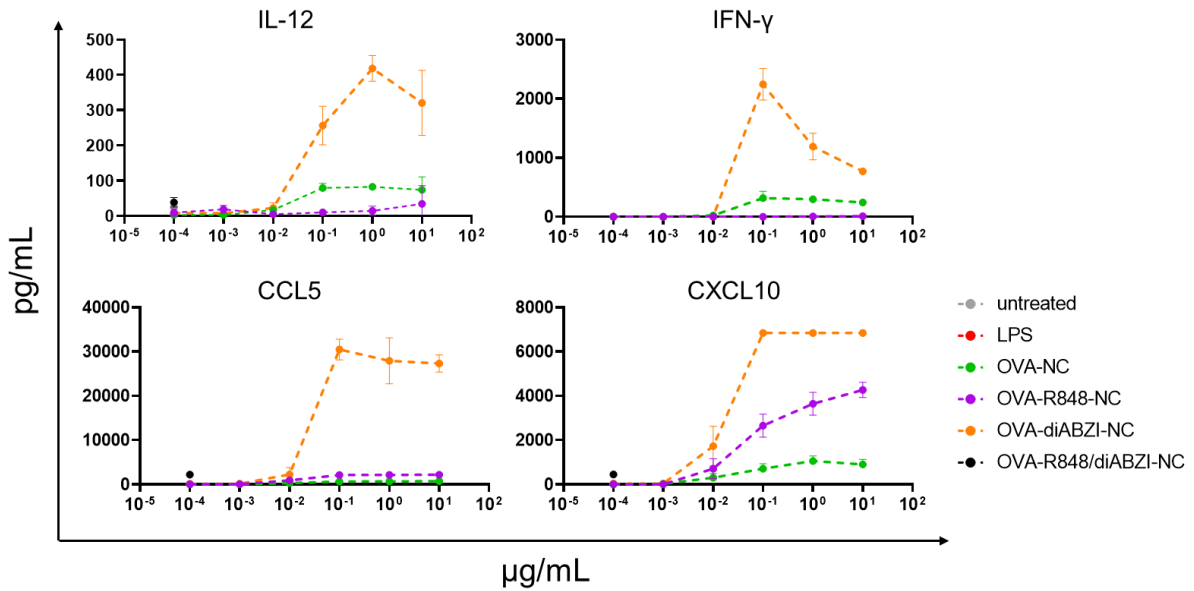


Figure 3. Secretion of pro-inflammatory cytokines by splenocytes *in vitro*. 4×10^5 cells were seeded into 96-well plates and treated with soluble R848 and diABZI compound 3 [10^{-4} to $10 \mu\text{g/mL}$] for 24 h ($n = 3$). LPS [100 ng/mL] served as positive control. The production of the pro-inflammatory cytokines IL-12, IFN- γ , CCL5, and CXCL10 was quantified using a bead-based immunoassay. Data represent mean \pm SD.

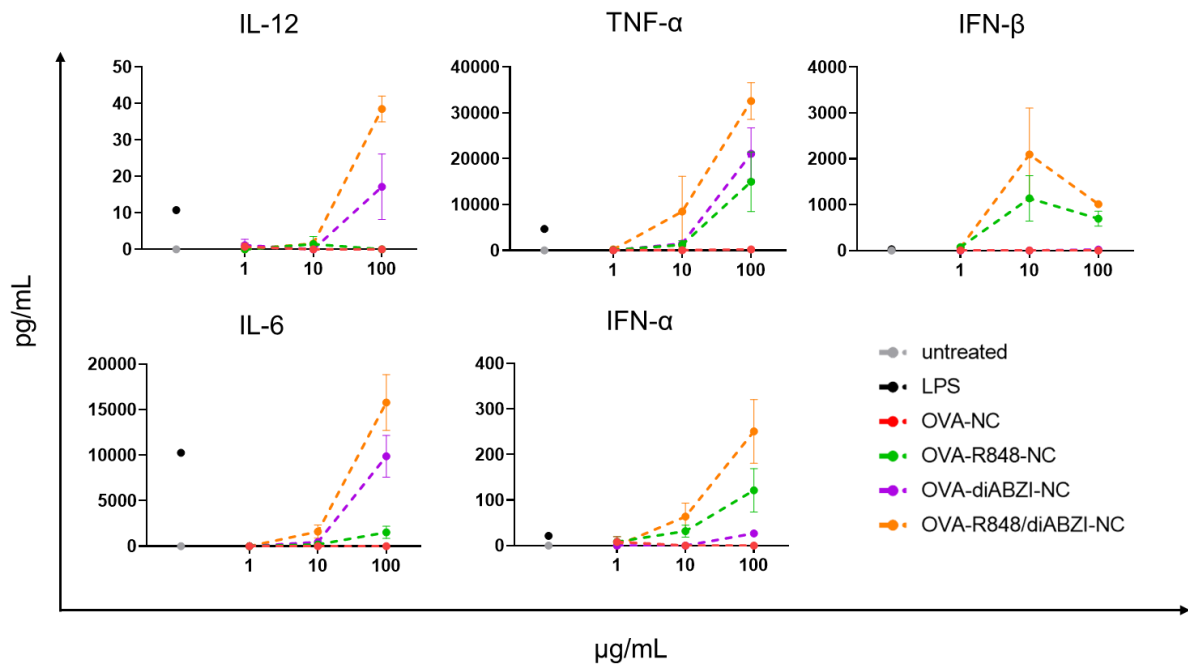


Figure 4. Secretion of pro-inflammatory cytokines by BMDCs *in vitro*. 2×10^5 cells were seeded into 12-well plates and treated with different OVA-NC formulations [1 to 100 $\mu\text{g/mL}$] for 24 h ($n = 3$). LPS [100 ng/mL] served as positive control. The production of the pro-inflammatory cytokines IL-12, TNF- α , IFN- β , IL-6 and IFN- α was quantified using a bead-based immunoassay. Data represent mean \pm SD.

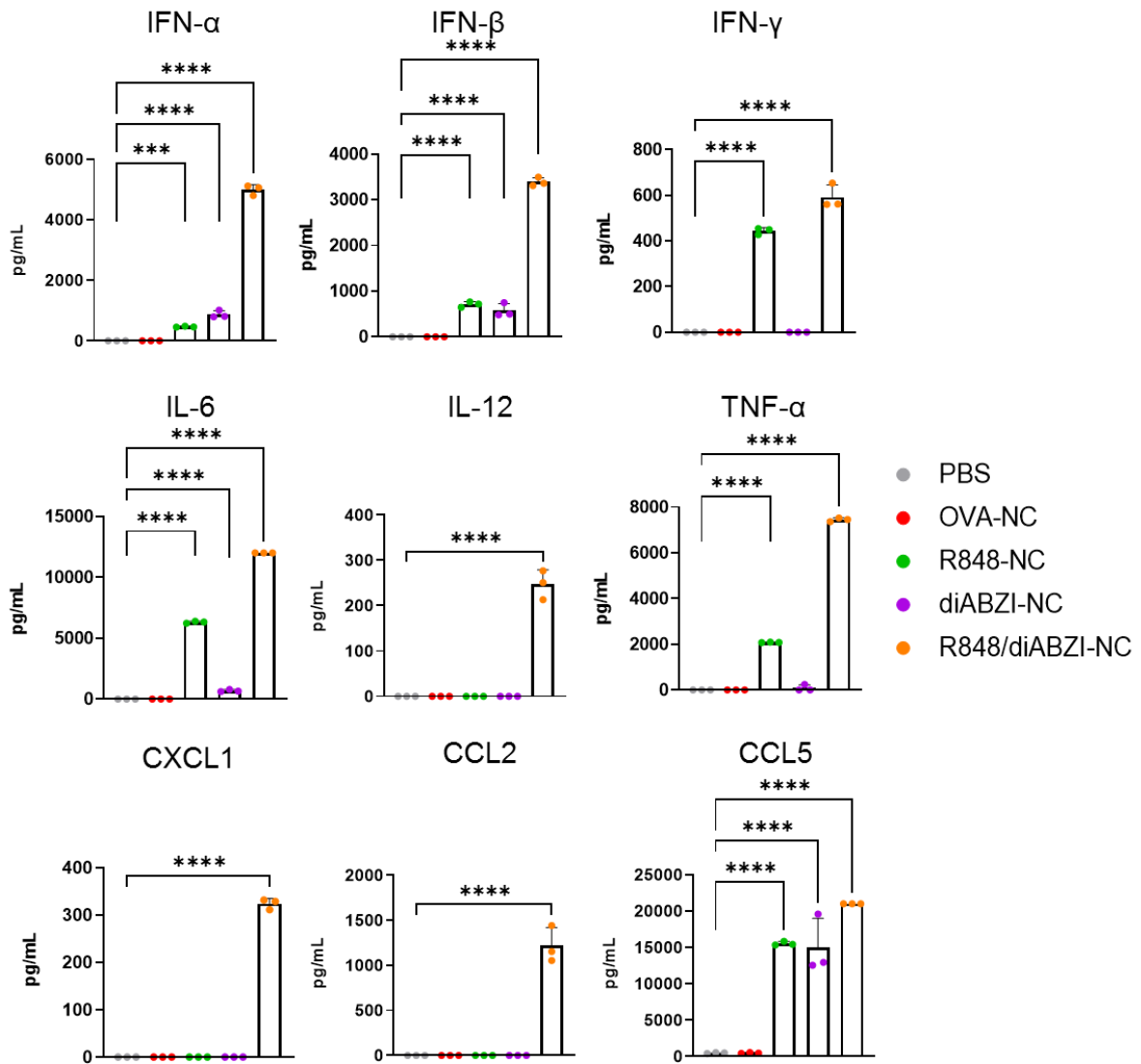


Figure 5. Secretion of pro-inflammatory cytokines by flt3-L BMDCs *in vitro*. 2.5×10^5 cells were seeded into 96-well plates and treated with different OVA-NC formulations [10 $\mu\text{g}/\text{mL}$] for 24 h ($n = 3$). The production of the pro-inflammatory cytokines IFN- α , IFN- β , IFN- γ , IL-6, IL-12, TNF- α , CXCL1, CCL2, and CCL5 was quantified using a bead-based immunoassay. Data represent mean \pm SD. Statistical analyses were performed using Ordinary one-way ANOVA and Tukey's post hoc test and significance was given with * $p < 0.05$, ** $p < 0.01$, *** $p < 0.001$, **** $p < 0.0001$.

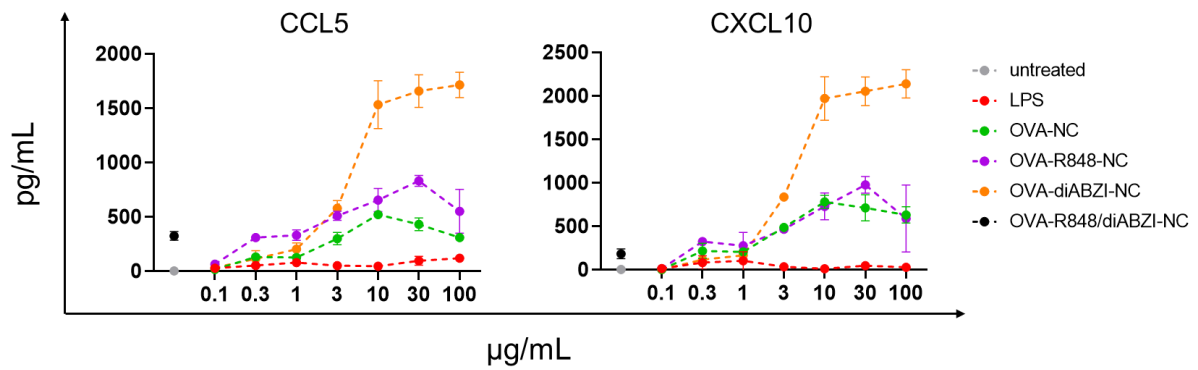


Figure 6. 2×10^6 splenocytes were seeded into 12-well plates and co-incubated with 0.1 – 100 $\mu\text{g}/\text{mL}$ OVA-NCs for 24 h. To quantify the secretion levels of pro-inflammatory cytokines, culture supernatants were analyzed with a bead-based assay. Data represent mean \pm SD, $n = 3$.

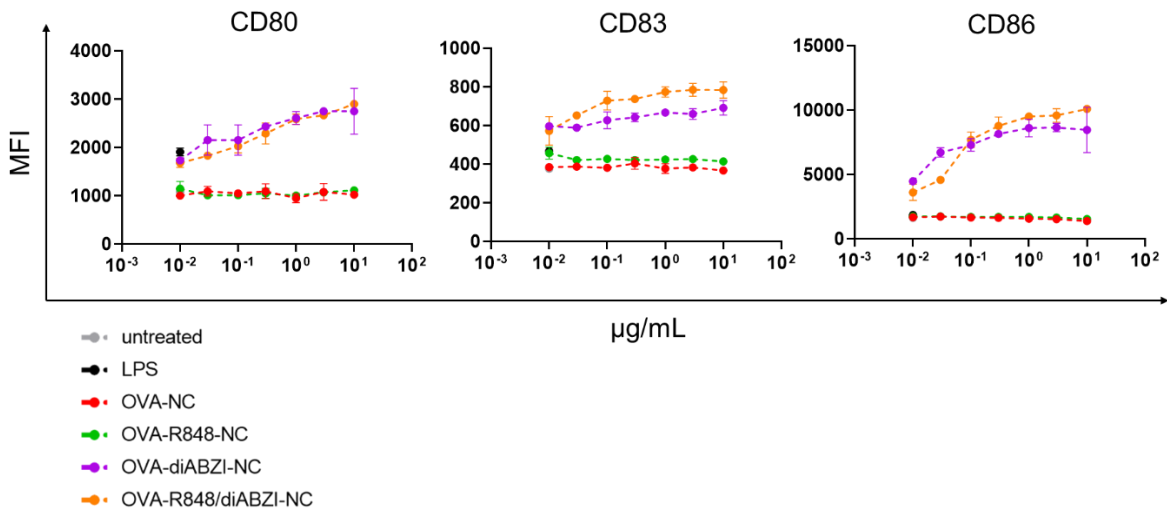


Figure 7. 2×10^5 moDCs were seeded into 96-well plates and treated with 10^{-3} - 10^2 $\mu\text{g}/\text{mL}$ OVA-NCs for 24 h. Non-loaded NCs and LPS [100 ng/mL] served as controls. Cells were harvested and analyzed for their expression levels of CD80, CD83, and CD86 via flow cytometry. Data represent mean \pm SD, $n = 3$.

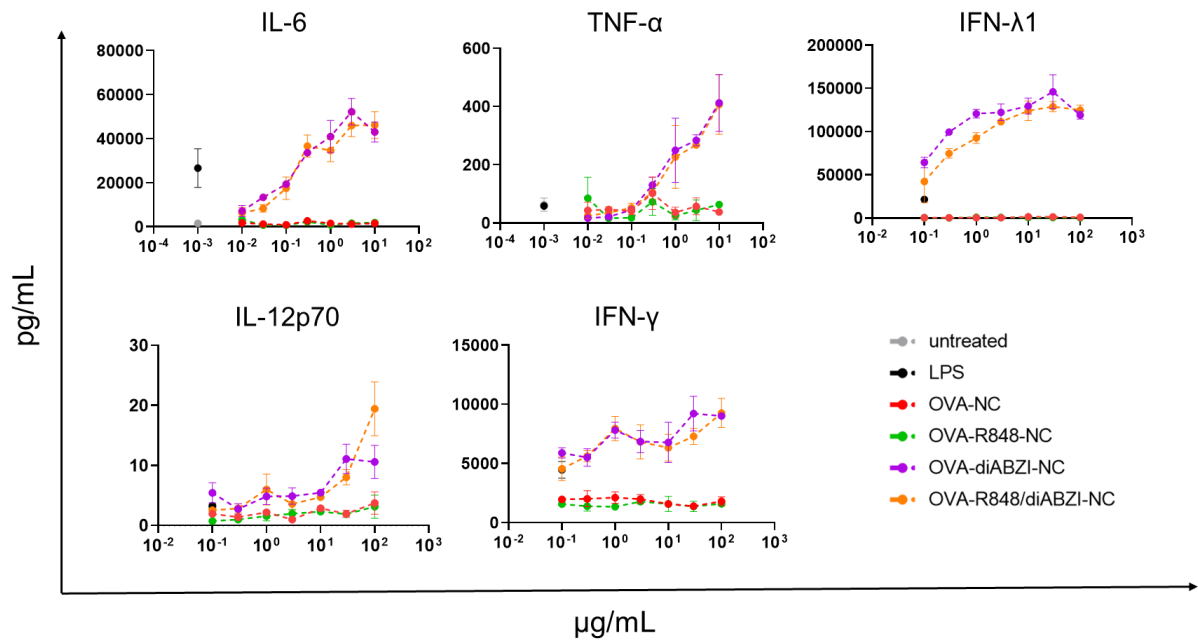


Figure 8. 2×10^5 moDCs were seeded into 96-well plates and co-incubated with 10^{-3} - 10^2 µg/mL OVA-NCs for 24 h. To quantify the secretion levels of IL-6, IL-12p70, TNF-α, IFN-γ, and IFN-λ1, culture supernatants were analyzed with a bead-based assay. Data represent mean ± SD, n = 3.

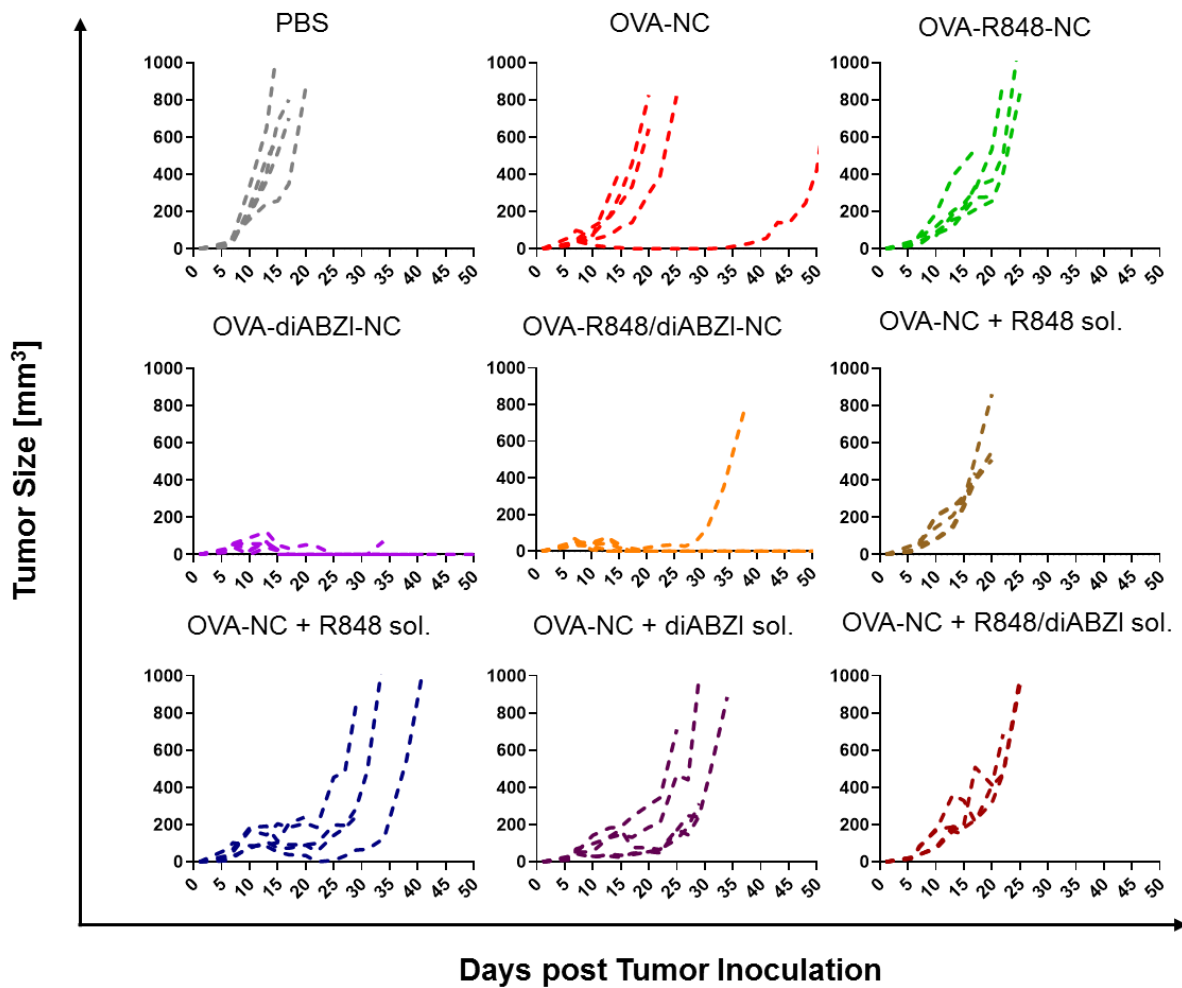


Figure 9. B16/F10-OVA tumor growth curves of individual mice of different treatment groups. C57BL/6J mice were injected with 5×10^5 B16/F10-OVA cells subcutaneously and treated at a tumor size of 25 to 50 mm^3 . Adjuvant-loaded OVA-NCs as well as non-loaded OVA-NCs and soluble adjuvants were injected subcutaneously at days 6, 13 and 20 post tumor cell inoculation ($3 \times 500 \mu\text{g}$). Treatment with PBS and non-loaded OVA-NCs served as controls ($n = 5$). Data represent mean \pm SD. Statistical analyses were performed using Ordinary one-way ANOVA and Tukey's post hoc test and significance was given with * $p < 0.05$, ** $p < 0.01$, *** $p < 0.001$, **** $p < 0.0001$.

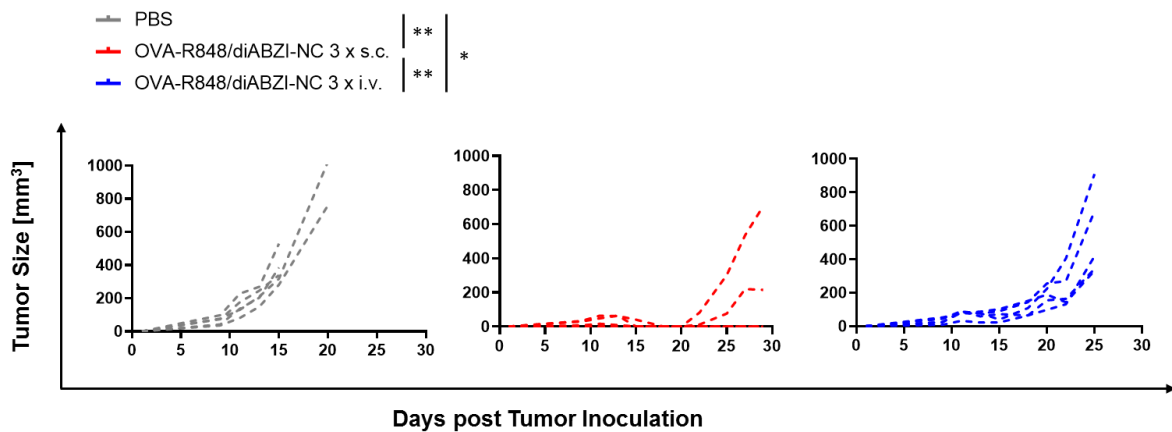


Figure 10. B16/F10-OVA tumor growth curves of individual mice of different treatment groups. C57BL/6J mice were injected with 5×10^5 B16/F10-OVA cells subcutaneously and treated at a tumor size of 25 to 50 mm³. OVA-R848/diABZI-NCs were injected subcutaneously or intravenously at days 6, 13 and 20 post tumor cell inoculation (3x 350 μ g). Treatment with PBS served as control (n = 5). Data represent mean \pm SD. Statistical analyses were performed using Ordinary one-way ANOVA and Tukey's post hoc test and significance was given with *p < 0.05, **p < 0.01, ***p < 0.001, ****p < 0.0001.

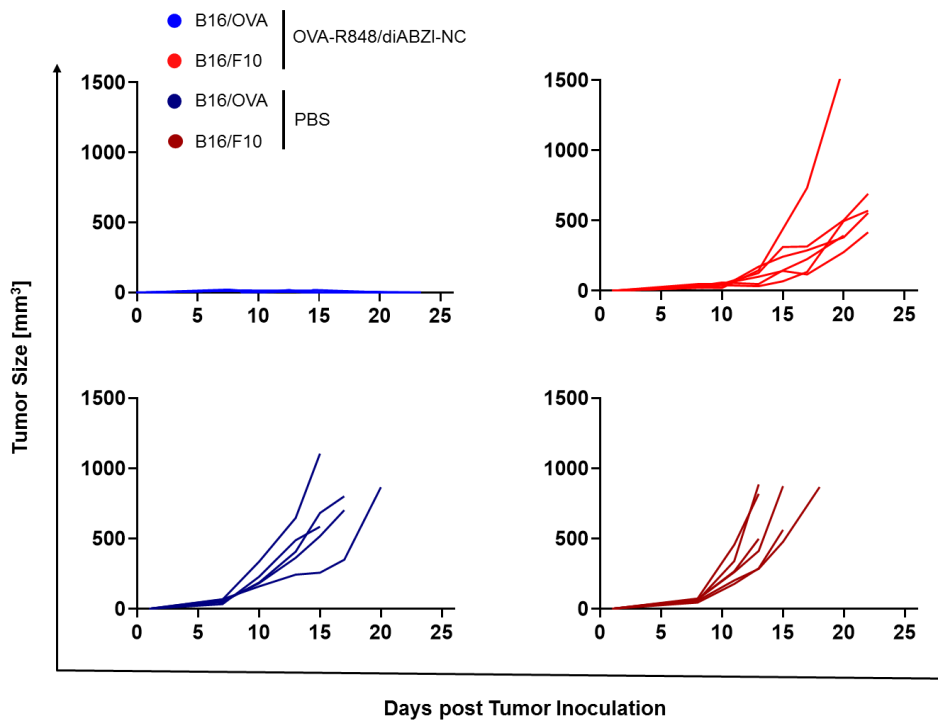


Figure 11. B16/F10-OVA and B16/F10 tumor growth curves of individual mice. C57BL/6J mice were injected with either 5×10^5 B16/F10-OVA cells or 5×10^5 B16/F10 cells subcutaneously and treated at a tumor size of 25 to 50 mm³. OVA-R848/diABZI-NCs were injected subcutaneously at days 6, 13 and 20 post tumor cell inoculation (3x 350 μ g). Treatment with PBS served as control (n = 4-6). Data represent mean \pm SD. Statistical analyses were performed using Ordinary one-way ANOVA and Tukey's post hoc test and significance was given with *p < 0.05, **p < 0.01, ***p < 0.001, ****p < 0.0001.

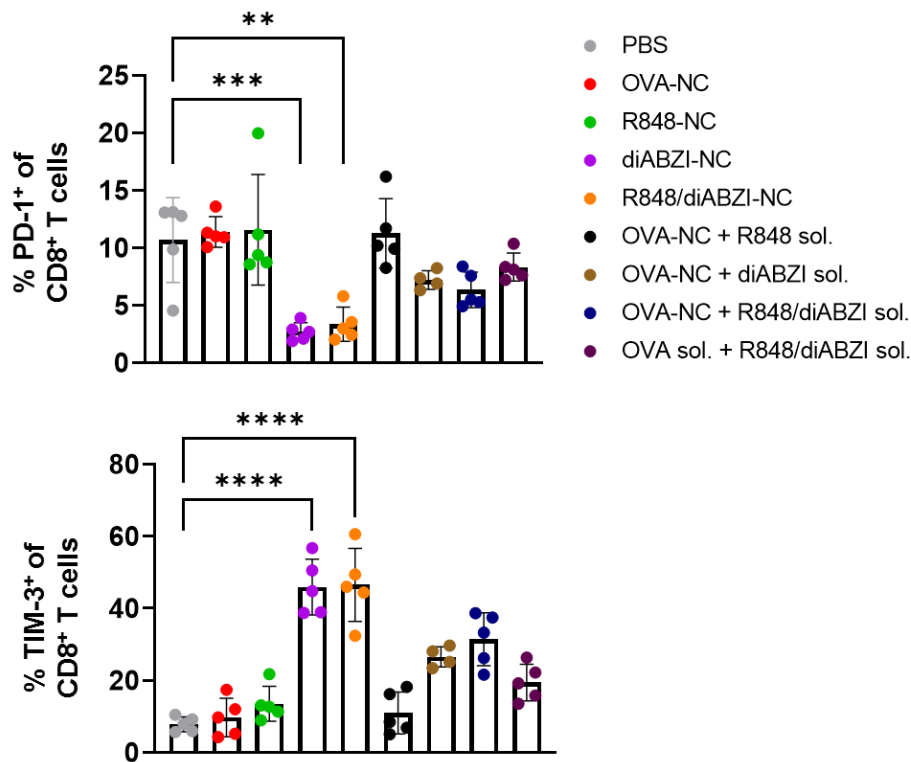


Figure 12. Expression of PD-1 and TIM-3 by tumor-infiltrating CD8⁺ T cells. C57BL/6J mice were injected subcutaneously with 350 μ g OVA-NCs into the tail base (n = 4-5). After 5 days, tumors were dissected and cell suspensions were generated. Cells were stained with antibodies specific for T cell surface markers, PD-1 as well as TIM-3 and further analyzed via flow cytometry. Data represent mean \pm SD. Statistical analyses were performed using Ordinary one-way ANOVA and Tukey's post hoc test and significance was given with *p < 0.05, **p < 0.01, ***p < 0.001, ****p < 0.0001.

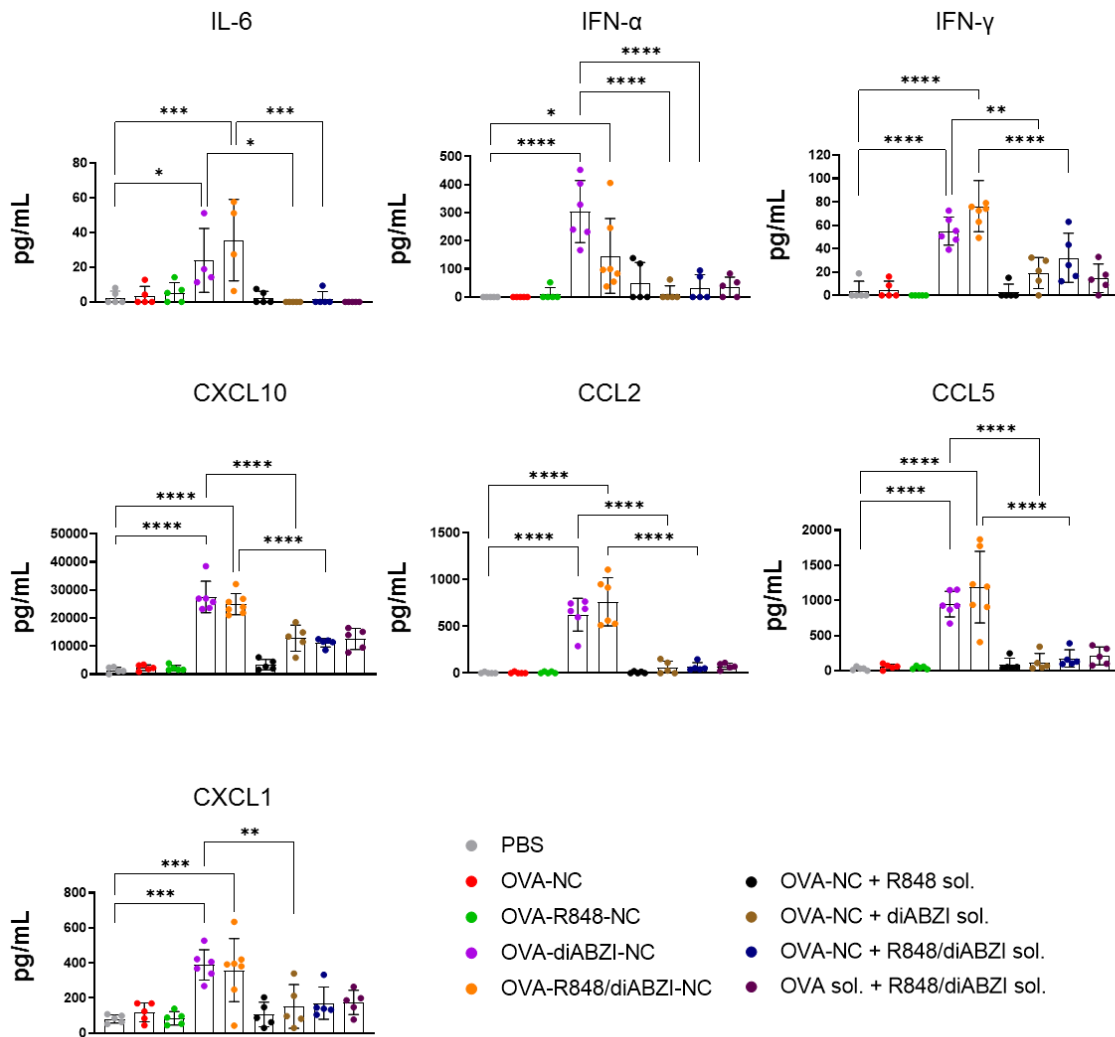


Figure 13. Adjuvant-loaded OVA-NCs induce secretion of pro-inflammatory cytokines by immune cells. B16/F10-OVA melanoma-bearing mice were treated with 350 μ g of different OVA-NC formulations after 6 days. Blood samples were collected 24 h after treatment and murine plasma was analyzed for IFN- γ , IFN- α and IL-6 with a bead-based immunoassay. Data represent mean \pm SD, n = 5-7. Statistical analyses were performed using Ordinary one-way ANOVA and Tukey's post hoc test and significance was given with *p < 0.05, **p < 0.01, ***p < 0.001, ****p < 0.0001.

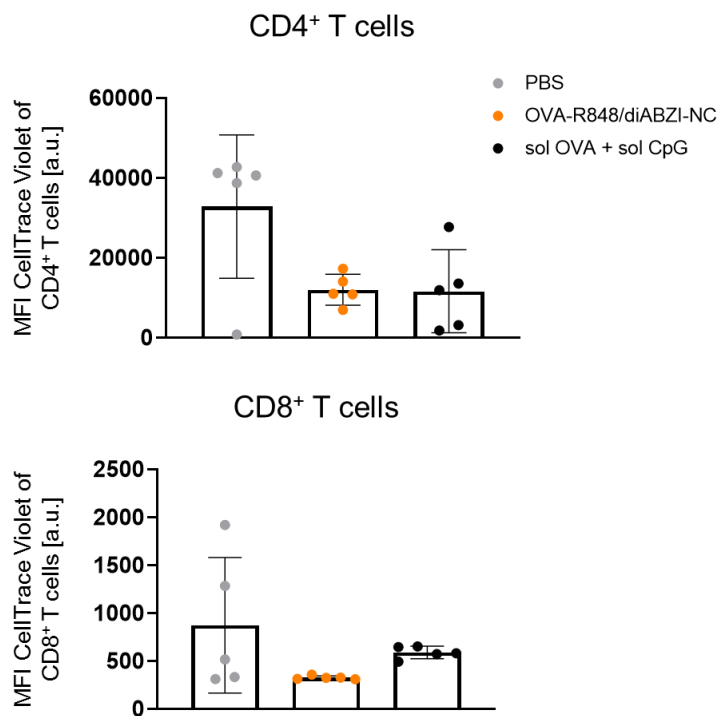


Figure 14. T cell proliferation is induced by R848/diABZI-loaded OVA-NCs *in vivo*. C57BL/6J mice were injected with OVA-R848/diABZI-NCs (350 μ g). PBS and CpG (ODN-1826) served as controls. 24 h afterwards, naïve CD8⁺ T cells and CD4⁺ T cells were isolated from either OT-Ix Ly5.1 or OT-IIxLy5.1 mice and stained with CellTrace Violet. 10⁶ cells of each T cell subtype were injected intravenously into the pretreated mice. After 72 h, inguinal lymph nodes were dissected and single cell suspensions were generated. Cells were stained with antibodies against T cell-specific surface markers and their proliferation analyzed via flow cytometry. Data represent mean \pm SD, n= 5. Statistical analyses were performed using Ordinary one-way ANOVA and Tukey's post hoc test and significance was given with *p < 0.05, **p < 0.01, ***p < 0.001, ****p < 0.0001.

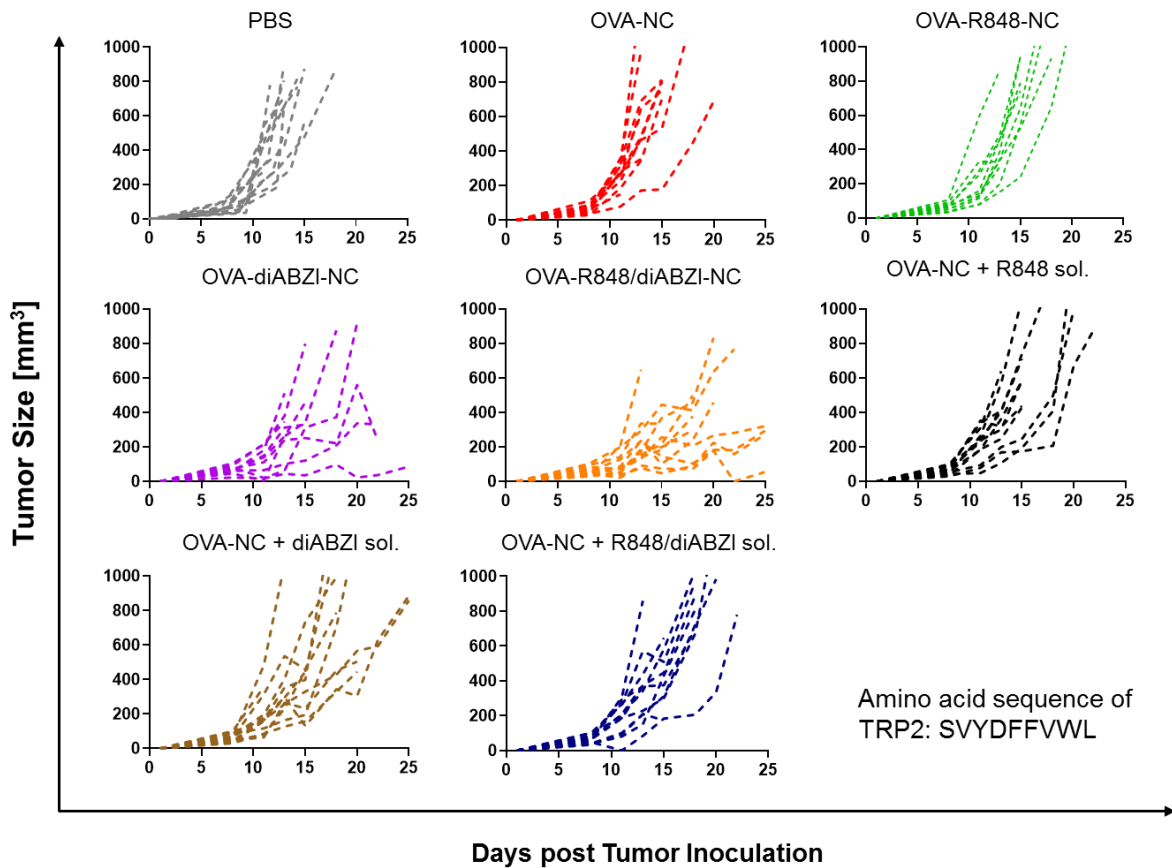


Figure 15. B16/F10 tumor growth curves of individual mice of different treatment groups. C57BL/6J mice were injected with 5×10^5 B16/F10 cells subcutaneously and treated at a tumor size of 25 to 50 mm^3 . Adjuvant-loaded OVA-TRP2-NCs as well as non-loaded OVA-TRP2-NCs and soluble adjuvants were injected subcutaneously at days 6, 13 and 20 post tumor cell inoculation (3x 350 μg). Treatment with PBS and non-loaded OVA-NCs served as controls ($n = 5$). Data represent mean \pm SD. Statistical analyses were performed using Ordinary one-way ANOVA and Tukey's post hoc test and significance was given with * $p < 0.05$, ** $p < 0.01$, *** $p < 0.001$, **** $p < 0.0001$.

Conclusion and Outlook

Nanocarriers (NCs) enable the protected and simultaneous transport of immunomodulatory molecules and tumor antigens. In the context of cancer treatment, the targeting of dendritic cells (DCs) with nanocarriers is of particular interest since they induce pro-inflammatory immune responses upon stimulation with adjuvants and are able to present encapsulated antigens to T cells. Subsequently, T cells specifically recognize antigen-expressing tumor cells and destroy them via secretion of granzyme and perforin.

Chapter A describes the synthesis of protein-based nanocarriers via copper-free azide-alkyne click reaction and the efficient encapsulation of the adjuvants resiquimod (R848), muramyl dipeptide (MDP) and polyinosinic:polycytidylic acid (Poly(I:C)) into the aqueous nanocapsule core. Furthermore, *in vitro* studies for the evaluation of NC uptake were performed. Additionally, the adjuvant-mediated induction of DC maturation was evaluated by analyzing the expression of CD80 and CD86 using flow cytometry. In summary, an efficient encapsulation of different adjuvants into NCs as well as their potential to stimulate DCs was demonstrated.

Chapter B deals with the encapsulation of R848 and MDP into ovalbumin (OVA)-based NCs to further induce OVA-specific immune responses *in vitro* and *in vivo*. It could be shown that R848 and MDP in combination triggered a superadditive production of different pro-inflammatory cytokines as well as strong DC maturation. In addition, *in vitro* T cell proliferation assays demonstrated a successful presentation of OVA peptides to naïve OT-I- and OT-II mouse-derived T cells upon NC uptake and their antigen-specific priming. Initial *in vivo* tumor studies revealed the potential of adjuvant-loaded OVA-NCs to reduce tumor growth in a B16/F10-OVA melanoma model. This chapter summarizes the simultaneous transport of antigen and adjuvants to DCs and the subsequent induction of OVA-specific T cell activation and anti-tumor responses. It further sets a focus on the advantage of combining R848 and MDP to induce a potent pro-inflammatory immune response.

In **chapter C**, a novel adjuvant combination for the treatment of B16/F10 melanoma was established. The simultaneous transport of diamidobenzimidazole (diABZI) and R848 in OVA-NCs triggered synergistic effects with respect to the expression of DC maturation markers and on the secretion of pro-inflammatory cytokines. Different *in vivo* studies were performed in order to achieve an optimal treatment regimen regarding applied NC doses and injections route. Furthermore, activation of immune cells as well as their infiltration into tumor-draining lymph nodes and melanoma tissue was confirmed. Furthermore, mice with B16/F10-OVA tumors were permanently cured by treatment with diABZI- and diABZI/R848-loaded NCs.

Encapsulation of the melanoma-specific antigen TRP2 in combination with diABZI and R848 also induced a significant reduction in tumor growth.

This nanovaccine can be further optimized by a combined encapsulation of different melanoma-associated antigens such as tyrosinase-related protein 1 (TRP1), gp100 or MelanA/MART-1. Encapsulation of other tumor-specific antigens into HSA- or OVA-NCs is also conceivable. These could be applied, for example, for the treatment of murine MC38 colon tumors or murine hepatocellular carcinoma. Especially with regard to personalized therapies, the presented protein-based NCs offer a versatile treatment tool as the encapsulation of patient-specific neoantigens is possible.

Another approach to improve the introduced nanovaccine is to investigate additional adjuvant combinations. These may also include anti-inflammatory compounds, such as rapamycin, with regard to the treatment of allergies or autoimmune diseases.

Our protein-based nanocapsules also offer the opportunity of conjugating DC-targeting antibodies or nanobodies onto the capsule surface. This allows both, increased uptake and targeted uptake into DC subtypes. In previous studies, our group demonstrated the efficient DC targeting by conjugating anti-CD11c and anti-Clec9a antibodies on mgHES-NCs. These antibodies could also be interesting for the project presented in this dissertation.

Combination therapy with immune checkpoint inhibitors, such as anti-PD-1 or anti-TIM-3 antibodies is also of interest in particular for the treatment of melanoma. This could enhance the effect of the adjuvant-loaded nanocarriers by bypassing the T cell inhibitory binding of immune checkpoints expressed by cancer cells. For this purpose, FDA-approved monoclonal antibodies, such as nivolumab (anti-PD-1), or antibodies currently included in clinical trials, may be used.

References

- [1] F. Garrido, T. Cabrera, N. Aptsiauri, *Int J Cancer* **2010**, 127, 249.
- [2] M. H. Lampen, T. van Hall, *Curr Opin Immunol* **2011**, 23, 293.
- [3] T. Blankenstein, P. G. Coulie, E. Gilboa, E. M. Jaffee, *Nat Rev Cancer* **2012**, 12, 307.
- [4] T. S. Lim, V. Chew, J. L. Sieow, S. Goh, J. P. Yeong, A. L. Soon, P. Ricciardi-Castagnoli, *Oncoimmunology* **2016**, 5, e1085146.
- [5] X. Y. Tang, Z. L. Luo, Y. L. Xiong, J. Yang, A. P. Shi, K. F. Zheng, Y. J. Liu, C. Shu, N. Ma, Q. Lu, J. B. Zhao, *Cancers (Basel)* **2022**, 14.
- [6] R. Reschke, M. Ziemer, *J Dtsch Dermatol Ges* **2020**, 18, 429.
- [7] F. S. Hodi, V. Chiarion-Sileni, R. Gonzalez, J. J. Grob, P. Rutkowski, C. L. Cowey, C. D. Lao, D. Schadendorf, J. Wagstaff, R. Dummer, P. F. Ferrucci, M. Smylie, A. Hill, D. Hogg, I. Marquez-Rodas, J. Jiang, J. Rizzo, J. Larkin, J. D. Wolchok, *Lancet Oncol* **2018**, 19, 1480.
- [8] T. J. Curiel, G. Coukos, L. Zou, X. Alvarez, P. Cheng, P. Mottram, M. Evdemon-Hogan, J. R. Conejo-Garcia, L. Zhang, M. Burow, Y. Zhu, S. Wei, I. Kryczek, B. Daniel, A. Gordon, L. Myers, A. Lackner, M. L. Disis, K. L. Knutson, L. Chen, W. Zou, *Nat Med* **2004**, 10, 942.
- [9] M. Gobert, I. Treilleux, N. Bendriss-Vermare, T. Bachelot, S. Goddard-Leon, V. Arfi, C. Biota, A. C. Doffin, I. Durand, D. Olive, S. Perez, N. Pasqual, C. Faure, I. Ray-Coquard, A. Puisieux, C. Caux, J. Y. Blay, C. Ménétrier-Caux, *Cancer Res* **2009**, 69, 2000.
- [10] D. I. Gaborovich, S. Nagaraj, *Nat Rev Immunol* **2009**, 9, 162.
- [11] S. Sakaguchi, T. Yamaguchi, T. Nomura, M. Ono, *Cell* **2008**, 133, 775.
- [12] K. Baruch, N. Rosenzweig, A. Kertser, A. Deczkowska, A. M. Sharif, A. Spinrad, A. Tsitsou-Kampeli, A. Sarel, L. Cahalon, M. Schwartz, *Nat Commun* **2015**, 6, 7967.
- [13] V. Bronte, P. Zanovello, *Nat Rev Immunol* **2005**, 5, 641.
- [14] P. C. Rodríguez, A. C. Ochoa, *Immunol Rev* **2008**, 222, 180.
- [15] R. Yang, Z. Cai, Y. Zhang, W. H. t. Yutzy, K. F. Roby, R. B. Roden, *Cancer Res* **2006**, 66, 6807.
- [16] B. Huang, P. Y. Pan, Q. Li, A. I. Sato, D. E. Levy, J. Bromberg, C. M. Divino, S. H. Chen, *Cancer Res* **2006**, 66, 1123.
- [17] S. Tiainen, R. Tumelius, K. Rilla, K. Hämäläinen, M. Tammi, R. Tammi, V. M. Kosma, S. Oikari, P. Auvinen, *Histopathology* **2015**, 66, 873.
- [18] J. Jou, K. J. Harrington, M. B. Zocca, E. Ehrnrooth, E. E. W. Cohen, *Clin Cancer Res* **2021**, 27, 689.
- [19] S. J. Paston, V. A. Brentville, P. Symonds, L. G. Durrant, *Front Immunol* **2021**, 12, 627932.

-
- [20] R. E. Hollingsworth, K. Jansen, *NPJ Vaccines* **2019**, 4, 7.
- [21] S. R. Pedersen, M. R. Sørensen, S. Buus, J. P. Christensen, A. R. Thomsen, *J Immunol* **2013**, 191, 3955.
- [22] A. Osipov, A. Murphy, L. Zheng, *Adv Cancer Res* **2019**, 143, 63.
- [23] Y. L. Vishweshwaraiah, N. V. Dokholyan, *Front Immunol* **2022**, 13, 1029069.
- [24] O. J. Finn, *Nat Rev Immunol* **2003**, 3, 630.
- [25] J. Rice, C. H. Ottensmeier, F. K. Stevenson, *Nat Rev Cancer* **2008**, 8, 108.
- [26] K. R. Porter, K. Raviprakash, *Curr Issues Mol Biol* **2017**, 22, 129.
- [27] M. A. Kutzler, D. B. Weiner, *Nat Rev Genet* **2008**, 9, 776.
- [28] S. Buchan, E. Grønevik, I. Mathiesen, C. A. King, F. K. Stevenson, J. Rice, *J Immunol* **2005**, 174, 6292.
- [29] L. Lambricht, A. Lopes, S. Kos, G. Sersa, V. Prémat, G. Vandermeulen, *Expert Opin Drug Deliv* **2016**, 13, 295.
- [30] M. Sällberg, L. Frelin, G. Ahlén, M. Sällberg-Chen, *Med Microbiol Immunol* **2015**, 204, 131.
- [31] S. Vasan, A. Hurley, S. J. Schlesinger, D. Hannaman, D. F. Gardiner, D. P. Dugin, M. Boente-Carrera, R. Vittorino, M. Caskey, J. Andersen, Y. Huang, J. H. Cox, T. Tarragona-Fiol, D. K. Gill, H. Cheeseman, L. Clark, L. Dally, C. Smith, C. Schmidt, H. H. Park, J. T. Kopycinski, J. Gilmour, P. Fast, R. Bernard, D. D. Ho, *PLoS One* **2011**, 6, e19252.
- [32] Y. L. Vishweshwaraiah, N. V. Dokholyan, *Adv Drug Deliv Rev* **2022**, 183, 114142.
- [33] J. Wei, A. M. Hui, *Cancer Treat Rev* **2022**, 107, 102405.
- [34] R. Tenchov, R. Bird, A. E. Curtze, Q. Zhou, *ACS Nano* **2021**, 15, 16982.
- [35] J. D. Beck, D. Reidenbach, N. Salomon, U. Sahin, Ö. Türeci, M. Vormehr, L. M. Kranz, *Mol Cancer* **2021**, 20, 69.
- [36] M. Diken, S. Kreiter, A. Selmi, C. M. Britten, C. Huber, Ö. Türeci, U. Sahin, *Gene Ther* **2011**, 18, 702.
- [37] L. Bialkowski, A. van Weijnen, K. Van der Jeught, D. Renmans, L. Daszkiewicz, C. Heirman, G. Stangé, K. Breckpot, J. L. Aerts, K. Thielemans, *Sci Rep* **2016**, 6, 22509.
- [38] D. A. Caruso, L. M. Orme, A. M. Neale, F. J. Radcliff, G. M. Amor, W. Maixner, P. Downie, T. E. Hassall, M. L. Tang, D. M. Ashley, *Neuro Oncol* **2004**, 6, 236.
- [39] A. Bonehill, S. Tuyaerts, A. M. Van Nuffel, C. Heirman, T. J. Bos, K. Fostier, B. Neyns, K. Thielemans, *Mol Ther* **2008**, 16, 1170.
- [40] S. Wilgenhof, A. M. T. Van Nuffel, D. Benteyn, J. Corthals, C. Aerts, C. Heirman, I. Van Riet, A. Bonehill, K. Thielemans, B. Neyns, *Ann Oncol* **2013**, 24, 2686.

References

- [41] B. De Keersmaecker, S. Claerhout, J. Carrasco, I. Bar, J. Corthals, S. Wilgenhof, B. Neyns, K. Thielemans, *J Immunother Cancer* **2020**, 8.
- [42] D. T. Le, D. M. Pardoll, E. M. Jaffee, *Cancer J* **2010**, 16, 304.
- [43] C. S. Higano, J. M. Corman, D. C. Smith, A. S. Centeno, C. P. Steidle, M. Gittleman, J. W. Simons, N. Sacks, J. Aimi, E. J. Small, *Cancer* **2008**, 113, 975.
- [44] E. J. Small, P. Fratesi, D. M. Reese, G. Strang, R. Laus, M. V. Peshwa, F. H. Valone, *J Clin Oncol* **2000**, 18, 3894.
- [45] D. L. Morton, L. J. Foshag, D. S. Hoon, J. A. Nizze, E. Famatiga, L. A. Wanek, C. Chang, D. G. Davtyan, R. K. Gupta, R. Elashoff, et al., *Ann Surg* **1992**, 216, 463.
- [46] E. C. Hsueh, R. K. Gupta, K. Qi, D. L. Morton, *J Clin Oncol* **1998**, 16, 2913.
- [47] J. A. Sosman, J. M. Unger, P. Y. Liu, L. E. Flaherty, M. S. Park, R. A. Kempf, J. A. Thompson, P. I. Terasaki, V. K. Sondak, *J Clin Oncol* **2002**, 20, 2067.
- [48] V. K. Sondak, J. A. Sosman, *Semin Cancer Biol* **2003**, 13, 409.
- [49] P. M. Santos, L. H. Butterfield, *J Immunol* **2018**, 200, 443.
- [50] L. H. Butterfield, *Front Immunol* **2013**, 4, 454.
- [51] J. G. Cyster, *J Exp Med* **1999**, 189, 447.
- [52] A. A. Itano, M. K. Jenkins, *Nat Immunol* **2003**, 4, 733.
- [53] P. Guermonprez, J. Valladeau, L. Zitvogel, C. Théry, S. Amigorena, *Annu Rev Immunol* **2002**, 20, 621.
- [54] L. Chen, *Nat Rev Immunol* **2004**, 4, 336.
- [55] C. Liu, D. Chu, K. Kalantar-Zadeh, J. George, H. A. Young, G. Liu, *Adv Sci (Weinh)* **2021**, 8, e2004433.
- [56] V. Mollica Poeta, M. Massara, A. Capucetti, R. Bonecchi, *Front Immunol* **2019**, 10, 379.
- [57] C. Macri, E. S. Pang, T. Patton, M. O'Keeffe, *Semin Cell Dev Biol* **2018**, 84, 11.
- [58] A. Gardner, Á. de Mingo Pulido, B. Ruffell, *Front Immunol* **2020**, 11, 924.
- [59] J. A. Villadangos, L. Young, *Immunity* **2008**, 29, 352.
- [60] H. Takahashi, Y. Nakagawa, K. Yokomuro, J. A. Berzofsky, *Int Immunol* **1993**, 5, 849.
- [61] R. A. Rosalia, E. D. Quakkelaar, A. Redeker, S. Khan, M. Camps, J. W. Drijfhout, A. L. Silva, W. Jiskoot, T. van Hall, P. A. van Veelen, G. Janssen, K. Franken, L. J. Cruz, A. Tromp, J. Oostendorp, S. H. van der Burg, F. Ossendorp, C. J. Melief, *Eur J Immunol* **2013**, 43, 2554.
- [62] R. J. Binder, K. M. Anderson, S. Basu, P. K. Srivastava, *J Immunol* **2000**, 165, 6029.
- [63] F. O. Nestle, S. Alijagic, M. Gilliet, Y. Sun, S. Grabbe, R. Dummer, G. Burg, D. Schadendorf, *Nat Med* **1998**, 4, 328.
- [64] F. J. Hsu, C. Benike, F. Fagnoni, T. M. Liles, D. Czerwinski, B. Taidi, E. G. Engleman, R. Levy, *Nat Med* **1996**, 2, 52.

References

- [65] V. F. Van Tendeloo, A. Van de Velde, A. Van Driessche, N. Cools, S. Anguille, K. Ladell, E. Gostick, K. Vermeulen, K. Pieters, G. Nijs, B. Stein, E. L. Smits, W. A. Schroyens, A. P. Gadisseur, I. Vrelust, P. G. Jorens, H. Goossens, I. J. de Vries, D. A. Price, Y. Oji, Y. Oka, H. Sugiyama, Z. N. Berneman, *Proc Natl Acad Sci U S A* **2010**, 107, 13824.
- [66] J. Rosenblatt, I. Avivi, B. Vasir, L. Uhl, N. C. Munshi, T. Katz, B. R. Dey, P. Somaiya, H. Mills, F. Campigotto, E. Weller, R. Joyce, J. D. Levine, D. Tzachanis, P. Richardson, J. Laubach, N. Raje, V. Boussiotis, Y. E. Yuan, L. Bisharat, V. Held, J. Rowe, K. Anderson, D. Kufe, D. Avigan, *Clin Cancer Res* **2013**, 19, 3640.
- [67] D. Schadendorf, S. Ugurel, B. Schuler-Thurner, F. O. Nestle, A. Enk, E. B. Bröcker, S. Grabbe, W. Rittgen, L. Edler, A. Sucker, C. Zimpfer-Rechner, T. Berger, J. Kamarashev, G. Burg, H. Jonuleit, A. Tüttenberg, J. C. Becker, P. Keikavoussi, E. Kämpgen, G. Schuler, *Ann Oncol* **2006**, 17, 563.
- [68] J. V. L. Niemi, A. V. Sokolov, H. B. Schioth, *Cancers (Basel)* **2022**, 14.
- [69] B. Pulendran, S. A. P. D. T. O'Hagan, *Nat Rev Drug Discov* **2021**, 20, 454.
- [70] I. Mellman, R. M. Steinman, *Cell* **2001**, 106, 255.
- [71] O. Takeuchi, S. Akira, *Cell* **2010**, 140, 805.
- [72] H. Sun, W. Hu, Y. Yan, Z. Zhang, Y. Chen, X. Yao, L. Teng, X. Wang, D. Chai, J. Zheng, G. Wang, *Hum Vaccin Immunother* **2021**, 17, 5546.
- [73] T. W. Dubensky, Jr., S. G. Reed, *Semin Immunol* **2010**, 22, 155.
- [74] A. Gołoś, A. Lutyńska, *Przegl Epidemiol* **2015**, 69, 731.
- [75] H. HogenEsch, *Vaccine* **2002**, 20 Suppl 3, S34.
- [76] J. W. Mannhalter, H. O. Neychev, G. J. Zlabinger, R. Ahmad, M. M. Eibl, *Clin Exp Immunol* **1985**, 61, 143.
- [77] M. Ulanova, A. Tarkowski, M. Hahn-Zoric, L. A. Hanson, *Infect Immun* **2001**, 69, 1151.
- [78] R. K. Gupta, *Adv Drug Deliv Rev* **1998**, 32, 155.
- [79] S. G. Reed, M. T. Orr, C. B. Fox, *Nat Med* **2013**, 19, 1597.
- [80] A. Kaur, J. Baldwin, D. Brar, D. B. Salunke, N. Petrovsky, *Curr Opin Chem Biol* **2022**, 70, 102172.
- [81] H. Sultan, A. M. Salazar, E. Celis, *Semin Immunol* **2020**, 49, 101414.
- [82] D. M. Klinman, *Nat Rev Immunol* **2004**, 4, 249.
- [83] D. Smirnov, J. J. Schmidt, J. T. Capecchi, P. D. Wightman, *Vaccine* **2011**, 29, 5434.
- [84] H. Hemmi, T. Kaisho, O. Takeuchi, S. Sato, H. Sanjo, K. Hoshino, T. Horiuchi, H. Tomizawa, K. Takeda, S. Akira, *Nat Immunol* **2002**, 3, 196.
- [85] M. Jurk, F. Heil, J. Vollmer, C. Schetter, A. M. Krieg, H. Wagner, G. Lipford, S. Bauer, *Nat Immunol* **2002**, 3, 499.

-
- [86] J. Ye, B. N. Mills, S. S. Qin, J. Garrett-Larsen, J. D. Murphy, T. P. Uccello, B. J. Han, T. G. Vrooman, C. J. Johnston, E. M. Lord, B. A. Belt, D. C. Linehan, S. A. Gerber, *J Immunother Cancer* **2022**, 10.
- [87] S. J. Dovedi, M. H. Melis, R. W. Wilkinson, A. L. Adlard, I. J. Stratford, J. Honeychurch, T. M. Illidge, *Blood* **2013**, 121, 251.
- [88] L. Zhou, Y. Zhang, Y. Wang, M. Zhang, W. Sun, T. Dai, A. Wang, X. Wu, S. Zhang, S. Wang, F. Zhou, *Adv Biosyst* **2020**, 4, e1900237.
- [89] L. Zitvogel, L. Galluzzi, O. Kepp, M. J. Smyth, G. Kroemer, *Nat Rev Immunol* **2015**, 15, 405.
- [90] G. Trinchieri, D. Santoli, *J Exp Med* **1978**, 147, 1314.
- [91] C. K. Lee, D. T. Rao, R. Gertner, R. Gimeno, A. B. Frey, D. E. Levy, *J Immunol* **2000**, 165, 3571.
- [92] M. Montoya, G. Schiavoni, F. Mattei, I. Gresser, F. Belardelli, P. Borrow, D. F. Tough, *Blood* **2002**, 99, 3263.
- [93] M. S. Diamond, M. Kinder, H. Matsushita, M. Mashayekhi, G. P. Dunn, J. M. Archambault, H. Lee, C. D. Arthur, J. M. White, U. Kalinke, K. M. Murphy, R. D. Schreiber, *J Exp Med* **2011**, 208, 1989.
- [94] B. N. Bidwell, C. Y. Slaney, N. P. Withana, S. Forster, Y. Cao, S. Loi, D. Andrews, T. Mikeska, N. E. Mangan, S. A. Samarajiwa, N. A. de Weerd, J. Gould, P. Argani, A. Möller, M. J. Smyth, R. L. Anderson, P. J. Hertzog, B. S. Parker, *Nat Med* **2012**, 18, 1224.
- [95] Z. von Marschall, A. Scholz, T. Cramer, G. Schäfer, M. Schirner, K. Oberg, B. Wiedenmann, M. Höcker, S. Rosewicz, *J Natl Cancer Inst* **2003**, 95, 437.
- [96] C. Yildirim, S. Nieuwenhuis, P. F. Teunissen, A. J. Horrevoets, N. van Royen, T. C. van der Pouw Kraan, *J Interferon Cytokine Res* **2015**, 35, 411.
- [97] K. E. Matthews, I. F. Hermans, J. M. Roberts, L. M. Ching, F. Ronchese, *Immunol Cell Biol* **2006**, 84, 383.
- [98] H. Lemos, E. Mohamed, L. Huang, R. Ou, G. Pacholczyk, A. S. Arbab, D. Munn, A. L. Mellor, *Cancer Res* **2016**, 76, 2076.
- [99] M. J. McKeage, J. Von Pawel, M. Reck, M. B. Jameson, M. A. Rosenthal, R. Sullivan, D. Gibbs, P. N. Mainwaring, M. Serke, J. J. Lafitte, C. Chouaid, L. Freitag, E. Quoix, *Br J Cancer* **2008**, 99, 2006.
- [100] P. N. Lara, Jr., J. Y. Douillard, K. Nakagawa, J. von Pawel, M. J. McKeage, I. Albert, G. Losonczy, M. Reck, D. S. Heo, X. Fan, A. Fandi, G. Scagliotti, *J Clin Oncol* **2011**, 29, 2965.
- [101] A. Y. Shih, K. L. Damm-Ganamet, T. Mirzadegan, *Biophys J* **2018**, 114, 32.

-
- [102] K. E. Sivick, A. L. Desbien, L. H. Glickman, G. L. Reiner, L. Corrales, N. H. Surh, T. E. Hudson, U. T. Vu, B. J. Francica, T. Banda, G. E. Katibah, D. B. Kanne, J. J. Leong, K. Metchette, J. R. Bruml, C. O. Ndubaku, J. M. McKenna, Y. Feng, L. Zheng, S. L. Bender, C. Y. Cho, M. L. Leong, A. van Elsas, T. W. Dubensky, Jr., S. M. McWhirter, *Cell Rep* **2018**, 25, 3074.
- [103] B. J. Francica, A. Ghasemzadeh, A. L. Desbien, D. Theodoros, K. E. Sivick, G. L. Reiner, L. Hix Glickman, A. E. Marciscano, A. B. Sharabi, M. L. Leong, S. M. McWhirter, T. W. Dubensky, Jr., D. M. Pardoll, C. G. Drake, *Cancer Immunol Res* **2018**, 6, 422.
- [104] J. B. Foote, M. Kok, J. M. Leatherman, T. D. Armstrong, B. C. Marcinkowski, L. S. Ojalvo, D. B. Kanne, E. M. Jaffee, T. W. Dubensky, Jr., L. A. Emens, *Cancer Immunol Res* **2017**, 5, 468.
- [105] Z. Deng, Y. Tian, J. Song, G. An, P. Yang, *Front Immunol* **2022**, 13, 887125.
- [106] A. Jekle, S. Thatikonda, S. Stevens, C. Williams, A. Kinkade, S. P. Ren, R. Jaisinghani, Q. L. Zhang, D. Misner, A. Stoycheva, J. Deval, S. Mukherjee, F. Gonzalez, S. Chanda, D. B. Smith, J. A. Symons, L. M. Blatt, L. Beigelman, *Cancer Research* **2020**, 80.
- [107] J. M. Ramanjulu, G. S. Pesiridis, J. Yang, N. Concha, R. Singhaus, S. Y. Zhang, J. L. Tran, P. Moore, S. Lehmann, H. C. Eberl, M. Muelbaier, J. L. Schneck, J. Clemens, M. Adam, J. Mehlmann, J. Romano, A. Morales, J. Kang, L. Leister, T. L. Graybill, A. K. Charnley, G. Ye, N. Nevins, K. Behnia, A. I. Wolf, V. Kasparcova, K. Nurse, L. Wang, A. C. Puhl, Y. Li, M. Klein, C. B. Hopson, J. Guss, M. Bantscheff, G. Bergamini, M. A. Reilly, Y. Lian, K. J. Duffy, J. Adams, K. P. Foley, P. J. Gough, R. W. Marquis, J. Smothers, A. Hoos, J. Bertin, *Nature* **2018**, 564, 439.
- [108] A. Amouzegar, M. Chelvanambi, J. N. Filderman, W. J. Storkus, J. J. Luke, *Cancers (Basel)* **2021**, 13.
- [109] H. A. Burris, M. R. Patel, D. C. Cho, J. M. Clarke, M. Gutierrez, T. Z. Zaks, J. P. Frederick, K. P. Hopson, K. Mody, A. Binanti-Berube, C. Robert-Tissot, B. G. Goldstein, B. Breton, J. Sun, S. Zhong, S. K. Pruitt, K. N. Keating, R. S. Meehan, J. F. Gainor, *Journal of Clinical Oncology* **2019**.
- [110] P. Couvreur, C. Vauthier, *Pharm Res* **2006**, 23, 1417.
- [111] S. M. Moghimi, A. C. Hunter, J. C. Murray, *Faseb j* **2005**, 19, 311.
- [112] P. Sabourian, G. Yazdani, S. S. Ashraf, M. Frounchi, S. Mashayekhan, S. Kiani, A. Kakkar, *Int J Mol Sci* **2020**, 21.
- [113] A. Gagliardi, E. Giuliano, E. Venkateswararao, M. Fresta, S. Bulotta, V. Awasthi, D. Cosco, *Front Pharmacol* **2021**, 12, 601626.
- [114] J. Simon, M. Fichter, G. Kuhn, M. Brueckner, C. Kappel, J. Schunke, T. Klaus, S. Grabbe, K. Landfester, V. Mailaender, *Nano Today* **2022**, 43.

-
- [115] M. Scherger, E. Bolli, A. R. P. Antunes, S. Arnouk, J. Stickdorn, A. Van Driessche, H. Schild, S. Grabbe, B. G. De Geest, J. A. Van Ginderachter, L. Nuhn, *Cells* **2020**, 9.
- [116] M. Kalkanidis, G. A. Pietersz, S. D. Xiang, P. L. Mottram, B. Crimeen-Irwin, K. Ardipradja, M. Plebanski, *Methods* **2006**, 40, 20.
- [117] K. Niikura, T. Matsunaga, T. Suzuki, S. Kobayashi, H. Yamaguchi, Y. Orba, A. Kawaguchi, H. Hasegawa, K. Kajino, T. Ninomiya, K. Ijiro, H. Sawa, *ACS Nano* **2013**, 7, 3926.
- [118] H. Ow, D. R. Larson, M. Srivastava, B. A. Baird, W. W. Webb, U. Wiesner, *Nano Lett* **2005**, 5, 113.
- [119] M. Benezra, O. Penate-Medina, P. B. Zanzonico, D. Schaer, H. Ow, A. Burns, E. DeStanchina, V. Longo, E. Herz, S. Iyer, J. Wolchok, S. M. Larson, U. Wiesner, M. S. Bradbury, *J Clin Invest* **2011**, 121, 2768.
- [120] S. Jiang, D. Prozeller, J. Pereira, J. Simon, S. Han, S. Wirsching, M. Fichter, M. Mottola, I. Lieberwirth, S. Morsbach, V. Mailänder, S. Gehring, D. Crespy, K. Landfester, *Nanoscale* **2020**, 12, 2626.
- [121] M. E. Moghadam, M. Sadeghi, H. Mansouri-Torshizi, M. Saidifar, *Eur J Pharm Sci* **2023**, 106477.
- [122] J. Fan, G. Fang, X. Wang, F. Zeng, Y. Xiang, S. Wu, *Nanotechnology* **2011**, 22, 455102.
- [123] C. Bharti, U. Nagaich, A. K. Pal, N. Gulati, *Int J Pharm Investig* **2015**, 5, 124.
- [124] Y. Yin, Y. Yan, B. Fan, W. Huang, J. Zhang, H. Y. Hu, X. Li, D. Xiong, S. L. Chou, Y. Xiao, H. Wang, *Research (Wash D C)* **2023**, 6, 0098.
- [125] T. Wang, M. Zou, H. Jiang, Z. Ji, P. Gao, G. Cheng, *Eur J Pharm Sci* **2011**, 44, 653.
- [126] S. D. Jazayeri, H. X. Lim, K. Shameli, S. K. Yeap, C. L. Poh, *Front Pharmacol* **2021**, 12, 682286.
- [127] M. L. Immordino, F. Dosio, L. Cattel, *Int J Nanomedicine* **2006**, 1, 297.
- [128] A. D. Bangham, M. M. Standish, J. C. Watkins, *J Mol Biol* **1965**, 13, 238.
- [129] A. G. Allison, G. Gregoriadis, *Nature* **1974**, 252, 252.
- [130] A. K. Giddam, M. Zaman, M. Skwarczynski, I. Toth, *Nanomedicine (Lond)* **2012**, 7, 1877.
- [131] P. Nordly, H. B. Madsen, H. M. Nielsen, C. Foged, *Expert Opin Drug Deliv* **2009**, 6, 657.
- [132] Y. Zhuang, Y. Ma, C. Wang, L. Hai, C. Yan, Y. Zhang, F. Liu, L. Cai, *J Control Release* **2012**, 159, 135.
- [133] N. Salomon, F. Vascotto, A. Selmi, M. Vormehr, J. Quinkhardt, T. Bukur, B. Schrörs, M. Löwer, M. Diken, Ö. Türeci, U. Sahin, S. Kreiter, *Oncoimmunology* **2020**, 9, 1771925.
- [134] S. Grabbe, H. Haas, M. Diken, L. M. Kranz, P. Langguth, U. Sahin, *Nanomedicine (Lond)* **2016**, 11, 2723.
- [135] X. Huang, N. Kong, X. Zhang, Y. Cao, R. Langer, W. Tao, *Nat Med* **2022**, 28, 2273.
- [136] Y. Zong, Y. Lin, T. Wei, Q. Cheng, *Adv Mater* **2023**, e2303261.

-
- [137] K. Swetha, N. G. Kotla, L. Tunki, A. Jayaraj, S. K. Bhargava, H. Hu, S. R. Bonam, R. Kurapati, *Vaccines (Basel)* **2023**, 11.
- [138] Z. Wan, R. Zheng, P. Moharil, Y. Liu, J. Chen, R. Sun, X. Song, Q. Ao, *Molecules* **2021**, 26.
- [139] X. Li, A. M. Aldayel, Z. Cui, *J Control Release* **2014**, 173, 148.
- [140] Q. Zeng, H. Li, H. Jiang, J. Yu, Y. Wang, H. Ke, T. Gong, Z. Zhang, X. Sun, *Biomaterials* **2017**, 122, 105.
- [141] L. Zhao, A. Seth, N. Wibowo, C. X. Zhao, N. Mitter, C. Yu, A. P. Middelberg, *Vaccine* **2014**, 32, 327.
- [142] S. Hamdy, A. Haddadi, R. W. Hung, A. Lavasanifar, *Adv Drug Deliv Rev* **2011**, 63, 943.
- [143] M. Diwan, P. Elamanchili, H. Lane, A. Gainer, J. Samuel, *J Drug Target* **2003**, 11, 495.
- [144] M. Kempf, B. Mandal, S. Jilek, L. Thiele, J. Vörös, M. Textor, H. P. Merkle, E. Walter, *J Drug Target* **2003**, 11, 11.
- [145] Y. Waeckerle-Men, M. Groettrup, *Adv Drug Deliv Rev* **2005**, 57, 475.
- [146] L. Josephson, C. H. Tung, A. Moore, R. Weissleder, *Bioconjug Chem* **1999**, 10, 186.
- [147] D. F. Nixon, C. Hioe, P. D. Chen, Z. Bian, P. Kuebler, M. L. Li, H. Qiu, X. M. Li, M. Singh, J. Richardson, P. McGee, T. Zamb, W. Koff, C. Y. Wang, D. O'Hagan, *Vaccine* **1996**, 14, 1523.
- [148] T. Warger, P. Osterloh, G. Rechtsteiner, M. Fassbender, V. Heib, B. Schmid, E. Schmitt, H. Schild, M. P. Radsak, *Blood* **2006**, 108, 544.
- [149] M. Diwan, P. Elamanchili, M. Cao, J. Samuel, *Curr Drug Deliv* **2004**, 1, 405.
- [150] S. Hamdy, P. Elamanchili, A. Alshamsan, O. Molavi, T. Satou, J. Samuel, *J Biomed Mater Res A* **2007**, 81, 652.
- [151] P. Elamanchili, C. M. Lutsiak, S. Hamdy, M. Diwan, J. Samuel, *J Immunother* **2007**, 30, 378.
- [152] K. Schroder, P. J. Hertzog, T. Ravasi, D. A. Hume, *J Leukoc Biol* **2004**, 75, 163.
- [153] S. Hamdy, O. Molavi, Z. Ma, A. Haddadi, A. Alshamsan, Z. Gobti, S. Elhasi, J. Samuel, A. Lavasanifar, *Vaccine* **2008**, 26, 5046.
- [154] M. Levit, A. Vdovchenko, A. Dzhuzha, N. Zashikhina, E. Katernyuk, A. Gostev, E. Sivtsov, A. Lavrentieva, T. Tennikova, E. Korzhikova-Vlakh, *Int J Mol Sci* **2021**, 22.
- [155] N. M. Molino, M. Neek, J. A. Tucker, E. L. Nelson, S. W. Wang, *Biomaterials* **2016**, 86, 83.
- [156] N. Hüppe, J. Schunke, M. Fichter, V. Mailänder, F. R. Wurm, K. Landfester, *Nanoscale Horiz* **2022**, 7, 908.
- [157] K. Piradashvili, M. Fichter, K. Mohr, S. Gehring, F. R. Wurm, K. Landfester, *Biomacromolecules* **2015**, 16, 815.

-
- [158] M. Fichter, K. Piradashvili, A. Pietrzak-Nguyen, L. Pretsch, G. Kuhn, S. Strand, M. Knuf, F. Zepp, F. R. Wurm, V. Mailänder, K. Landfester, S. Gehring, *Biomaterials* **2016**, 108, 1.
- [159] G. Baier, M. Fichter, A. Kreyes, K. Klein, V. Mailänder, S. Gehring, K. Landfester, *Biomacromolecules* **2016**, 17, 148.
- [160] Y. Wang, L. Zhang, Z. Xu, L. Miao, L. Huang, *Mol Ther* **2018**, 26, 420.
- [161] S. Gao, J. Wang, Z. Zhu, J. Fang, Y. Zhao, Z. Liu, H. Qin, Y. Wei, H. Xu, X. Dan, L. Yang, Q. Xu, *Immunotherapy* **2023**, 15, 57.
- [162] J. Nagasaki, T. Ishino, Y. Togashi, *Cancer Sci* **2022**, 113, 3303.
- [163] D. S. Chen, I. Mellman, *Immunity* **2013**, 39, 1.
- [164] A. Ribas, J. D. Wolchok, *Science* **2018**, 359, 1350.
- [165] Y. Liu, W. N. Crowe, L. Wang, W. J. Petty, A. A. Habib, D. Zhao, *Nano Res* **2023**, 16, 5300.
- [166] X. Gao, G. Lei, B. Wang, Z. Deng, J. Karges, H. Xiao, D. Tan, *Adv Sci (Weinh)* **2023**, 10, e2205241.
- [167] Y. Cheng, C. Wang, H. Wang, Z. Zhang, X. Yang, Y. Dong, L. Ma, J. Luo, *BMC Med* **2022**, 20, 411.
- [168] N. Pippa, M. Gazouli, S. Pispas, *Vaccines (Basel)* **2021**, 9.
- [169] S. V. Khairnar, P. Pagare, A. Thakre, A. R. Nambiar, V. Junnuthula, M. C. Abraham, P. Kolimi, D. Nyavanandi, S. Dyawanapelly, *Pharmaceutics* **2022**, 14.
- [170] S. M. Gheibi Hayat, M. Darroudi, *J Cell Physiol* **2019**, 234, 12530.
- [171] M. C. Operti, A. Bernhardt, S. Grimm, A. Engel, C. G. Figdor, O. Tagit, *Int J Pharm* **2021**, 605, 120807.
- [172] M. E. Pichichero, *Vaccine* **2014**, 32, 3886.
- [173] R. Aspinall, G. Del Giudice, R. B. Effros, B. Grubeck-Loebenstien, S. Sambhara, *Immun Ageing* **2007**, 4, 9.
- [174] S. H. van der Burg, R. Arens, F. Ossendorp, T. van Hall, C. J. Melief, *Nat Rev Cancer* **2016**, 16, 219.
- [175] S. Valastyan, R. A. Weinberg, *Cell* **2011**, 147, 275.
- [176] O. Veiseh, F. M. Kievit, R. G. Ellenbogen, M. Zhang, *Adv Drug Deliv Rev* **2011**, 63, 582.
- [177] M. F. Roelofs, L. A. Joosten, S. Abdollahi-Roodsaz, A. W. van Lieshout, T. Sprong, F. H. van den Hoogen, W. B. van den Berg, T. R. Radstake, *Arthritis Rheum* **2005**, 52, 2313.
- [178] A. I. Tikhvatulin, A. S. Dzharullaeva, N. M. Tikhvatulina, D. V. Shcheblyakov, M. M. Shmarov, I. V. Dolzhikova, P. Stanhope-Baker, B. S. Naroditsky, A. V. Gudkov, D. Y. Logunov, A. L. Gintsburg, *PLoS One* **2016**, 11, e0155650.
- [179] C. G. Da Silva, M. G. M. Camps, T. Li, A. B. Chan, F. Ossendorp, L. J. Cruz, *Biomaterials* **2019**, 220, 119417.

-
- [180] K. Landfester, C. K. Weiss, *Modern Techniques for Nano- and Microreactors/-Reactions* **2010**, 229, 1.
- [181] H. C. Kolb, M. G. Finn, K. B. Sharpless, *Angew Chem Int Ed Engl* **2001**, 40, 2004.
- [182] J. E. Moses, A. D. Moorhouse, *Chem Soc Rev* **2007**, 36, 1249.
- [183] K. Piradashvili, J. Simon, D. Paßlick, J. R. Höhner, V. Mailänder, F. R. Wurm, K. Landfester, *Nanoscale Horiz* **2017**, 2, 297.
- [184] L. M. Gaetke, C. K. Chow, *Toxicology* **2003**, 189, 147.
- [185] J. M. Siebert, G. Baier, A. Musyanovych, K. Landfester, *Chem Commun (Camb)* **2012**, 48, 5470.
- [186] M. Tarhini, H. Greige-Gerges, A. Elaissari, *Int J Pharm* **2017**, 522, 172.
- [187] D. Paßlick, K. Piradashvili, D. Bamberger, M. Li, S. Jiang, D. Strand, R. W. P. K. Landfester, M. Bros, S. Grabbe, V. Mailänder, *J Control Release* **2018**, 289, 23.
- [188] M. Neek, T. I. Kim, S. W. Wang, *Nanomedicine* **2019**, 15, 164.
- [189] E. D. Goddard-Borger, R. V. Stick, *Org Lett* **2007**, 9, 3797.
- [190] A. Thomas, H. Schlaad, B. Smarsly, M. Antonietti, *Langmuir* **2003**, 19, 4455.
- [191] A. Gardner, B. Ruffell, *Trends Immunol* **2016**, 37, 855.
- [192] K. Ni, H. C. O'Neill, *Immunol Cell Biol* **1997**, 75, 223.
- [193] J. Couzin-Frankel, *Science* **2013**, 342, 1432.
- [194] E. S. Bergmann-Leitner, W. W. Leitner, *Vaccines (Basel)* **2014**, 2, 252.
- [195] B. Guy, *Nat Rev Microbiol* **2007**, 5, 505.
- [196] S. E. Girardin, I. G. Boneca, J. Viala, M. Chamailard, A. Labigne, G. Thomas, D. J. Philpott, P. J. Sansonetti, *J Biol Chem* **2003**, 278, 8869.
- [197] L. Alexopoulou, A. C. Holt, R. Medzhitov, R. A. Flavell, *Nature* **2001**, 413, 732.
- [198] E. D. Goddard-Borger, R. V. Stick, *Organic letters* **2007**, 9, 3797.
- [199] R. L. Sabado, S. Balan, N. Bhardwaj, *Cell Res* **2017**, 27, 74.
- [200] E. S. Trombetta, I. Mellman, *Annu Rev Immunol* **2005**, 23, 975.
- [201] S. Akira, K. Takeda, *Nat Rev Immunol* **2004**, 4, 499.
- [202] J. Kwon, S. F. Bakhoun, *Cancer Discov* **2020**, 10, 26.
- [203] T. Li, Z. J. Chen, *J Exp Med* **2018**, 215, 1287.
- [204] C. Pasare, R. Medzhitov, *Semin Immunol* **2004**, 16, 23.
- [205] S. Meixlsperger, C. S. Leung, P. C. Rämer, M. Pack, L. D. Vanoaica, G. Breton, S. Pascolo, A. M. Salazar, A. Dzionek, J. Schmitz, R. M. Steinman, C. Münz, *Blood* **2013**, 121, 5034.
- [206] K. McKenna, A. S. Beignon, N. Bhardwaj, *J Virol* **2005**, 79, 17.
- [207] F. M. Marincola, E. M. Jaffee, D. J. Hicklin, S. Ferrone, *Adv Immunol* **2000**, 74, 181.

References

- [208] J. Landsberg, J. Kohlmeyer, M. Renn, T. Bald, M. Rogava, M. Cron, M. Fatho, V. Lennerz, T. Wölfel, M. Hölzel, T. Tüting, *Nature* **2012**, 490, 412.
- [209] R. V. Parry, J. M. Chemnitz, K. A. Frauwirth, A. R. Lanfranco, I. Braunstein, S. V. Kobayashi, P. S. Linsley, C. B. Thompson, J. L. Riley, *Mol Cell Biol* **2005**, 25, 9543.
- [210] B. H. Kang, H. K. Lee, *Int J Mol Sci* **2022**, 23.
- [211] A. Ladányi, *Pigment Cell Melanoma Res* **2015**, 28, 490.
- [212] A. G. Sikora, N. Jaffarad, Y. Hailemichael, A. Gelbard, S. W. Stonier, K. S. Schluns, L. Frasca, Y. Lou, C. Liu, H. A. Andersson, P. Hwu, W. W. Overwijk, *J Immunol* **2009**, 182, 7398.
- [213] S. Bhatnagar, V. Revuri, M. Shah, P. Larson, Z. Shao, D. Yu, S. Prabha, T. S. Griffith, D. Ferguson, J. Panyam, *Cancers (Basel)* **2022**, 14.
- [214] M. Merad, P. Sathe, J. Helft, J. Miller, A. Mortha, *Annu Rev Immunol* **2013**, 31, 563.
- [215] M. Bros, E. Montermann, A. Cholaszczyńska, A. B. Reske-Kunz, *Int Immunopharmacol* **2016**, 35, 174.
- [216] M. Fichter, M. Dedters, A. Pietrzak-Nguyen, L. Pretsch, C. U. Meyer, S. Strand, F. Zepp, G. Baier, K. Landfester, S. Gehring, *Vaccine* **2015**, 33, 838.
- [217] D. Hofmann, S. Tenzer, M. B. Bannwarth, C. Messerschmidt, S. F. Glaser, H. Schild, K. Landfester, V. Mailänder, *ACS Nano* **2014**, 8, 10077.
- [218] S. Tenzer, D. Docter, S. Rosfa, A. Wlodarski, J. Kuharev, A. Rekik, S. K. Knauer, C. Bantz, T. Nawroth, C. Bier, J. Sirirattanapan, W. Mann, L. Treuel, R. Zellner, M. Maskos, H. Schild, R. H. Stauber, *ACS Nano* **2011**, 5, 7155.
- [219] R. A. Bradshaw, A. L. Burlingame, S. Carr, R. Aebersold, *Mol Cell Proteomics* **2006**, 5, 787.
- [220] S. Han, R. da Costa Marques, J. Simon, A. Kaltbeitzel, K. Koynov, K. Landfester, V. Mailänder, I. Lieberwirth, *Nat Commun* **2023**, 14, 295.
- [221] J. C. Silva, M. V. Gorenstein, G. Z. Li, J. P. Vissers, S. J. Geromanos, *Mol Cell Proteomics* **2006**, 5, 144.
- [222] M. Jurk, A. Kritzler, B. Schulte, S. Tluk, C. Schetter, A. M. Krieg, J. Vollmer, *Eur J Immunol* **2006**, 36, 1815.
- [223] G. M. Lynn, C. Sedlik, F. Baharom, Y. Zhu, R. A. Ramirez-Valdez, V. L. Coble, K. Tobin, S. R. Nichols, Y. Itzkowitz, N. Zaidi, J. M. Gammon, N. J. Blobel, J. Denizeau, P. de la Rochere, B. J. Francica, B. Decker, M. Maciejewski, J. Cheung, H. Yamane, M. G. Smelkinson, J. R. Francica, R. Laga, J. D. Bernstock, L. W. Seymour, C. G. Drake, C. M. Jewell, O. Lantz, E. Piaggio, A. S. Ishizuka, R. A. Seder, *Nat Biotechnol* **2020**, 38, 320.
- [224] T. Su, Y. Zhang, K. Valerie, X. Y. Wang, S. Lin, G. Zhu, *Theranostics* **2019**, 9, 7759.

-
- [225] Z. J. Roberts, N. Goutagny, P. Y. Perera, H. Kato, H. Kumar, T. Kawai, S. Akira, R. Savan, D. van Echo, K. A. Fitzgerald, H. A. Young, L. M. Ching, S. N. Vogel, *J Exp Med* **2007**, 204, 1559.
- [226] G. J. Rustin, C. Bradley, S. Galbraith, M. Stratford, P. Loadman, S. Waller, K. Bellenger, L. Gumbrell, L. Folkes, G. Halbert, *Br J Cancer* **2003**, 88, 1160.
- [227] L. J. Cruz, R. A. Rosalia, J. W. Kleinovink, F. Rueda, C. W. Löwik, F. Ossendorp, *J Control Release* **2014**, 192, 209.
- [228] T. Fujimura, R. Okuyama, T. Ohtani, Y. Ito, T. Haga, A. Hashimoto, S. Aiba, *Clin Exp Dermatol* **2009**, 34, 793.
- [229] A. M. Fathallah, R. B. Bankert, S. V. Balu-Iyer, *Aaps j* **2013**, 15, 897.
- [230] S. T. Hwang, *J Invest Dermatol* **2012**, 132, 1070.
- [231] D. Leveque, *Anticancer Res* **2014**, 34, 1579.
- [232] C. G. Kim, Y. C. Kye, C. H. Yun, *Pharmaceutics* **2019**, 11.
- [233] H. Raskov, A. Orhan, J. P. Christensen, I. Gögenur, *Br J Cancer* **2021**, 124, 359.
- [234] D. Hendriks, Y. He, I. Koopmans, V. R. Wiersma, R. J. van Ginkel, D. F. Samplonius, W. Helfrich, E. Bremer, *Oncoimmunology* **2016**, 5, e1202390.
- [235] S. Singhal, P. S. Bhojnagarwala, S. O'Brien, E. K. Moon, A. L. Garfall, A. S. Rao, J. G. Quatromoni, T. L. Stephen, L. Litzky, C. Deshpande, M. D. Feldman, W. W. Hancock, J. R. Conejo-Garcia, S. M. Albelda, E. B. Eruslanov, *Cancer Cell* **2016**, 30, 120.
- [236] C. Beauvillain, Y. Delneste, M. Scotet, A. Peres, H. Gascan, P. Guermonprez, V. Barnaba, P. Jeannin, *Blood* **2007**, 110, 2965.
- [237] A. Bajnok, M. Ivanova, J. Rigó, Jr., G. Toldi, *Mediators Inflamm* **2017**, 2017, 8045161.
- [238] C. Cambiaggi, M. T. Scupoli, T. Cestari, F. Gerosa, G. Carra, G. Tridente, R. S. Accolla, *Immunogenetics* **1992**, 36, 117.
- [239] M. López-Cabrera, A. G. Santis, E. Fernández-Ruiz, R. Blacher, F. Esch, P. Sánchez-Mateos, F. Sánchez-Madrid, *J Exp Med* **1993**, 178, 537.
- [240] J. Reddy, P. Chastagner, L. Fiette, X. Liu, J. Thèze, *Int Immunol* **2001**, 13, 135.
- [241] A. L. Jackson, H. Matsumoto, M. Janszen, V. Maino, A. Blidy, S. Shye, *Clin Immunol Immunopathol* **1990**, 54, 126.
- [242] S. Simon, N. Labarriere, *Oncoimmunology* **2017**, 7, e1364828.
- [243] Y. Wolf, A. C. Anderson, V. K. Kuchroo, *Nat Rev Immunol* **2020**, 20, 173.
- [244] Á. de Mingo Pulido, K. Hänggi, D. P. Celas, A. Gardner, J. Li, B. Batista-Bittencourt, E. Mohamed, J. Trillo-Tinoco, O. Osunmakinde, R. Peña, A. Onimus, T. Kaisho, J. Kaufmann, K. McEachern, H. Soliman, V. C. Luca, P. C. Rodriguez, X. Yu, B. Ruffell, *Immunity* **2021**, 54, 1154.
- [245] Z. Xu, Y. Wang, L. Zhang, L. Huang, *ACS Nano* **2014**, 8, 3636.

References

- [246] E. A. Vasievich, S. Ramishetti, Y. Zhang, L. Huang, *Mol Pharm* **2012**, 9, 261.
- [247] L. Sfondrini, D. Besusso, V. Bronte, B. Macino, A. Rossini, M. P. Colombo, S. Ménard, A. Balsari, *Cancer Immunol Immunother* **2004**, 53, 697.

Acknowledgements

At this point I would like to thank those who have supported and accompanied me during the period of writing the dissertation.

In particular, I would like to thank [redacted] for the opportunity to perform the scientific work in his research group. Thanks to his expert advice and supervision, it was possible to develop an interesting and innovative project. Only with his support as a contact person and motivator I was able to complete my dissertation successfully.

I would like to thank [redacted] for supervising my doctoral thesis, [redacted] for her willingness to serve as a reviewer and [redacted] for chairing the oral examination.

Special thanks go to [redacted] and [redacted] from the Max Planck Institute for Polymer Research in Mainz. The joint collaboration was always characterized by close scientific exchange, good communication and reliability. Their support and the synthesis of the nanocapsule formulations provided me with the opportunity to perform the presented experiments.

Furthermore, I would like to thank [redacted] for his professional and moral support both, in performing the experiments and writing the dissertation. I would also like to sincerely thank my colleagues and [redacted] for their constructive and motivating collaboration, which has greatly enhanced the last year.

I would like to thank [redacted] for his understanding and caring way of backing me up. Last but not least, I would like to thank my family and especially my parents for their unconditional support during difficult phases as well as for paving the way until I submitted my dissertation.